

# Life Extension Activities in Fast Breeder Test Reactor

**B.Anandapadmanaban, A.Babu, S.Sridhar, K.Dinesh, G.Srinivasan**

Indira Gandhi Centre for Atomic Research, Kalpakkam, India

**Abstract.** Fast Breeder Test Reactor (FBTR) has completed 26 years of operation and is currently under periodic safety review by the Atomic Energy Regulatory Board of India for life extension. Over a period of time, based on the operational feedback, maintenance difficulties and obsolescence, several major components have been replaced. These include the Neutronic channels, UPS, computers of the Central Data Processing System, main boiler feed pumps, four control rod drive mechanisms, two control rods, central canal plug, deaerator lift pumps, reheaters of the steam water system, station batteries, DM plant, Nitrogen plant, starting air system of the emergency diesel generators and isolation dampers of the reactor containment building. Due to obsolescence, 6.6kV MOCB were replaced with VCB and 415V electro-mechanical relays were replaced with numerical relays. Regarding the non-replaceable components, residual life assessment has been carried out based on the operational history vis-à-vis the design limits for each component. The life limiting mechanism of heat transport systems of FBTR are creep and fatigue. Creep-fatigue damage has been assessed from operational cycles and found to be insignificant. However, the major life limiting factor has been found to be the irradiation induced loss of ductility of the Grid Plate which supports the core. The fast flux at the grid plate location was measured using Np foils and SS samples irradiated. The estimated residual life of the grid plate, based on the results, has been assessed as 6.52 effective full power years.

## 1. INTRODUCTION

The Fast Breeder Test Reactor (FBTR) located at Kalpakkam, India is a plutonium carbide fuelled, two loop fast reactor with sodium as the primary/secondary coolant. The first criticality of this reactor was achieved on 18<sup>th</sup> Oct.1985 with a 23 subassembly core rated for 10.5MWt with 320w/cm linear heat rating. The core has been expanded progressively and the target burn up was increased based on the results of Post Irradiation Examination (PIE) conducted on fuel at various burn up levels. The reactor has been operated up to a power level of 20.3MWt/4.2MWe with a sodium temperature of 482°C max.

The reactor has completed 27 years of successful mission mode operation at various power levels for material irradiation, reactor physics experiments and power generation. It is in continuous operation and simultaneously undergoing periodic safety review by the Atomic Energy Regulatory Board of India. The periodic safety review covers the Actual physical condition of the plant, Review of Safety Analysis, Equipment qualification, Ageing management, Safety performance, Implementation of feedback from other nuclear power plants, Procedures used for handling normal & off-normal situations, maintenance, testing, inspection, radiation protection etc., Organization & administration structure, Human resource development, Emergency planning measures and Environmental impact.

Over a period of time, several major components have been replaced mainly to address obsolescence, degradation and operational convenience. These include the Neutronic channels, UPS, Computers of the Central Data Processing System, Main boiler feed pumps, four Control Rod Drive Mechanisms, Central canal plug of reactor, two Control rods, Deaerator lift pumps, Reheaters of the steam water system, Station Batteries, Emergency chiller units, Air handling units, Starting air system of emergency Diesel Generators, Quick isolation dampers of the reactor containment building, DM plant and Nitrogen plant.

For non-replaceable components, residual life assessment has been carried out based on the operational history vis-à-vis the design limits for each component. The life limiting mechanism of heat transport systems of FBTR are creep and fatigue. Since the reactor has operated only upto a temperature of 444°C till 2007, the creep effect is insignificant. The total number of thermal cycles seen by the reactor components as of 2007 was 163, as against the design cycle of 2000 for most of the components. After 2007, till this date, the reactor has experienced very few thermal cycles. As such all the heat transport system components have sufficient design life for safe operation for another 20years or more. The major life limiting factor for the reactor is found to be the neutronic fluence on the grid plate which supports the core. The fast flux at the grid plate location was measured using Np foils and the residual life of the reactor has been assessed to be 6.52 effective full power years.

## 2. DESCRIPTION

Fig.1 gives the schematic of FBTR. The heat generated in the reactor core is removed by two parallel hydro-dynamically coupled primary sodium loops which in turn transfer the heat to two independent secondary sodium loops through intermediate heat exchangers. Each secondary sodium loop is

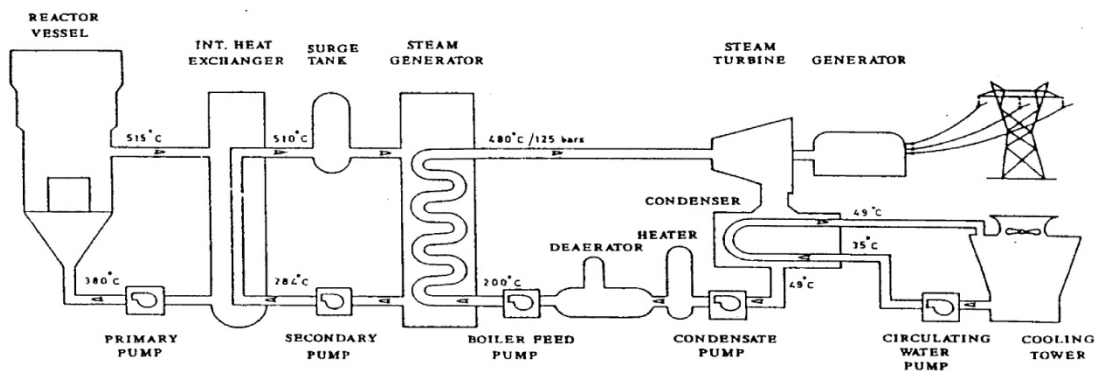


FIG. 1. Simplified Schematic of FBTR.

provided with two once-through serpentine type steam generator (SG) modules. The steam from the SG in both the loops is fed to a common steam water circuit comprising a Turbo- Generator (TG) and a 100% capacity Dump Condenser (DC). In the case of non-availability of turbine, reactor operation could be continued at full power by dumping the steam in the DC. The material of construction is austenitic stainless steel for reactor vessel, primary and secondary sodium circuits, which has good ductility and creep resistance at high temperature. Sudden ruptures are quite unlikely and the "leak before break" criterion is applicable.

## 3. DESIGN LIFE ASSESSMENT AND OPERATION HISTORY OF STRUCTURES, SYSTEMS AND COMPONENTS

The reactor has a nominal design life of 20 years, corresponding to the operating temperatures at 40 MWt. However, the reactor has been operated upto a maximum power level of only 20.3 MWt. The maximum sodium outlet temperature achieved is 490°C as against the design temperature of 520°C. Steam temperature reached so far is 470°C as against the design temperature of 480°C.

### 3.1. Reactor Nuclear Systems

The sodium heat transport systems including reactor are designed as per ASME Sec-III, applying code cases 1331, 1592 or N-47 for the high temperature components. The life of almost all the components is governed by creep-fatigue. The primary and secondary sodium system components are designed for a creep life of  $1.5 \times 10^5$ h at 520°C. The combination of sodium which have good thermal conductivity, with stainless steel having poor thermal conductivity and high coefficient of thermal

expansion, makes the sodium systems prone to thermal stresses during reactor shutdown and during incidents like trips of various pumps in the heat transport chain. All sodium system components have been design checked for 2000 cycles and IHX tube-sheet for 1000 cycles of hot and cold shocks.

Though the fuel was initially rated for 35 GWd/t, the burnup has been progressively enhanced based on PIE at 25, 50, 100, 155 GWd/t burnup. For some of the subassemblies other than fuel, viz. Nickel, steel and control rods, whose design life could not be quantified, a programme for periodic replacement followed by PIE is in place.

Periodic visual inspection of the Reactor Vessel internals is carried out every two years using periscope. The condition of Reactor Vessel (RV), internal piping and other components inside RV was found to be good.

Metallic bellows in Control Rod Drive Mechanisms failed four times, warranting the replacement of the lower part of the mechanisms. The failures were due to entry of sodium into the interspace of mechanism through the SS bellows made of 0.125 mm thick discs after prolonged exposure to sodium, resulting in seizure of gripper mechanism or translation mechanism.

Biological shield cooling coils embedded in borated concrete, surrounding the reactor block developed leaks in the year 2000, after 15 years of service due to crevice corrosion in some of the embedded socket weld joints. Sealants and sealing procedure were developed in house and sealing is done as and when any leak develops.

The Central Canal Plug (CCP), which houses three thermocouples for monitoring the outlet temperature of the central SA, was replaced by a CCP of modified design, which allows above core irradiation and has four thermocouples instead of three for monitoring the outlet temperature of the central SA. The instrumentation for the reactor vessel Displacement Measuring Device has been replaced by a microprocessor-based system as the existing system became obsolete. The inflatable seals on the reactor assembly, which had failed during commissioning, were replaced in 2004. All accessible elastomeric seals on the reactor assembly were also replaced during this time.

Performance of sodium systems has been satisfactory so far. There was no leak in the pipeline & equipment. Sodium purity has been maintained extremely well with plugging temperatures less than 105°C. There were only two failures of bellows-sealed sodium service valves in secondary sodium system and one valve leak in primary sodium purification circuit due to a manufacturing defect. These were replaced.

Each of the four sodium pumps has been in operation for more than 165,000 h. There were no bearing failures. The oil leak through mechanical seals is monitored and the seal box is replaced as and when seal leak rate exceeds a specified limit. As the pumps are located in the cold legs of the loops, there is no concern for creep and fatigue damage due to thermal shocks.

One secondary cold trap was replaced during initial period of operation consequent on plugging by oxides/ hydroxides due to a design deficiency coupled with procedural error in operating the cold trap with large impurity ingress after a modification work in secondary sodium system. The cold trap removed from the circuit has been cleaned, modified and kept as a spare in addition to the one spare of modified design..

### **3.2. Conventional Systems**

These systems are all accessible for maintenance/ replacement, and hence there is no specific design life for these systems, except for some individual components (e.g. batteries, bearings, belts, seals, electronic cards etc.). The components in these systems are being inspected on a regular basis and retrofitting or replacement is planned based on their condition or whenever they become obsolete. The reactor went critical in 1985, and all the conventional systems have been in continuous operation since

then. Civil structures including the Reactor Containment Building (RCB) were ready in 1975 and have seen a life of 37 years.

#### **4. AGEING MANAGEMENT**

Ageing management addresses the residual life assessment of components which are passive, non-replaceable / replaceable with difficulty, taking into account their life degrading mechanisms.

The life limiting mechanisms of heat transport system are creep & fatigue. Though the reactor has completed 27 calendar years of operation, it was operated upto a temperature of 444°C till 2007, the creep effect is insignificant. The maximum achieved temperature is well below the creep range for SS. The reactor has seen 270 LOR & 169 scrams so far and most of them are at low reactor power. Hence the stresses due to hot and cold shocks are less than at nominal design power (40 MWt) conditions. From creep-fatigue considerations, the reactor has not seen much life. Data on various incidents such as secondary sodium pump trip, MBFP trip and SG depressurization are regularly logged for predicting the life of SG modules.

Residual life assessment has been carried out based on the operation history vis-à-vis the design limit for each component as part of Periodic Safety Review. Preliminary assessment shows that the plant systems have exhausted less than 10% of its original design life even though the reactor is 27 years old. However, the major life limiting factor has been found to be the neutronic fluence on the grid plate which supports the core. Irradiation induced loss of ductility limits the fluence on the GP. Though the reactor has operated at low power (max. of 20.3MWt) w.r.to its nominal design power (40 MWt), the incident flux on the reactor components is governed by the LHR rather than the reactor power. An assessment of the residual life of the grid plate was done by measurement of fast flux in the grid plate location using Np foils and irradiation of SS samples to dpa levels at the Grid Plate location. For a 10% residual ductility criterion, the residual life has been assessed to be 6.52 effective full power years. For other reactor components, life limit from neutron-induced embrittlement is longer. The limiting fluence for the reactor vessel will be reached in 47 EFPY and hence there is no concern. A material surveillance programme is being evolved to monitor the material property degradation due to fluence.

#### **5. EQUIPMENT QUALIFICATION AND LIFE EXTENSION ACTIVITIES**

Equipment qualification refers to the ability of the replaceable equipment to meet the functional requirements on demand, accomplished by periodic surveillance, maintenance and replacement. All systems have been well maintained by periodical preventive maintenance (PM) programme. Components like batteries, bearings, belts, elastomeric seals, electronic cards etc. which have specified life are periodically replaced based on the manufacturer's recommendations or results of surveillance checks & condition monitoring. Other components are overhauled by replacing the aged/worn out/degraded parts and put back in service.

##### **5.1. Nuclear systems**

On the nuclear systems, periodic PM is carried out on sodium pump drives. Sodium pump seals are replaced whenever oil leak exceeds the specified value. The remote operation mechanical links of primary sodium valves are relubricated at specific intervals and the ease of operation is ensured. Piping hangers in the primary and secondary systems are periodically inspected and reset if required. Availability of Argon compressors in the primary cover gas circuit, blowers & HX in the PHEC & RPC circuits and thermo fluid pumps & HX in the primary & secondary cold trap cooling circuits is ensured by regular PM. The electronics of all the sodium instrumentation is also maintained by periodic servicing. Whenever required, entry is made into the normally inaccessible primary purification cabin to attend to problems in leak detectors and valves.

## **5.2. Air locks**

The rubber seals of Material air lock and Personal air lock are being replaced at specified periodicity. A regular PM is in place to maintain these air locks which are in constant use for personal and material access into the Reactor Containment Building. The actuators of the air locks are serviced and aged components are being replaced as a part of PM.

## **5.3. Auxiliary support systems**

The DM plant has been replaced with higher capacity plant to enhance the capacity from 1 to 3 m<sup>3</sup>/h plant in 1996. The cryogenic nitrogen plant has been replaced by a state-of-the art plant based on PSA (pressure switch adsorption) principle in 1996. The capacity of the plant has been augmented by adding one more PSA tower and a Nitrogen booster compressor. The contact type heaters in the steam water circuit were replaced by non-contact type, since level fluctuations were high in the contact type, resulting in several reactor trips.

## **5.4. Civil Structures**

RCB leak test is carried out every two years since 1985 at a test pressure of 150mb(g). The leak rates have been found to be well below the acceptance level of 0.077% v/v per hour. The major contributor to the leaks has been found to be cable penetrations and micro cracks in concrete. Cable penetrations are repaired and resin-hardener mix coating is applied over the leaking area on concrete surface.

The 150mm thick RCC sump wall of cooling tower has developed cracks at some places and water started leaking. Leaks were arrested by pressure grouting cement slurry mixed with water proofing chemical. All leaks have been arrested. The metallic structures are generally maintained by periodical coal tar epoxy painting and are replaced when extensively corroded.

Periodic visual inspection is carried out on the RCC tunnel connecting cooling tower and service water intermediate sump. Structure is found intact without any cracks or spalls. Periodic repainting of the internal surface with epoxy paint is done.

## **5.5. Electrical Systems**

The two 10 MVA, 33 kV / 6.6 kV main transformers and ten 6.6 kV / 433 V auxiliary load center transformers and circuit breakers are in service for the past 32 years. There was no major fault or breakdown in these equipments. Major reconditioning of these transformers was done at the supplier's facility considering their age and to increase the residual life further. The servicing involved vacuum treatment for the core and windings, total replacement of oil, gaskets and radiator valves.

All the 18 nos. of 6.6 kV Minimum Oil Circuit Breakers (MOCB) were replaced with Vacuum Circuit Breakers (VCB) as the MOCB breakers became obsolete. The VCBs & their carriage were retrofitted into the existing 6.6KV panels. 15 nos of LT air circuit breakers which were in service for the past 30 years were also replaced with new model breakers as they became obsolete.

Due to performance degradation, the 220 V, 1 $\phi$ , 50 Hz UPS was replaced in 1998 by a state-of-the-art system. The tubular batteries in the 220 V 1 $\phi$  UPS, 220V, 48V & 24V DC control power supply systems and in the Ward Leonard drives have been replaced by high performance Plante' cells. The batteries are being replaced with a periodicity of 7 to 10 years.

36 nos. lightning masts and 52 nos. earth pits around the plant in the electrical grounding system were totally serviced and renovated.

Motors/Generators in all systems including sodium pump drives have been replaced by spares, whenever need arose. The machines taken out are serviced, rewound if required and kept as spares.

Power cables, which had failed 10 times in the penetration to RCB, were normalized by replacing the penetration joints. Failures were analyzed and found to be due to overheating as the spacing between cable joints were very short. Hence, the cable penetration joint assembly was redesigned by increasing the length (from 300 to 600mm) thereby giving more space between the individual cable core joints and introduction of a spacer disc to keep uniform radial clearance and testing the joint for contact resistance. The cable removed from RCB penetration in the wake of a cable fire incident was tested and found to have a residual life of more than 20 years.

The 30 years old electromagnetic protective relays (48nos.) which became obsolete were replaced with state of the art numerical relays.

### ***5.6. Instrumentation & Control Systems***

The neutronic channels were totally replaced in 1998 by state-of-the-art, maintenance friendly channels due to frequent failure of the old channels. The grounding of the signal cables were improved to eliminate noise pick up.

The two computers of Central Data Processing System (CDPS) were replaced one by one in 1988 and in 1992. These two systems were again replaced with discless embedded systems in 2006 & 2009. The CDPS function as a data acquisition system has been progressively increased over the years by adding industrial PCs for real-time logging of various plant parameters and history memorization. These PCs are periodically replaced/updated whenever required.

The Mass Spectrometer signals in Steam Generator Leak Detection System (SGLDS) were replaced by sputter- ion pump signals for sensing presence of hydrogen in sodium due to tube leak in steam generator. This has obviated the need for expensive mass spectrometers and their spares. For further improving the system reliability/availability, triplication of SGLDS in each secondary loop has been done.

Similarly, the Reactor Vessel Displacement Measurement Device controller was also replaced with embedded system in 2011. A number of analog indicators have been replaced with digital indicators, especially in temperature measurement channels. Old recorders have been replaced with chart-less recorders which have less wear and tear as there are no moving parts like motors and pens in such recorders. Particulate Activity Monitors have been replaced with micro-controller based ones. Linear power supply units in some systems have been upgraded to light-weight SMPS systems which offer higher efficiency.

### ***5.7. Mechanical Equipment***

The flywheel casings of Ward Leonard 100 & Ward Leonard 500 which were experiencing high vibration due to damage in the bearing housing were replaced with spare housings. Sodium pump seals are replaced whenever the oil leak past the seals is excessive. Bearings are replaced based on condition monitoring.

The main boiler feed water pumps were replaced by indigenous make, maintenance-friendly pumps due to obsolescence. The performance of the new pumps was found excellent and they were found very robust in withstanding transients.

The deaerator lift pumps were also replaced with pumps of new design as the balancing discs of existing pumps were found getting jammed due to shaft movement whenever selected on auto standby.

The valves provided in the inter seal argon supply to Control Rod Drive Mechanisms and Core thermocouples were diaphragm valves. The valve diaphragms were found getting deformed by repeated closing/opening operations and getting into the inlet/outlet port of the valve, thereby blocking the argon flow partially or fully. The absence of argon in the inter space also had a role in the failure

of CRDM bellows and seizure of gripper assemblies. The diaphragm valves were replaced with ball valves.

Service water pipelines in several areas have been replaced consequent on scaling or pinholes. The remaining pipelines were chemically descaled. At present, service water system chemistry is being maintained by proprietary chemicals and the system performance is satisfactory. Carbon Steel tube bundles in all process HX have been replaced with Cupro-nickel or admiralty brass to minimize corrosion / deposition problems.

Frequent start failures were observed in Emergency power diesel generators during surveillance tests. The DG sets were commissioned in 1982. On failure analysis, the reason for start failure was found to be due to malfunctioning of some of the pneumatic circuit components (ageing), Poor quality of starting air (presence of oil & moisture) hampering the operation of pneumatic components and obsolescence of the other components. As the starting circuit system is very critical for diesel generators, the existing obsolete system was replaced with an upgraded version sourced from original equipment manufacturer. An air drier was introduced in the starting air system to prevent moisture entry to the pneumatic components.

The 30 year old underground fire water system piping network made of CI was replaced with an above ground fully welded CS piping network as the old system was prone to leakages at the joints and frequent pipe line cracks due to corrosion. Also the existing negative suction fire water pumps were replaced with submersible pumps as their foot valves could not sustain the pressure of 6.5-7.5 kg/cm<sup>2</sup> which is to be maintained in the system as per the latest fire safety norms to prevent fatigue damage due to frequent pressurization & depressurization.

FBTR cooling tower which acts as the ultimate heat sink for the plant consists of 4 cells each having independent induced draft fans. The cooling tower is cross flow with splash type fill arrangement. Treated wood was used for fill material and drift eliminators. Due to poor ageing resistance of the wood, frequent replacement of fills involving large downtime was required. The decay of wood had resulted in choking and deposition in various heat exchangers, strainers and pipelines. The wooden fills were replaced with PVC fills of proprietary design. The wooden drift eliminators were changed with cellular PVC drift eliminators, reducing the drift losses. Performance testing of the cooling tower indicated a heat removal capability of 39MWt which is about 30% higher than earlier estimated capability of 30MWt with wooden fills.

The aged rubber lined piping of DM plant acid/alkali systems were replaced with Vinyl ester based FRP piping. The storage tanks for acid were also replaced. The expansion rubber bellows in condenser cooling water system which have a definite life are being replaced periodically.

The ventilation of Turbine building and steam generator building where ambient temperature was very high was augmented by providing high capacity supply fans and additional exhaust fans. The roof exhaust fans in all the buildings, which are usually difficult to approach for routine maintenance, have been taken out, serviced and reinstalled. The exhaust fans of service building and battery rooms were replaced. All the hoods, which got corroded, have been replaced.

The reactor containment building isolation dampers which required frequent maintenance were replaced with high performance butterfly dampers of failsafe design.

## **6. LIFE EXTENSION PLANS**

Even though the reactor has operated for 27 years, sufficient residual life is available for the irreplaceable components by virtue of operation at lower power and lower temperatures so far. The ultimate life of the reactor is governed by the neutron-induced embrittlement of the Grid Plate.

In order to conserve the residual life of the nuclear heat transport systems, the fatigue damage due to thermal shocks is minimized by suitable measures. Periodic assessment of creep-fatigue damage is

done from plant operating history. Most of the earlier reactor trips have occurred from the steam water system due to level fluctuations in the capacities of the contact type LP heaters. The trips due steam water system were significantly reduced by replacing LP heaters by non-contact type in 2004.

In the wake of the incident in a Japanese nuclear plant, periodical inspection of high pressure steam pipelines and lines handling wet steam is done looking for erosion/thinning. A surveillance programme is in place for pipeline condition monitoring.

As part of Plant life extension studies beyond 2025, tube bundles of one IHX will be removed and tube & tube sheets inspected for their condition. Tube surfaces will be studied for carburization. One pump will be dismantled and inspected for shaft straightness and condition of the impeller and hydrostatic bearings. When the SG reaches its design limit depressurization cycles, expansion bends on the steam side could be removed and assessed for residual life. If required, a SG module may be taken out and inspected.

In order to improve the performance, it is planned to replace the existing low-level amplifiers with isolation amplifiers which offer better CMRR in the instrumentation systems. Ward-Leonard drive systems for the sodium pumps will be replaced with latest drive system with additional equipment protection. The ageing LOR and SCRAM logic circuits are being considered for revamping as maintenance of these systems have become difficult due to obsolescence of components.

## **7. SEISMIC QUALIFICATION**

FBTR is designed based on the design of Rapsodie-Fortissimo in Cadarache, France. All nuclear systems are designed for high seismic levels of Cadarache. FBTR site is located in Zone 3 of moderate seismic activity. The Reactor vessel of Rapsodie was designed for a seismic level of 0.2g(H) & 0.4g(V). For FBTR, the Reactor containment building, steam generator building were designed for 0.1g(H) and 0.05g(V) and the other buildings were designed for 0.05g (H) and 0.025g(V).

Seismic reevaluation of FBTR was undertaken because of the revised seismic design criteria and high Design Basis Ground Motion (DBGM) found during geotechnical evaluation for Prototype Fast Breeder Reactor located at the same site. Re-evaluation activities started in the year 2007. The main objectives of seismic re-evaluation were Review the seismic capacity of safety related Structures, Systems & Components to achieve Safety functions such as Safe shutdown of reactor, Maintaining the plant in safe shutdown condition for prolonged period, Long term decay heat removal and Containment/Confinement of Radioactive inventory.

The Methodology followed for seismic reevaluation was Determination of peak ground acceleration that can be withstood without compromising plant safety, Review based on Review Basis Ground Motion (RBGM), Enhancement of seismic capacity of Safety related SSC, Criteria recommended by IAEA for seismic re-evaluation of plants, Derivation of Seismic Margin & Seismic core damage frequency, Preparation of Event trees & Fault trees from plant logic diagram and their usage for detailed safety analysis, Determination of Seismic capacity of components based on standardized methodology, Qualification of Civil structures & certain mechanical components by analysis, Qualification of Other components by experience based methodology & plant walk down, and Seismic qualification of Certain active components like relays, switches, dampers etc. by testing.

The seismic re-evaluation indicated the need for Seismic upgradation of FBTR with respect to civil structures & mechanical systems and Design review for systems of offsite power, primary pump drive and secondary pump drive. The Easy fixes identified based on plant walk down are being corrected. The battery banks were supported on seismically qualified anchored supports. It is planned to seismically retrofit the Cable trays, AC ducts and Unreinforced Masonry Walls.

## **8. FLOOD PROTECTION MEASURES**

Consequent to the Tsunami of 2004 at Kalpakkam coast, the design basis flood level of FBTR has been revised upwards. As an immediate measure post Tsunami, an Emergency Operating procedure has been kept in place to protect the plant & personnel. Also a Tsunami warning system is made available in Control room which gets input from USGS & EMSC. Reactor will be shutdown on confirmation of Tsunami from Tsunami warning centre, Hyderabad & Andamans.

The revision in the Design Basis Flood Level (DBFL) has called for additional flood protection measures since the present Finished Floor Level (FFL) of FBTR is not high enough for the revised DBFL. A new flood safe & seismically qualified building will be constructed to house the primary & secondary sodium pump drives, two seismically qualified diesel generator sets and an alternate emergency control room. In addition, adequate no. of electrical/Diesel powered dewatering pump sets will be strategically located at various plant locations for pumping out water from the buildings. All the external openings in the plant will be provided with ramps of suitable height to prevent entry of flood waters into the building.

## **9. CONCLUSION**

The unit cost of nuclear power is high compared to the cost of power generated from fossil fuels. The high cost is attributed to the high installation cost of a nuclear plant. In order to have an economical pricing, the nuclear plants have to be designed for longer lives or by extending the life by suitable requalification programme at the end of design life. Since FBTR has to play a major role in the testing of advanced fuels for the future high performance fast reactors, it has to operate well beyond 2025. Even though conventional systems have aged, the nuclear systems are relatively fresh. It is possible to extend the reactor life beyond 2025 by refurbishing and requalifying the aged components and by adopting suitable operational strategies to minimize the ageing of irreplaceable components, especially the grid plate. Simultaneously, the safety of the plant also can be upgraded to the current standards by adopting suitable measures.

# Restoration work for obstacle and upper core structure in reactor vessel of experimental fast reactor “Joyo” (2)

**M. TAKAMATSU, T. Ashida, T. KOBAYASHI, H. KAWAHARA,  
H. ITO, A. NAGAI**

Japan Atomic Energy Agency, Oarai, Japan

**Abstract.** In the experimental fast reactor Joyo, it was confirmed that the top of the irradiation test Sub-Assembly (S/A) of “MARICO-2” (material testing rig with temperature control) had bent onto the in-vessel storage rack (IVS) as an obstacle and had damaged the Upper Core Structure (UCS). This incident necessitates the replacement of the UCS and the retrieval of MARICO-2 S/A for Joyo re-start. Along with four stages involving jack-up and retrieval of the existing damaged UCS (ed-UCS), retrieval of the MARICO-2 S/A, and installation of the new UCS (n-UCS) in the restoration work plan, current conditions at Joyo are being carefully investigated, and the results are applied to the designs of special handling equipment, which is being manufactured and scheduled for operation in 2014.

## 1. Introduction

Since Joyo with a MK-I breeder core attained initial criticality in 1977 as the first sodium-cooled fast reactor in Japan, it has been upgraded several times and is now being operated as a high-performance irradiation test bed with a MK-III core<sup>[1]</sup>. During the 15th periodic inspection in 2007, in-vessel observation using techniques developed specifically for Joyo revealed that the top of the MARICO-2 S/A had bent onto the IVS as an obstacle and had damaged the UCS<sup>[2][3]</sup> (refer to Figure 1). This incident necessitates four-stage restoration work involving jack-up and retrieval of the ed-UCS, retrieval of the MARICO-2 S/A, and installation of the n-UCS for Joyo re-start. Because the replacement of the UCS was not expected in the original design and the bent MARICO-2 S/A cannot be retrieved with the existing handling equipment, specific design and development of new handling equipment are required while considering severe conditions such as (1) high radioactivity, (2) high temperatures and radiation doses, (3) primary sodium coolant retained in the Reactor Vessel (R/V), and (4) sodium deposition. This paper details the process leading to the restoration work plan, which involves jack-up and retrieval of ed-UCS, retrieval of MARICO-2 S/A, and installation of n-UCS, along with the development of equipment.

## 2. Plant description and current status of Joyo

The structure of the R/V, Rotating Plug (R/P), UCS, and MARICO-2 are shown in Figures 2 and 3. The following subsections describe the specifications and the current status to be considered in the design and development of the equipment.

### 2.1. Reactor vessel (R/V)

The R/V is approximately 10 m high with an internal diameter of approximately 3.6 m, which includes sub-assemblies and in-vessel structures (UCS, core support plate, IVS, etc.). Because the R/V is always filled with a sodium coolant to remove decay heat, the top of the R/V is covered with R/Ps to seal it completely. The sodium inlet and outlet piping are located on the lower and upper parts of the R/V, respectively. The surface level of sodium is usually maintained above the sodium outlet piping (GL-6500mm level) with an inert gas as a cover gas. The surface level of sodium can be changed by draining it during maintenance. The restoration work must be conducted without removing the fuel

S/A. During the restoration work, the level is maintained at 50 mm below the top of the fuel S/A. The temperature of sodium is approximately 200deg-C, and the temperature of the cover gas is approximately 140~160deg-C.

## **2.2. Rotating plugs(R/P)**

The R/Ps installed on top of the R/V consist of large and small R/P, approximately 4,730 and 2,870 mm in diameter. The center of the large R/P is aligned with the center of the R/V, whereas the center of the small R/P is 500 mm off-center. Access to the sub-assembly is controlled by rotating the large and small R/Ps. The UCS is installed on the small R/P. In addition, there are one center hole and ten other holes for the control rod on the UCS, in-vessel inspection hole (A) and fuel handling hole on the small R/P, and an in-vessel inspection hole (B) on the large R/P. The in-vessel observation was concluded using the existing holes. However, because the diameter of the existing holes is insufficient for the retrieval of the MARICO-2 S/A<sup>[2]</sup>, the retrieval is performed using the hole through which the ed-UCS is extracted.

## **2.3. Upper core structure (UCS)**

The UCS is installed on the small R/P. Six control rod drive mechanisms are installed through the holes on the UCS. The UCS contains cylindrical shield layers in the upper part and thermal striping prevention plates, flow-regulating grids, and thermocouple sleeves for S/A outlet temperature measurements are installed in the lower part. The diameters of the UCS top plate, upper part, middle part, and lower part are approximately 1,350, 1,130, 1,010, and 1,060 mm, respectively, and the UCS is approximately 6,330 mm high.

## **2.4. Irradiation test equipment “MARICO-2”**

MARICO-2 is on-line instrumented material irradiation equipment for testing the creep rupture strength of fuel cladding materials under the fast neutron irradiation environment. It is approximately 11 m high. There is a handling head at the top of the MARICO-2 S/A that connects with the MARICO-2 upper guide tube by latch fingers. The height of the MARICO-2 S/A is approximately 2.3 m. After the irradiation test, the S/A was expected to be disconnected and placed in the transfer pot on the IVS in order to transfer the S/A to a post-irradiation examination facility. The failure of disconnecting the S/A was found to be a cause of this incident. In addition, it was confirmed that the MARICO-2 S/A is stuck in the transfer pot owing to its deformation.

## **3. Outline of the restoration work plan**

The restoration work plan is outlined in Figure 4. The restoration work can be divided into the following four stages. A detailed description of each stage is provided below along with points to be considered while developing the equipment.

### **3.1. Jack-up of ed-UCS**

This is the first stage of the restoration work. A temporary pit cover, guide tube, and screw jack-up equipment, among other components are installed above the R/Ps. The primary objectives in this stage are to (1) shear the sodium bridges [deposited sodium in the gap between the ed-UCS and the Guide Sleeve (GS) of the small R/P] without deforming the GS owing to the consequent overload on the sodium bridges' shearing resistances (refer to Figure 5), and (2) jack-up the ed-UCS to 1000 mm through the small-diameter part of the GS, where the gap between the ed-UCS and GS is quite narrow (5 mm at the minimum), without deforming the bolts of the ed-UCS thermal shielding plate owing to the resistance caused by interference and contact between the ed-UCS and GS (refer to Figure 5).

### **3.2. Retrieval of ed-UCS**

A door valve, cask, and wire jack-up equipment, among other equipment are installed on the temporary pit cover and the guide tube. The ed-UCS is retrieved into the cask using wire jack-up equipment in this stage. Because the dose rate of the ed-UCS surface is quite high owing to the activation over 30 years of operation, one of the design requirements for the cask is to provide a dose rate of  $<2$  mSv/h on the cask surface according to previous results related to modifications to light water reactors. The other design requirement is to reduce the weight of the cask as much as possible in order to meet the maximum allowable weight capacity of the crane in the reactor containment vessel.

### **3.3. Retrieval of MARICO-2 S/A**

As mentioned above, the MARICO-2 S/A must be retrieved through the hole from which the ed-UCS is extracted. However, to avoid contact, the ed-UCS cannot be set just above the MARICO-2 S/A. Furthermore, because the driving mechanisms of the R/Ps are removed before the first stage (jack-up of ed-UCS), it is impossible to adjust the hole position above the MARICO-2 S/A. Therefore, an offset arm to reach the MARICO-2 S/A is required as part of the MARICO-2 S/A retrieval equipment.

### **3.4. Installation of n-UCS**

The procedure for installing the n-UCS is almost the same as the reversed procedure for retrieving the ed-UCS. The key issue is how to guide the n-UCS to the required position. The measure is currently under consideration.

## **4. Design and development of principal equipment**

Considering all points described in the previous section, further considerations and experiments have been performed to apply the results to the design of equipment.

### **4.1. Investigation of allowable load for ed-UCS jack-up and retrieval**

Figure 6 shows a schematic diagram of screw jack-up equipment as representative jack-up equipment. To prevent the deformation of the ed-UCS and GS, the allowable load is investigated as shown in Figure 7 using “Abaqus/Standard Version 6.7-1” with 3-D modeling to consider (1) wringing force, (2) sodium bridge shearing force, and (3) resistance caused by interference and contact between the ed-UCS and GS.

#### **(1) Wringing force**

The ed-UCS has been positioned on the small R/P in tight contact with its own weight (16.5 ton) for over 30 years. Assuming that the contacting surface of the ed-UCS has been vacuumed by this tight contact, the ed-UCS has been pushed against the small R/P by atmospheric pressure. This pushing force is defined as the wringing force. The wringing force is evaluated as approximately 3.37 ton.

Deformation at the point of force application (the contacting surface of the ed-UCS on the small R/P) is unlikely owing to its thick structure. However, in the case that the sodium bridge shearing is incomplete, there may be a risk of GS deformation due to the rapid release of the wringing force. Therefore, the jack-up speed is limited to below 2 mm/h to prevent permanently deforming the GS.

#### **(2) Sodium bridge shearing force**

To prevent deforming the GS by the sodium bridge shearing force, the allowable pulling force is evaluated as approximately 0.72 ton. Based on this evaluation, the maximum speed of screw jack-up is established to be 1 mm/s (sodium bridge shearing force at the maximum speed is estimated to be below approximately 0.53 ton).

#### **(3) Resistance caused by interference and contact between the ed-UCS and GS**

The evaluation results for the allowable pulling force concerning the resistance caused by interference and the contact between the ed-UCS and GS are 1.09 ton (pulling height: 444 to 842 mm) and 1.73 ton (pulling height: over 842 mm), respectively.

#### **4.2. Measure for inclination control**

With regard to the above resistance, a strict inclination control is required because of the narrow gap (min. 5 mm) between the ed-UCS and GS. Assuming a conservative 2.5 mm gap, the allowable inclination is estimated as 0.6925/1000 mm/mm. To achieve a strict control, the following two measures are implemented in the design of the jack-up equipment, as shown in Figure 6.

(1) Applying three-point suspension

Three screw or wire jacks are located uniformly in a concentric configuration. These jacks are synchronized in principle. In addition, these jacks can operate independently according to demand to precisely regulate the inclination.

(2) Inclination monitoring with level- and load-measuring devices

There are two level-measuring devices set at an appropriately relative position on a hanging plate and three load-measuring devices on the jack-up equipment. The inclination of the UCS is directly measured with the two level-measuring devices, and then, the load between the jacks is equalized with the three load-measuring devices.

#### **4.3. Visual monitoring equipment for UCS replacement**

To visually monitor the inclination and the gap between the ed-UCS and GS, special monitoring equipment has been developed. Figure 8 shows a schematic diagram of the monitoring equipment for the UCS fitting area as typical monitoring equipment. This equipment is installed into the R/V with two video scopes through an inspection hole (A) in order to provide a view of the UCS fitting area. Figure 8 also compares photographs of the actual UCS fitting area with video scopes and radiation-resistant fiberscopes. It is apparent that the video scopes provide better quality and clearer photographs than the fiberscopes. However, because a dim area still remains, an improvement in lighting strength is required to obtain high-quality photographs.

#### **4.4. Cask for ed-UCS retrieval**

The maximum dose rate on the ed-UCS surface is estimated to be approximately 54 Sv/h in the axial direction and 124 Sv/h in the horizontal direction as of October 1, 2012 on the basis of in-vessel dose rate measurement results<sup>[4]</sup>. Figure 9 shows the dose rate distribution on the ed-UCS surface and the result of the shielding design. Although a general cask has one or two kinds of thicknesses from a manufacturing viewpoint, this cask has four kinds of thicknesses in order to optimize cask design while avoiding an excessive safety margin. As shown in Figure 9, the dose rate on the cask surface proved to be below 1 mSv and met the requirement. In addition, separable wire jack-up equipment and door-valve are featured in this cask. It is advantageous for weight reduction, and the total weight of the cask including the ed-UCS is estimated to be 93.4 ton, which can be handled by the existing crane (maximum allowable weight capacity of crane in reactor containment vessel: 100 ton).

#### **4.5. MARICO-2 S/A retrieval equipment**

Figure 10 shows a schematic diagram of the retrieval equipment for MARICO-2 S/A. As mentioned above, this equipment needs an offset arm to reach the MARICO-2 S/A. Furthermore, as it is confirmed that the MARICO-2 S/A is stuck in the transfer pot on account of its deformation, this equipment is also required to retrieve the MARICO-2 S/A together with the transfer pot. To satisfy these requirements, a pantograph mechanism and a latch finger mechanism for MARICO-2 S/A retrieval equipment are currently being developed on the basis of remote control techniques demonstrated in the fuel handling machine. Figure 11 shows the results of an in-vessel test using a preliminary latch finger mechanism as an example of the developments. The in-vessel test results demonstrated that the preliminary latch finger can successfully be inserted into the transfer pot, and then, the transfer pot can be gripped and extracted together with the MARICO-2 S/A.

#### 4.6. Visual monitoring equipment for MARICO-2 S/A retrieval

To confirm the latch finger insertion and the transfer pot gripping shown in Figure 11, special monitoring equipment is also required for MARICO-2 S/A retrieval. This equipment is installed into the R/V with fiberscopes through an inspection hole (B) in order to provide a view of latch finger insertion and transfer pot gripping. Because the dose rate in this area is estimated to be approximately 300 Gy/h, the high-radiation-resistant fiberscope (allowable dose: 500,000 Gy) developed for Joyo<sup>[5]</sup> is employed according to past experience.

### 5. Conclusion

In this preparative work for the restoration of Joyo, a series of equipment needed for the restoration work on Joyo has been successfully designed and developed. The n-UCS and all necessary equipment are currently being manufactured. A full ex-vessel test is scheduled in 2013 to verify performance and establish the final work procedure, and then, the replacement of the UCS and the retrieval of the MARICO-2 S/A will be conducted in 2014.

The restoration work on Joyo will provide valuable experience and insight into further improvements and verification of repair techniques for sodium-cooled fast reactors. Ultimately, Joyo will play a key role not only in fast reactor cycle technology development but also a wide variety of science and technology fields including the fast neutron irradiation bed.

### Acronyms list

ed-UCS	existing damaged UCS
GS	guide sleeve
IVS	in-vessel storage rack
MARICO	<u>m</u> aterial testing <u>r</u> ig with temperature <u>c</u> ontrol
n-UCS	new UCS
R/P	rotating plug
R/V	reactor vessel
S/A	subassembly
UCS	upper core structure

### ACKNOWLEDGEMENTS

We would like to thank to Mitsubishi Heavy Industries Ltd. and Fuji Electric Co. Ltd. for their valuable assistance. We would also like to thank the members of the experimental fast reactor department of JAEA for their dedicated contributions.

### REFERENCES

- [1] T. Aoyama, T. Sekine, et al., "Core performance tests for the JOYO MK-III upgrade" Nuclear Engineering and Design 237, pp.353-368 (2007).
- [2] T. Sekine, T. Ashida, et al., "Restoration work for obstacle and upper core structure in reactor vessel of experimental fast reactor Joyo" Proceedings of International Conference on Fast Reactors and Related Fuel Cycles (FR09), December 7-11, 2009, Kyoto, Japan
- [3] M. Takamatsu, K. Imaizumi, et al., "Development of observation techniques in reactor vessel of experimental fast reactor Joyo" Proceedings of the 17th International Conference on Nuclear Engineering (ICONE17), July 12-16, 2009, Brussels, Belgium
- [4] S. Maeda, H. Naito, et al., "Measurement and Analysis of In-vessel Component Activation and Gamma Dose Rate Distribution in Joyo" Progress in Nuclear Science and Technology, 1 pp.182-185 (2011)
- [5] H. Naito, W. Itagaki et al., "Inspection and Repair Techniques in the Reactor vessel of the Experimental Fast Reactor Joyo-Development of a High Radiation Resistant Fiberscope -" JAEA-Technology 2012-009 (2012)

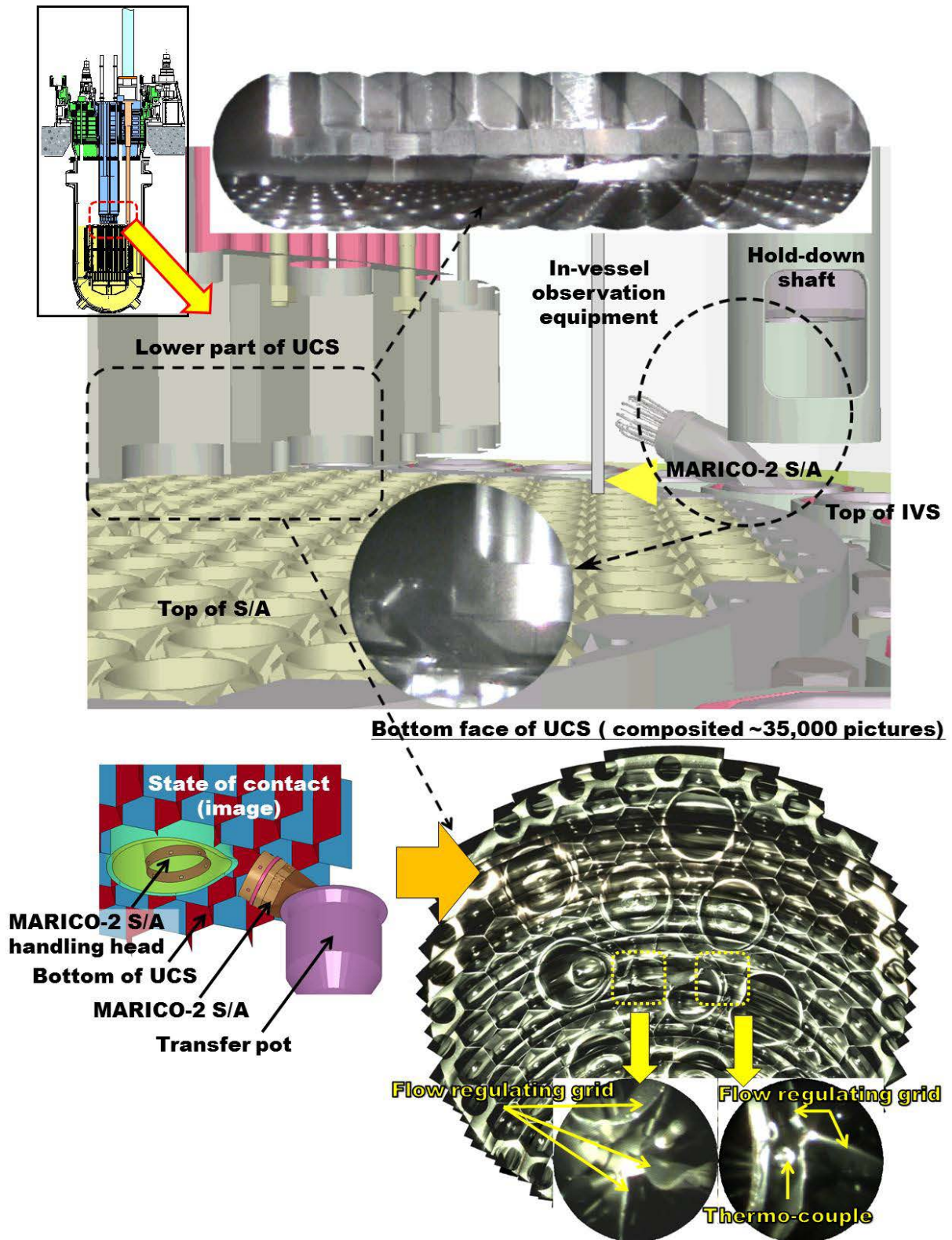


FIG. 1. Observation results for UCS and MARICO-2 S/A

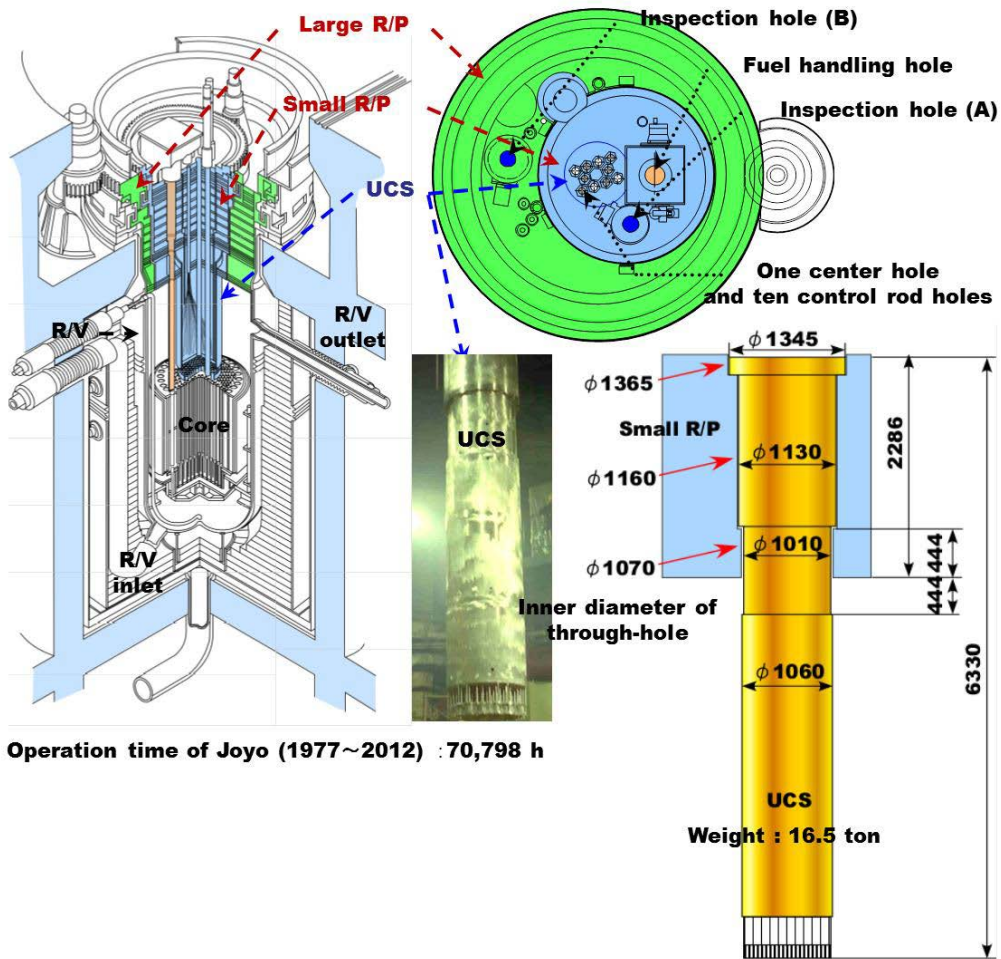


FIG. 2. Structure of R/V, R/P, and UCS

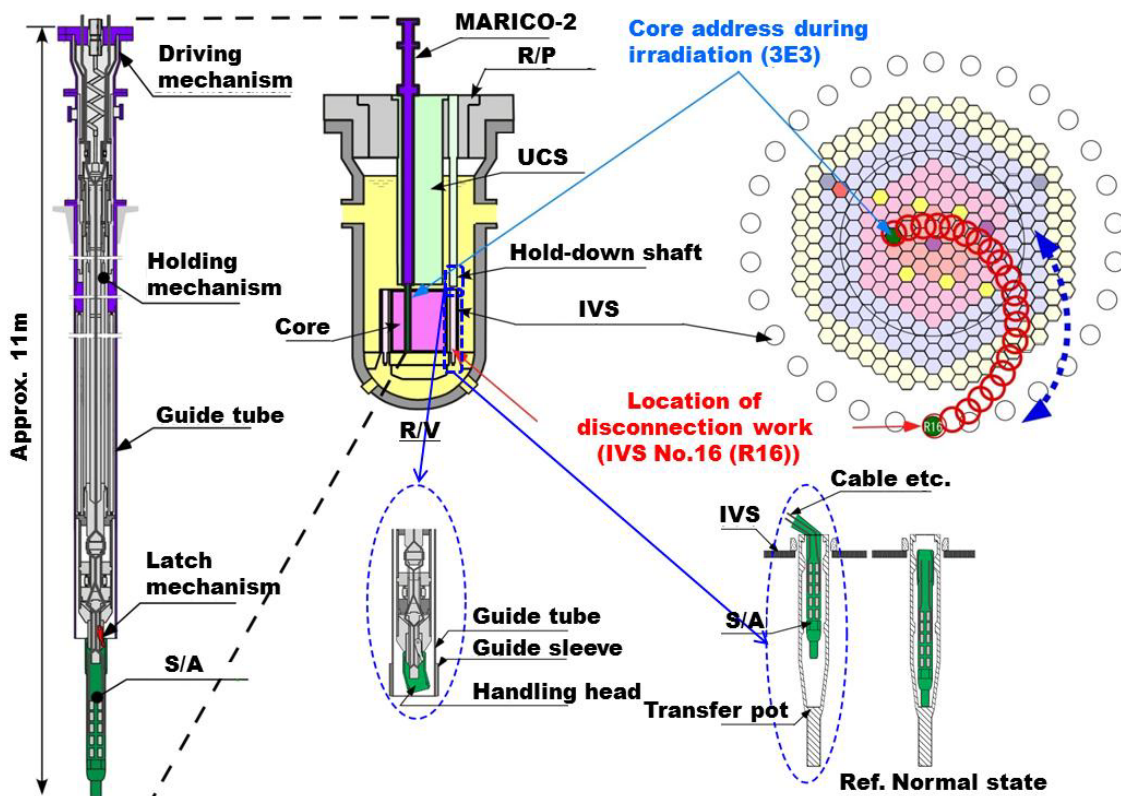


FIG. 3. Structure of MARICO-2

- (1) Jack up ed-UCS to 1000mm using screw jack-up equipment.
- (2) Retrieve ed-UCS into cask using wire jack-up equipment.
- (3) Retrieve MARICO-2 S/A through the hole from which ed-UCS is extracted.
- (4) Install n-UCS.

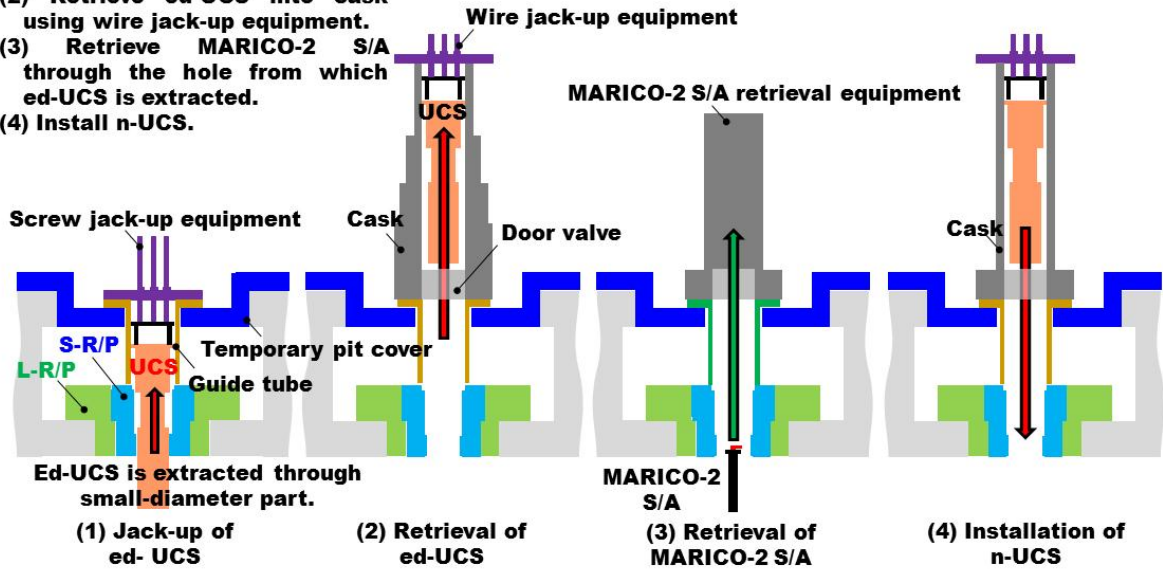


FIG. 4. Outline of restoration work plan

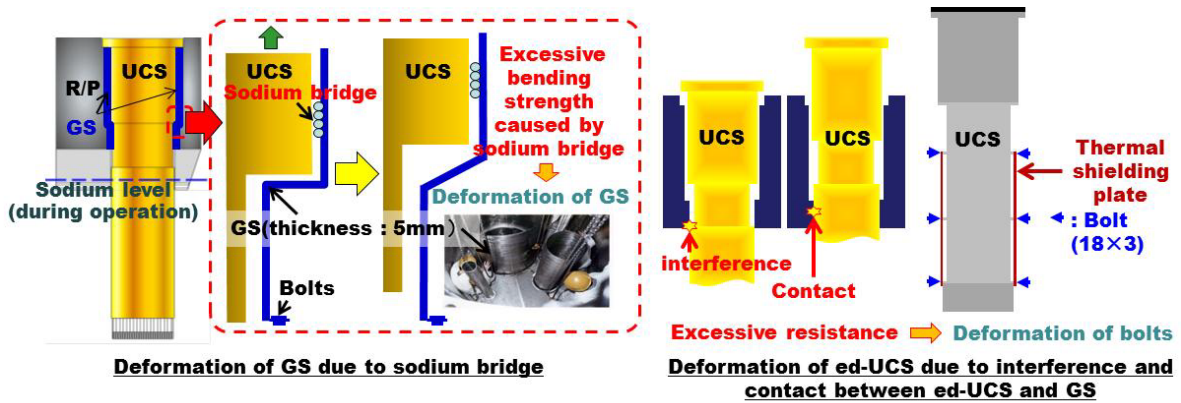


FIG. 5. Risks of deformation during ed-UCS jack-up

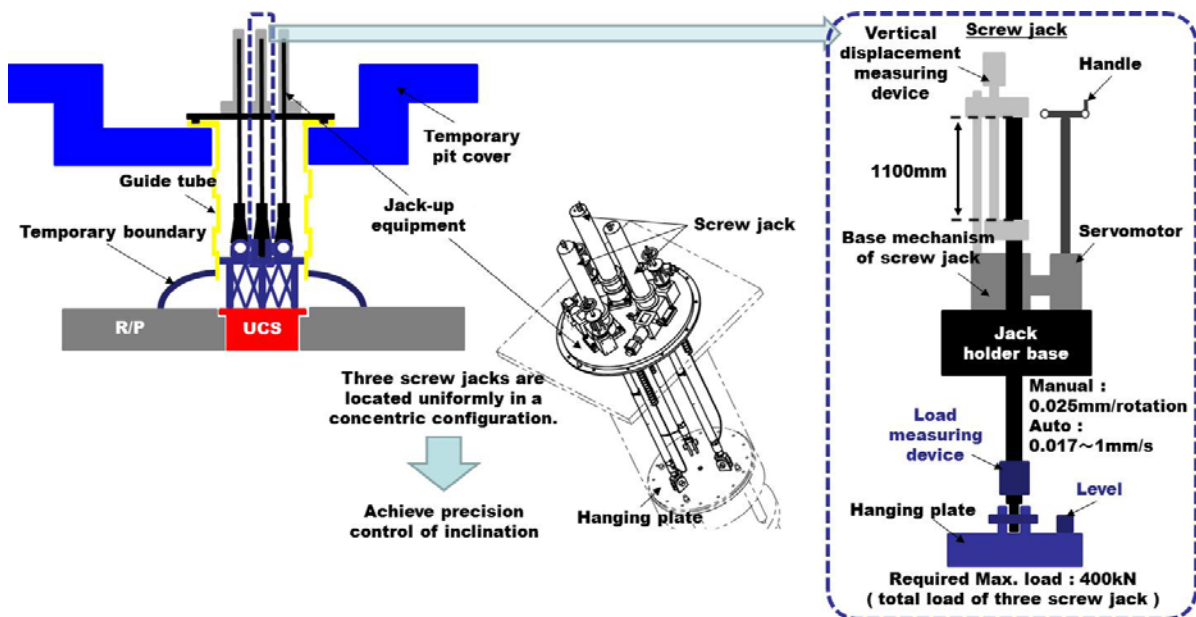


FIG. 6. Schematic diagram of screw jack-up equipment

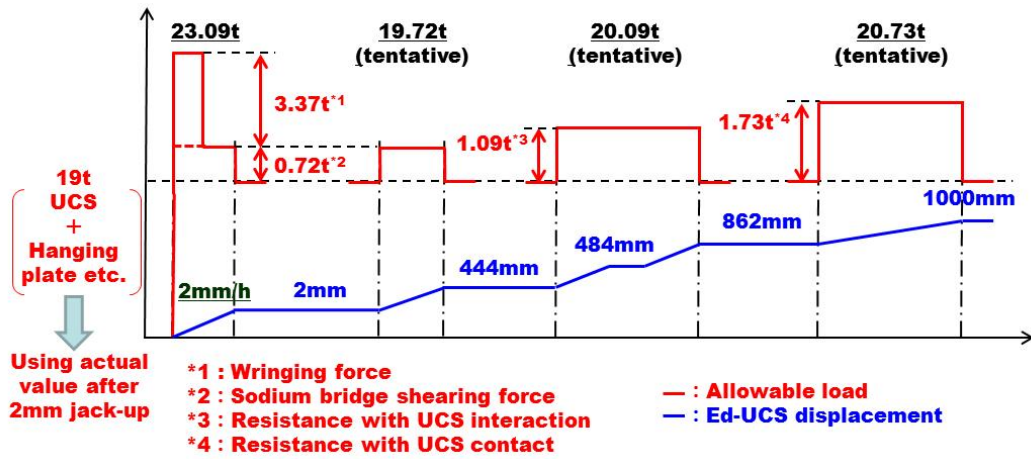


FIG. 7. Allowable load during ed-UCS jack-up

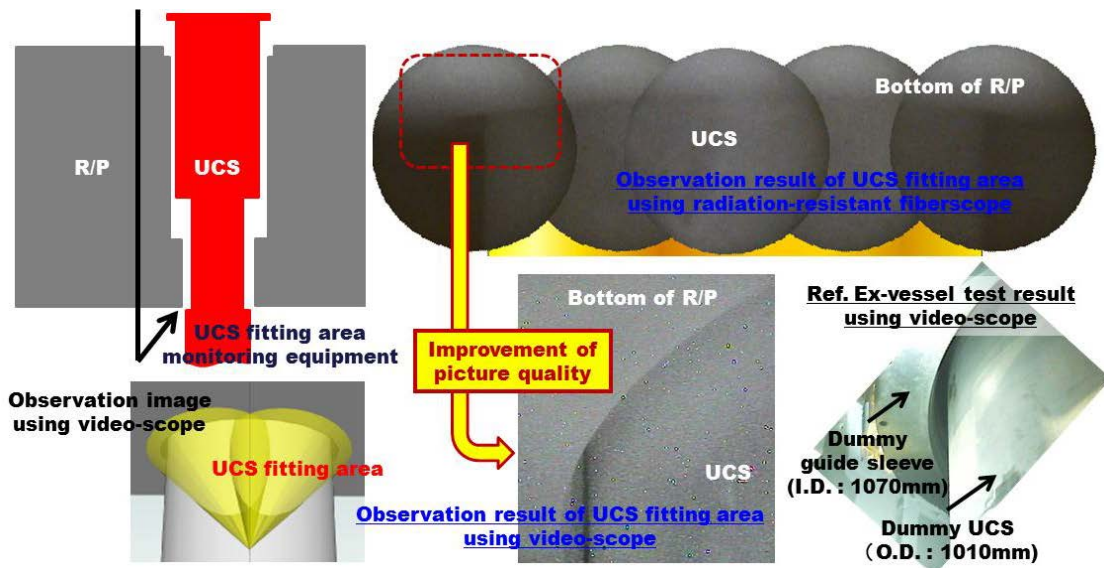


FIG. 8. Schematic diagram of monitoring equipment for UCS fitting area

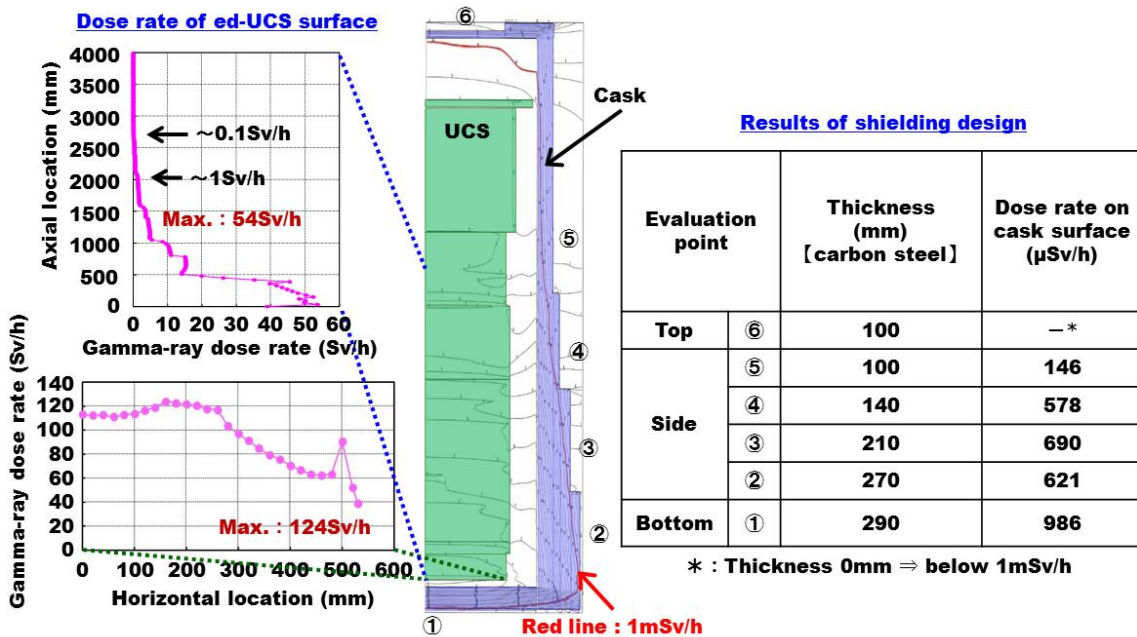


FIG. 9. Dose rate distribution on the ed-UCS surface and shielding design results

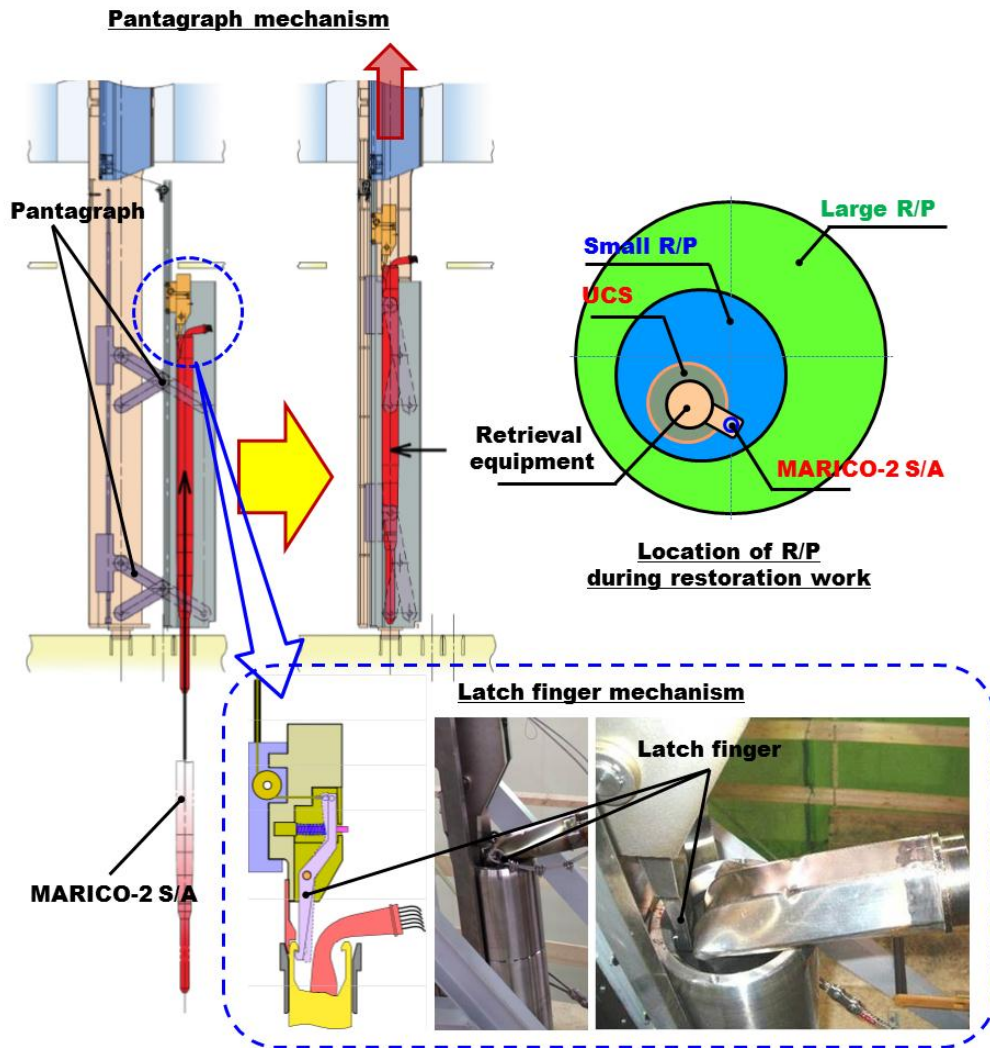


FIG. 10. Schematic diagram of MARICO-2 S/A retrieval equipment

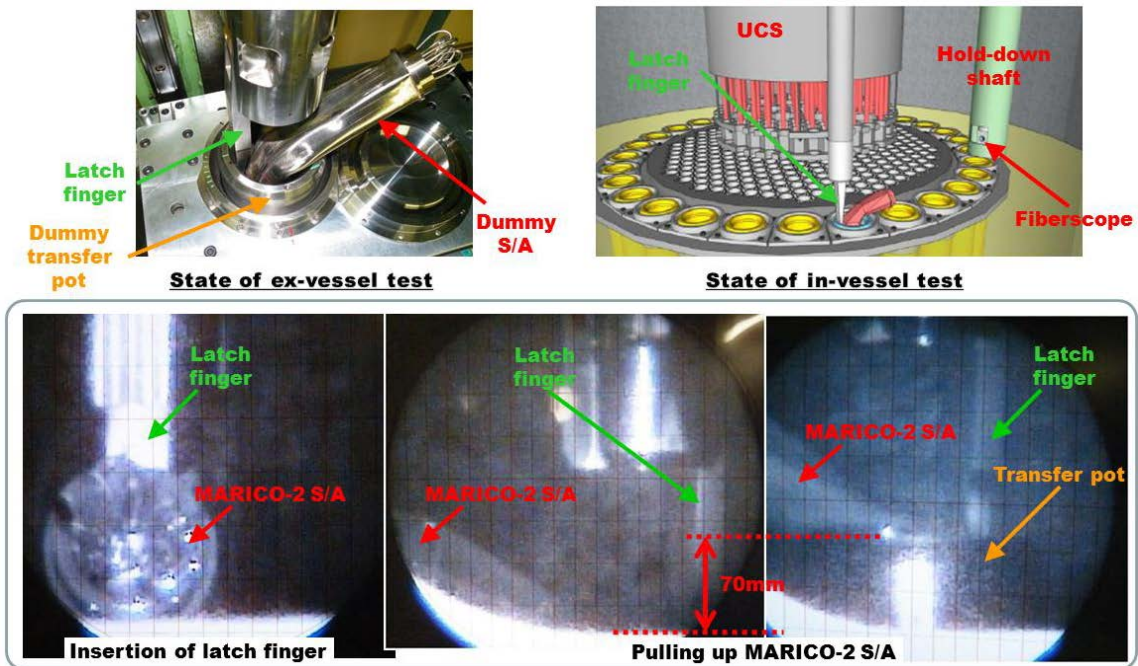


FIG. 11. In-vessel test using preliminary latch finger mechanism

# Evaluation of Feedback Reactivity in Monju Start-Up Test

A. Kitano, T. Miyagawa<sup>a</sup>, Y. Ohkawachi, T. Hazama

Japan Atomic Energy Agency

*Presented by Error! Unknown document property name.*

**Abstract.** The feedback reactivity measurement was conducted in Monju Start-up test in 2010. The total feedback reactivity was evaluated together with its two reactivity components related either to power or to the core inlet coolant temperature. The corresponding calculated values were evaluated by simulating temperature distribution in the core under experimental conditions of the power and the inlet coolant temperature. The calculated and measured values of the feedback reactivity showed a reasonable agreement.

## 1. Introduction

The feedback reactivity due to power increase is a key parameter in the safety of reactor operation. Its design accuracy can be validated with the total feedback effect measured during reactor operation; however, if an error exists, the reason is difficult to identify since the feedback effect consists of various effects, such as the Doppler effect and expansion effect of core structures. Thermal property data used in the calculation also causes an error. An attempt to separate the feedback reactivity into three components due to power, the average coolant temperature, and the grid plate temperature is reported [1]. The results are physically reasonable but measurement uncertainty of each component is more than 10%.

In this paper, a new method is presented to measure the feedback reactivity. The total feedback reactivity is evaluated together with its two reactivity components related to the power and the isothermal temperature. The power component is associated mainly with temperature change in fuel pellets. The isothermal component is with subsequent change in the core inlet temperature. The reactivity is evaluated in the self-stability test performed at zero power level in the Japanese prototype fast reactor Monju. In the test, the self-stability is demonstrated for a positive reactivity insertion at critical. The reactor power first increases, then decreases by the feedback reactivity effect, and finally becomes stable. At zero power, the phenomena proceeds much slower than those observed at high power due to small feedback effect; thus the behavior can be more easily followed.

The corresponding calculated values are evaluated by simulating temperature distribution in the core under experimental conditions of the power and the inlet coolant temperature. It is confirmed that the calculated and measured values show good agreement.

## 2. Feedback reactivity measurement in Monju start-up test

### 2.1. Brief description of Monju start-up test

The core configuration of Monju is shown in *FIG.1*. The core consists of inner and outer core regions surrounded by radial blanket and shielding. The control rods are classified into Fine Control Rod (FCR), Coarse Control Rod (CCR) and Back-up Control Rod (BCR). The neutron detectors located outside of the reactor vessel are classified into Source Range Monitor (SRM), Wide Range Monitor (WRM) and Power Range Monitor (PRM). WRM signal is used in the feedback reactivity experiment.

---

<sup>a</sup> Present affiliation: The Japan Atomic Power Company, Tokyo, Japan

Monju has restarted its operation after about 14 year suspension since the sodium leakage accident. The System start-up test (SST) has been also restarted and reactor physics tests were carried out in the restart core [2][3][4].

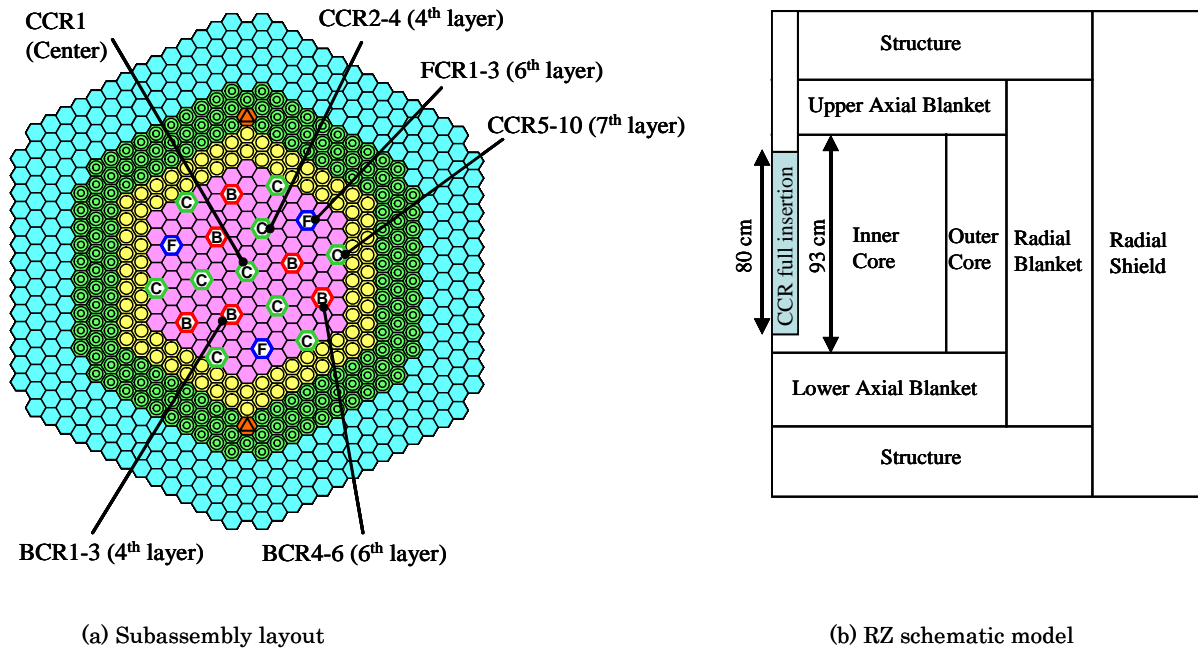


FIG. 1. Monju core configuration.

## 2.2. Feedback reactivity experiment

The feedback reactivity experiment was conducted in the SST in June, 2010. The original purpose is to demonstrate the self-stability feature after a reactivity insertion at zero power level. FIG.2 shows the plant condition during the experiment. The reactor is operated at around 200°C with the primary coolant flow rate 49% of the rated value. The secondary loop is in operation with the coolant flow rate 7% of the rated value. The air cooler, which is the main heat removal system during the experiment, is effective without active air ventilation.

The experiment was carried out in the following procedure: First, the initial condition was confirmed for the reactor power (WRM count rate) and the reactor vessel (R/V) inlet coolant temperature at a critical state with the central control rod withdrawn by 400 mm and the other control rods fully withdrawn. Then a positive reactivity was inserted by a withdrawal of the central control rod. The power and the coolant temperature were monitored till the parameters became stable. This procedure was repeated for three cases with reactivity insertions of  $+2\phi$ ,  $+4\phi$  and  $+6\phi$ .

The time history of the power and the coolant temperature is shown in FIG.3. The timing of the reactivity insertion is adjusted to 18 minutes in all the cases. The reactivity insertion takes six seconds for the  $+6\phi$  case. After the reactivity insertion, the reactor power sharply increases to the peak, then decreases to the minimal value, and finally becomes stable. The coolant temperature follows the same trend with time delay and smaller variation. From the result, we can confirm the reactor has the self-stability feature.

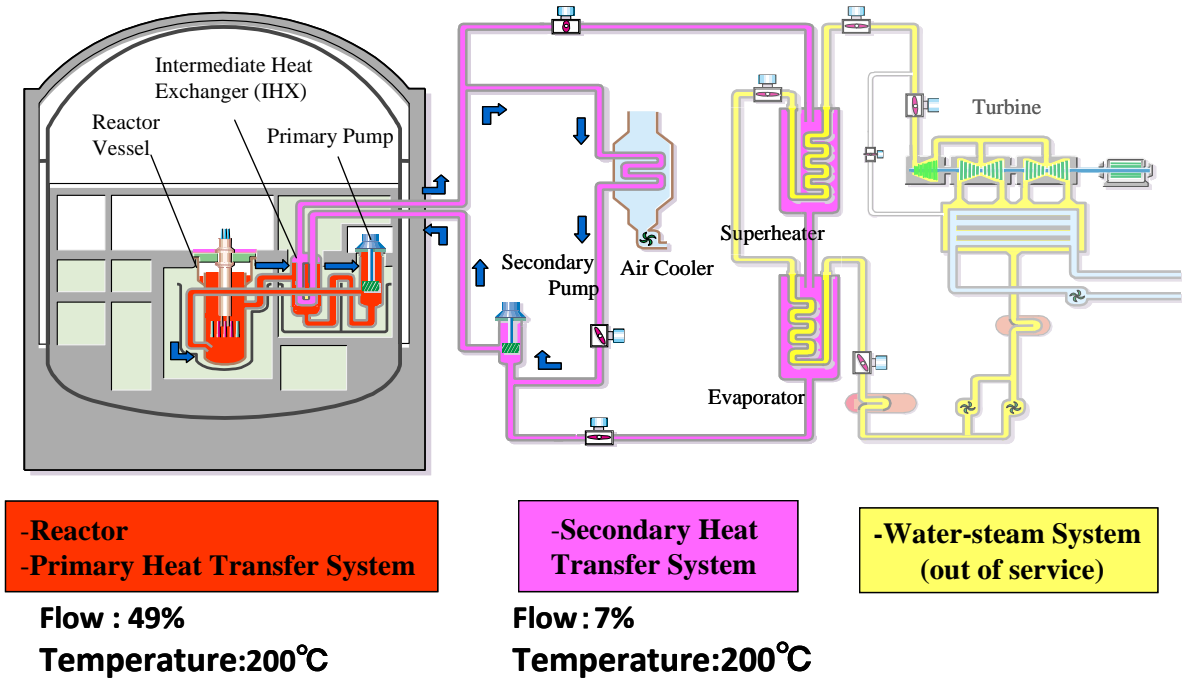


FIG. 2. Plant condition in the feedback experiment

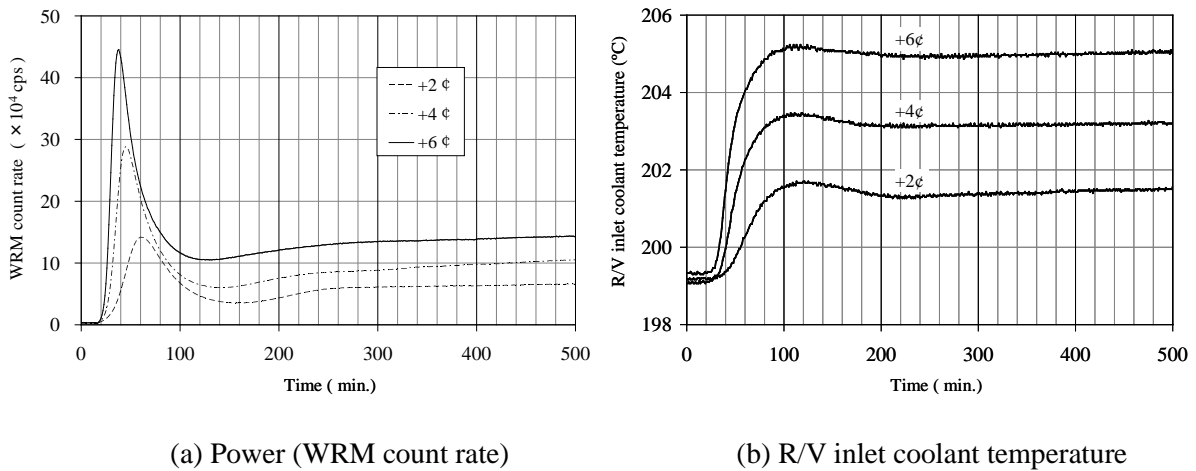


FIG. 3. History of power and R/V inlet coolant temperature

### 3. Evaluation of feedback reactivity

The feedback reactivity can be expressed by

$$\rho_{feedback} = k_D \ln\left(\frac{T_F}{T_0}\right) + k_F \Delta T_F + k_C \Delta T_{in} + (k_{Na} + k_S) \Delta T_m \quad (1)$$

$k_D$  : Fuel Doppler coefficient  $T(\Delta k/\Delta T)$

$k_C$  : Core support plate temperature coefficient ( $\Delta k/k/^\circ C$ )

$k_F$  : Fuel temperature coefficient ( $\Delta k/k/^\circ C$ )

$k_{Na}$  : Coolant temperature coefficient ( $\Delta k/k/^\circ C$ )

$k_S$  : Structure temperature coefficient ( $\Delta k/k/^\circ C$ )

$T_F$  : Fuel temperature ( $^\circ C$ )

$T_{in}$  : R/V inlet coolant temperature ( $^\circ C$ )

$T_m$  : Coolant temperature in the core ( $^\circ C$ )

$T_0$  : Initial core (coolant) temperature ( $^\circ C$ )

$\Delta T$  : Change from  $T_0$  ( $^\circ C$ ).

In the small reactivity range observed in the experiment (about  $2.0 \times 10^{-4} \Delta k/k$  at the maximum), the Doppler reactivity, the first term of Eq. (1), can be a linear function of the fuel temperature. It is also assumed that thermal properties, such as conductivity and gap conductance are constant over the small temperature range in the experiment; thus, the following relation is satisfied:

$$\Delta T_F = \Delta T_m + a \Delta n_{WRM} , \quad (2)$$

$$\Delta T_m = \Delta T_{in} + b \Delta n_{WRM} . \quad (3)$$

$\Delta n_{WRM}$  : Change of WRM count rate from initial value (cps)

a, b : Constant.

Then the feedback reactivity becomes a function of the two variables as

$$\rho_{feedback} = K_R \Delta n_{WRM} + K_{in} \Delta T_{in} \quad (4)$$

$K_R$  : Reactivity coefficient on the WRM count rate ( $\Delta k/k/cps$ )

$K_{in}$  : Reactivity coefficient on the R/V inlet temperature ( $\Delta k/k/^\circ C$ ).

$K_R$  is related to the power coefficient and  $K_{in}$  is equivalent to the isothermal temperature coefficient.

At the peak and the minimum point (or bottom) of the power history, the reactivity becomes zero. The inserted positive reactivity is balanced by the negative feedback reactivity. In the experiment, we have six data of various

combinations of  $\rho_{feedback}$ ,  $\Delta n_{WRM}$ , and  $\Delta T_{in}$  as summarized in Table 1. The value of  $\rho_{feedback}$ , or inserted positive reactivity, was evaluated by the asymptotic period method with  $n_{WRM}$  data after the reactivity insertion.

Table 1. Measured data at the power peak and power bottom

Case	$\rho_{feedback}$ (% $\Delta k/k$ )	$\Delta n_{WRM}$ (cps)	$\Delta T_{in}$ ( $^{\circ}C$ )
+2 $\phi$ , power bottom	$7.496 \times 10^{-3}$	32106	2.34
+4 $\phi$ , power bottom	$1.386 \times 10^{-2}$	57546	4.25
+6 $\phi$ , power bottom	$1.959 \times 10^{-2}$	102286	5.84
+2 $\phi$ , power peak	$7.496 \times 10^{-3}$	138781	1.07
+4 $\phi$ , power peak	$1.386 \times 10^{-2}$	285819	1.55
+6 $\phi$ , power peak	$1.959 \times 10^{-2}$	442343	2.00

We can evaluate the two parameters by fitting the data to Eq. (4). The parameters are obtained as  $K_R = -3.2 \times 10^{-10}$   $\Delta k/k/cps$  and  $K_{in} = -2.8 \times 10^{-5}$   $\Delta k/k/^{\circ}C$ . FIG.4 shows dispersion of measured data for the fitted line obtained with the parameters substituted in Eq. (4). Good fitting accuracy is confirmed in both parameters.

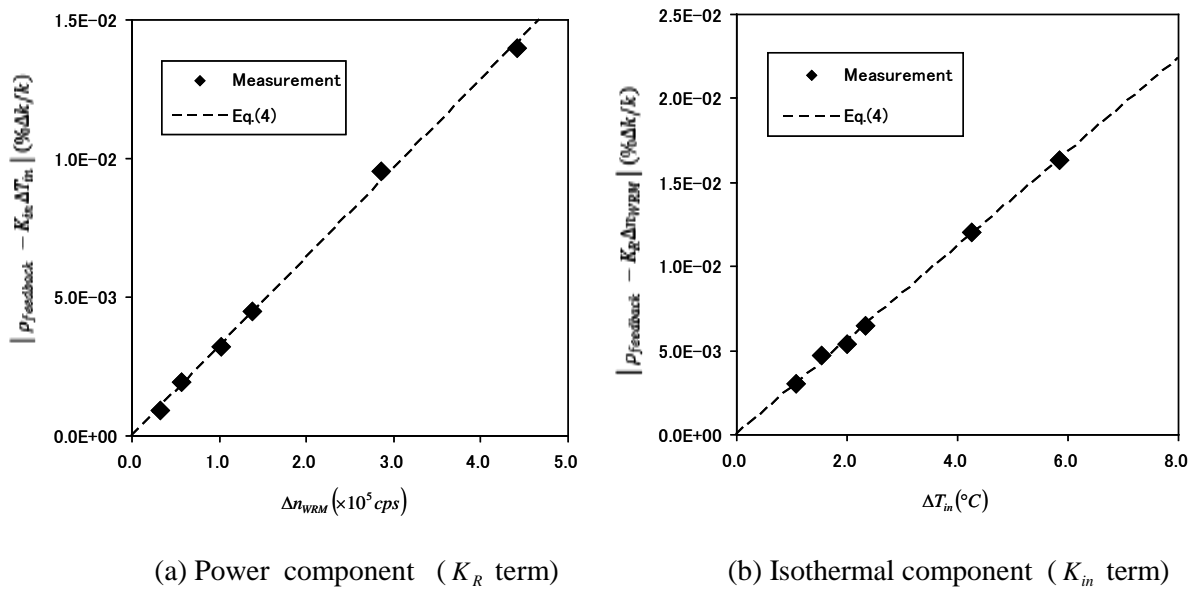


FIG. 4. Accuracy of fitting procedure

## 4. Calculation of feedback reactivity

### 4.1. Calculation method

The calculation method is based on a deterministic calculation scheme depicted in FIG.5. The effective cross section is calculated from a 70-energy-group constant set based on JENDL-3.3 with SLAROM-UF [5]. The core calculation is made in the three-dimensional Tri-Z model with DIF3D [6].

The feedback reactivity is calculated based on Eq. (1) for regions: three regions of the inner core, the outer core, and the radial blanket. The core fuel region is further divided into six regions in the axial direction.

The Doppler and temperature coefficients are calculated by the first order perturbation theory with forward and adjoint flux of the initial critical condition. The Doppler coefficient is calculated by increasing the cross section temperature by 10°C. The temperature coefficients are calculated from the density coefficient and the geometry coefficient. The Doppler effect is taken into account in the calculation of the temperature coefficients for the structure and coolant as well.

The average temperature in each region is calculated for the experimental conditions of  $T_{in}$  and power converted from  $n_{WRM}$  in Table 1. Temperature distribution in each subassembly is calculated by the subchannel code COBRA4-MJ and the distribution is averaged by volume to obtain the temperature of each material in Eq. (1). The effective temperature due to the crystalline binding effect [7] is considered in the Doppler effect in fuel.

Then the feedback reactivity is evaluated for the regions from the Doppler coefficient, the temperature coefficients, and the average temperature.

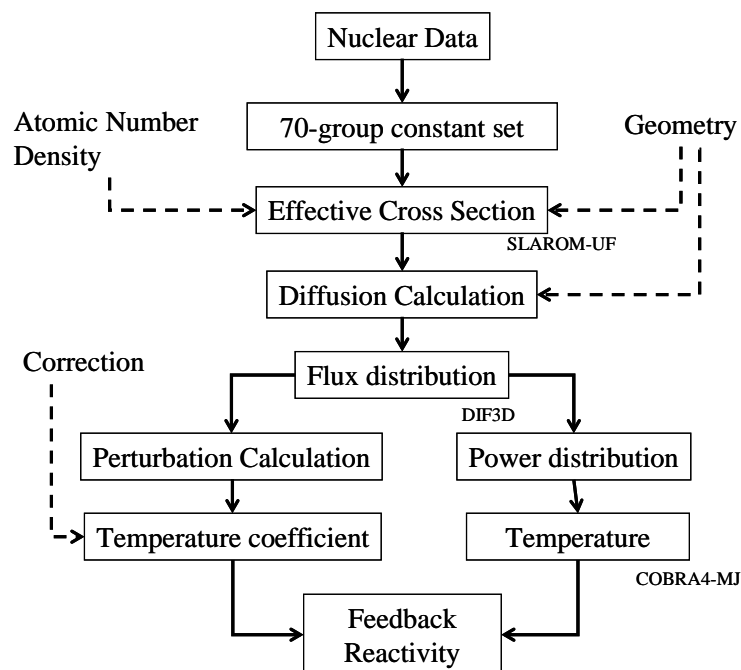


FIG. 5. Calculation flow of feedback reactivity

## 4.2. Comparison with measurement

FIG.6 compares the measured and calculated values of the feedback reactivity. Good agreement is confirmed in general. When closely examined, the values for the power bottom show slightly larger discrepancy of 6% than that for the power peak of 3%.

Calculated values of the two parameters  $K_R$  and  $K_{in}$  are evaluated from the corresponding reactivity divided by either  $\Delta n_{WRM}$  or  $\Delta T_{in}$ . They are obtained as  $K_R = -3.0 \times 10^{-10} \Delta k/k/cps$  and  $K_{in} = -3.1 \times 10^{-5} \Delta k/k/^\circ C$ . The corresponding C/E values are 0.92 for  $K_R$  and 1.09 for  $K_{in}$ . The calculated parameters are almost the same in all the experiment cases, which supports the validity of the simple representation of the feedback reactivity in Eq. (4).

The error in  $K_R$  and  $K_{in}$  is propagated to the feedback reactivity through their contribution shown in FIG.7. We can see that the error in the reactivity for the power bottom is dominantly determined by that in  $K_{in}$ . The error in the reactivity for the power peak is smaller due to cancellation of the errors in  $K_R$  and  $K_{in}$ . FIG.8 shows the axial temperature distribution in the inner core region, which explains the difference in the contribution of  $K_R$  and  $K_{in}$  terms.

The overestimation in the calculated  $K_{in}$  is consistent with those reported in the isothermal temperature reactivity evaluation [4], where presence of a bias is suspected in the measured value.

The error in  $K_R$  would be in the accuracy of WRM-power conversion factor. In this study, the value is determined from heat balance in the air cooling system, where the temperature change in the system is small ( $\sim 6^\circ C$ ). The conversion factor should be examined more carefully together with uncertainty.

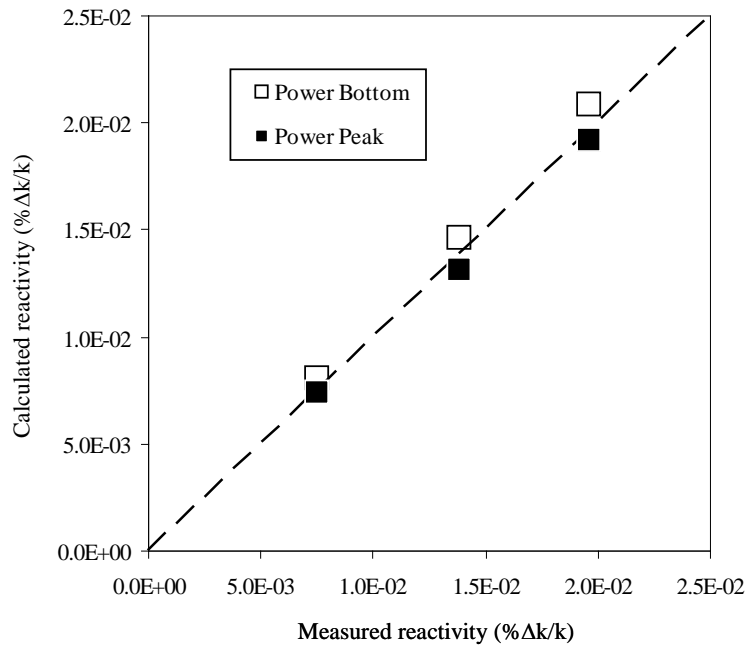


FIG. 6. Comparison of measured and calculated feedback reactivity

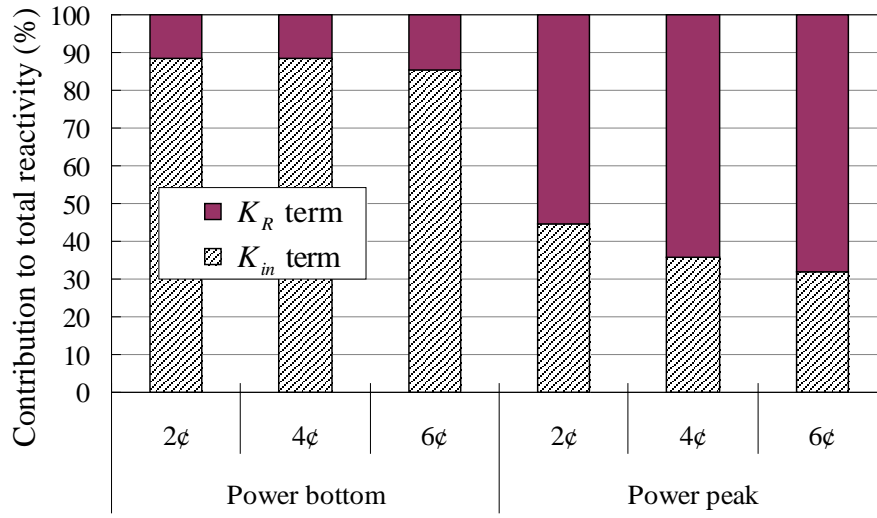
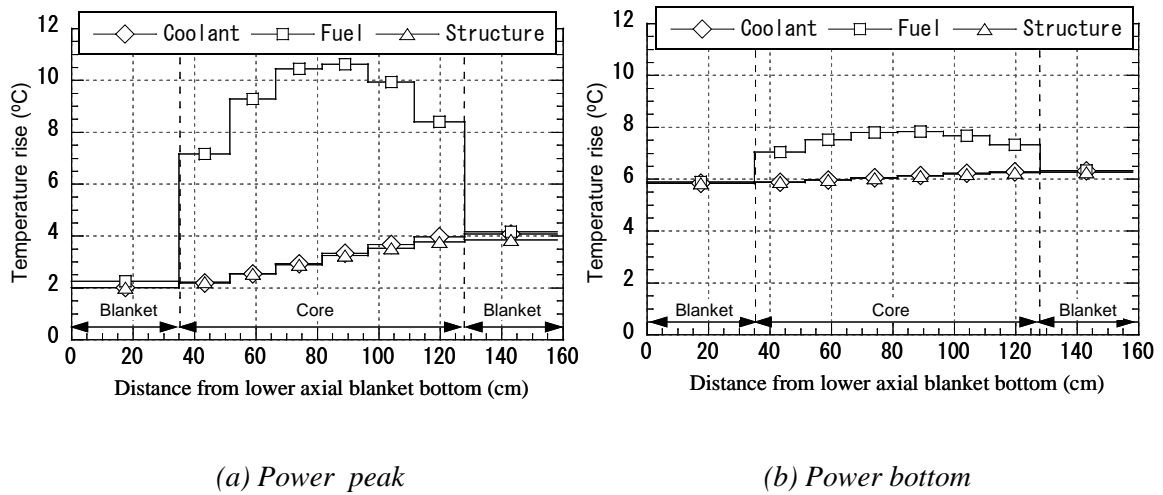


FIG. 7. Contribution of  $K_R$  and  $K_{in}$  terms to total feedback reactivity



(a) Power peak

(b) Power bottom

FIG. 8. Axial temperature distribution in the inner core region ( $6c$  insertion case)

## 5. Conclusion

The self-stability feature of the reactor was demonstrated in Monju. It was confirmed that after a reactivity insertion, the reactor became stable without a control rod operation. The two reactivity parameters that determines the feedback reactivity were evaluated through a fitting procedure of measured data as

$$K_R = -3.2 \times 10^{-10} \Delta k/k/cps$$

$$K_{in} = -2.8 \times 10^{-5} \Delta k/k/^\circ C.$$

Calculation accuracy was evaluated for the feedback reactivity and the two parameters. The accuracy for the feedback reactivity is reasonable with the largest error of 6%. That for the two parameters has larger error of about 10%. The reason of the error need to be further examined in the measured and calculated values.

## ACKNOWLEDGEMENTS

We would like to thank all the staff in Monju and Fuel fabrication sections. We are also indebted to A. Takegoshi for the calculation work.

## REFERENCES

- [1] M. Vanier et al., "SuperPhenix Reactivity and Feedback Coefficients," *Nucl. Sci. Eng.*, **106**, 30 (1990).
- [2] T. HAZAMA, A. KITANO and Y. KISHIMOTO, "Criticality Evaluation for the Monju Restart Core," *Nucl. Technol.*, **179**, 250 (2012).
- [3] K. TAKANO, M. FUKUSHIMA, T. HAZAMA and T. SUZUKI, "Control Rod Worth Evaluation for the Monju restart Core," *Nucl. Technol.*, **179**, 266 (2012).
- [4] T. MOURI, S. MARUYAMA, T. HAZAMA and T. SUZUKI, "Isothermal Temperature Coefficient Evaluation for the Monju Restart Core," *Nucl. Technol.*, **179**, 286 (2012).
- [5] T. Hazama, G.Chiba, et al., "Development of a Fine and Ultra-Fine Group Cell Calculation Code SLAROM-UF for Fast Reactor Analyses", *J. Nucl. Sci. Technol.*, **43**, 8, 908 (2006).
- [6] "DIF3D 7.0: Code System for Solving Finite Difference Diffusion Theory Problems", RSIC, CCC-649(1997).
- [7] A. T. D. BUTLAND, "A Note on Crystalline Binding in Uranium Dioxide and Its Effect on the Doppler Broadening of Uranium Resonances," *Ann. Nucl. Sci. Eng.*, **1**, 575 (1974).

## **Evaluation on coolability of the reactor core in Monju by natural circulation under earthquake and subsequent tsunami event**

**F.Yamada, Y.Fukano, H.Nishi, M.Konomura**

Japan Atomic Energy Agency (JAEA)

1 Shiraki, Tsuruga-shi, Fukui-ken, 919-1279 Japan

**Abstract.** The core cooling capability by natural circulations at a station black-out event, induced by an earthquake and a subsequent tsunami attack, has been evaluated in detail, referring to the accident of the Fukushima Dai-ichi Nuclear Power Station of Tokyo Electric Power Company (F1). The plant dynamics computer code: Super-COPD [1] has been used for the evaluation, which has been verified by the analyses of the preliminary test results on the natural circulation in Monju [2]. As a result it was concluded that the natural circulations of the coolant sodium will enable the decay heat removal of the core as far as the sodium coolant flow circuits are intact and secured.

### **1. Introduction**

The decay heat of the core in Monju should be safely removed after the reactor shut-down by the insertion of the control rods at an earthquake. Therefore the coolant in the heat transport systems (HTSs) is forced to be circulated by rotating the circulation pumps. The power to these pumps will be supplied by an alternating-current (AC) fed by the emergency diesel generators even at a loss of off-site power supply. Then the decay heat of the core can be safely released to the atmosphere by switching the heat sink from the steam generators to the air coolers.

However it can be imagined to lose all the AC power supply (Station Black-Out: SBO) at a beyond-the-design-basis huge tsunami attack. Such a tsunami will destroy the sea-water pumps of the component cooling water system and will result in a diesel generator shut-down. Therefore the Monju plant is designed to be able to cool down the core by the natural circulations induced by the temperature difference of the coolant without the forced convection by the circulation pumps. Around the 24m-difference in height between the core and the air coolers enables this natural circulation. Moreover the equipment, which enables natural circulations, is located high over 21m above sea level (*See FIG. 1.*).

The core cooling capability by natural circulations at a SBO has been investigated in detail based on these design considerations. A SBO event can be induced by an earthquake and a subsequent huge tsunami attack, referring to the F1 accident. Super-COPD has been used for the investigation, which has been verified by the analyses of the preliminary test results on the natural circulation in Monju [3].

### **2. Basic sequence of events**

A basic sequence of events after an earthquake and a subsequent tsunami has been assumed as shown below (*See FIG. 2.*)[4]. The decay heat removal capability by the natural circulations has been evaluated by Super-COPD, simulating this sequence of events.

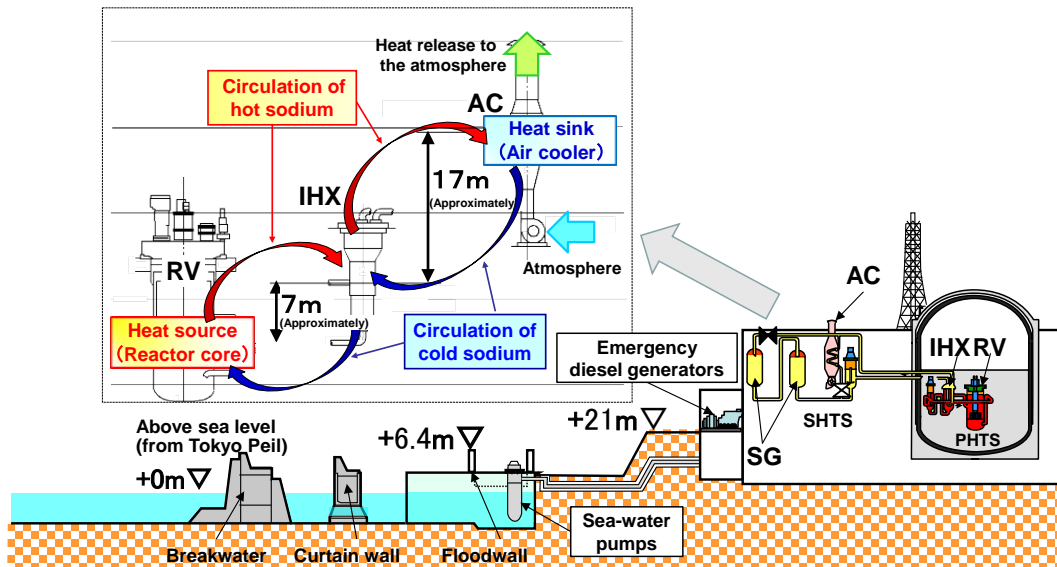


FIG. 1. Schematic view of difference in height and natural circulation in Monju plant

It has been assumed in the basic sequence of events that an earthquake occurred just after starting the commercially-based full power operation. A simultaneous loss of off-site power supply has also been assumed. A subsequent beyond-the-design-basis huge tsunami attack has been assumed after 13 minutes. This tsunami would lead the plant to a SBO event. The main circulation-pump motors and air cooler blowers have been assumed to be disabled by the occurrence of a SBO. Then the heat transport systems (HTSs) have been assumed to be transitioned into a natural circulation mode. The natural circulations would be controlled by the outlet temperature control system of the air coolers to maintain the temperature at a certain setup value (by controlling the apertures of the vanes and dampers). Therefore the power to these vanes and dampers would be supplied by the permanently-installed batteries and the newly-equipped power-supply vehicles, as one of the emergency safety measures. After achieving a cold shut-down state (Primary HTS sodium temperature: 180 to 250 degrees-Celsius), it has been assumed that a single set of primary and secondary HTSs has been returned to a forced circulation mode by the pony-motors powered by a restored single diesel generator.

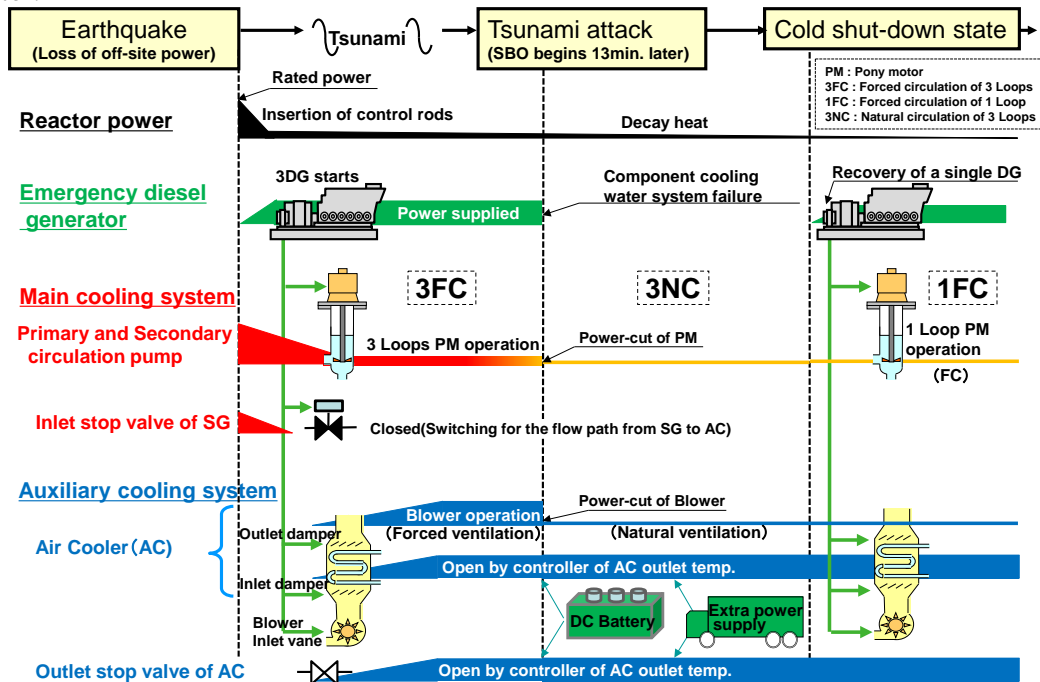


FIG. 2. Sequence of events after an earthquake and a subsequent tsunami

### 3. Analytical results based on basic sequence of events

The following analytical results have been derived based on the numerical simulation by Super-COPD for the basic sequence of events.

#### 3.1 Immediately after earthquake (from 0 to 13 minutes)

The reactor is automatically and immediately shut-down by inserting the control rods into the core activated by the earthquake and the loss of off-site power supply. The main circulation pumps of the primary and secondary HTSs are switched to and operated at a low flow-rate mode circulated by the pony motors. The air cooler blowers are also activated. The core decay heat is removed by the forced circulations of the coolant sodium. Then the heat removal capability of the air coolers is sufficient to cool down the core decay heat. The fuel assembly outlet temperature does not exceed the initial temperature (See FIG. 3.).

#### 3.2 After tsunami (from 13 minutes to 3 days or more)

After 13 minutes, a SBO occurs due to the tsunami attack. The pony motors for the main circulation pumps of the primary and secondary HTSs and the blowers for the air coolers are disabled. The core flow rate is decreased due to the pony motor shut-down. Then the fuel assembly outlet temperature increases (See FIG. 3.). This temperature rise of the core sodium causes buoyancy effect. Natural circulations are induced and initiated by this buoyancy effect. Then the core decay heat is transported to the air coolers and safely released to the atmosphere by the natural circulations of the sodium in the primary and secondary HTSs. A cold shut-down state is achieved approximately 3 days later. The primary HTS sodium is gradually cooled down to the cold shut-down state (See FIG. 4.).

Low-flow-rate forced circulations of a single set of primary and secondary HTSs are restored by the pony-motor driven pump circulations powered by a restored single diesel generator approximately 3 days later. The cold shut-down state is maintained by this low-flow-rate operation. The temperature difference between the reactor vessel inlet and outlet is reduced by these forced circulations for the restored HTSs (See FIG. 4.).

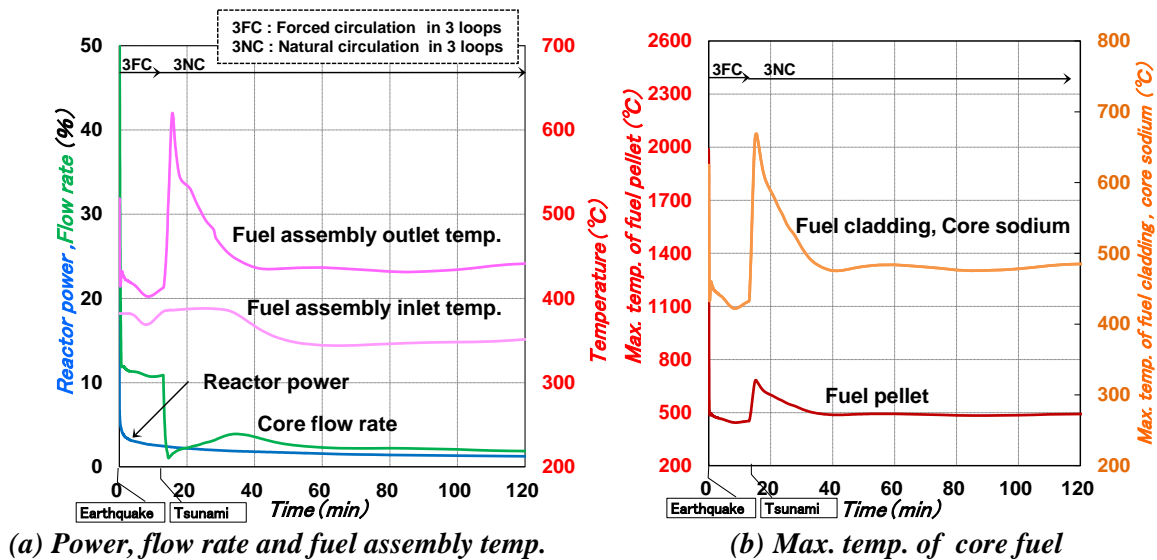


FIG. 3. Analytical results of Base case (0s. ~120min.)

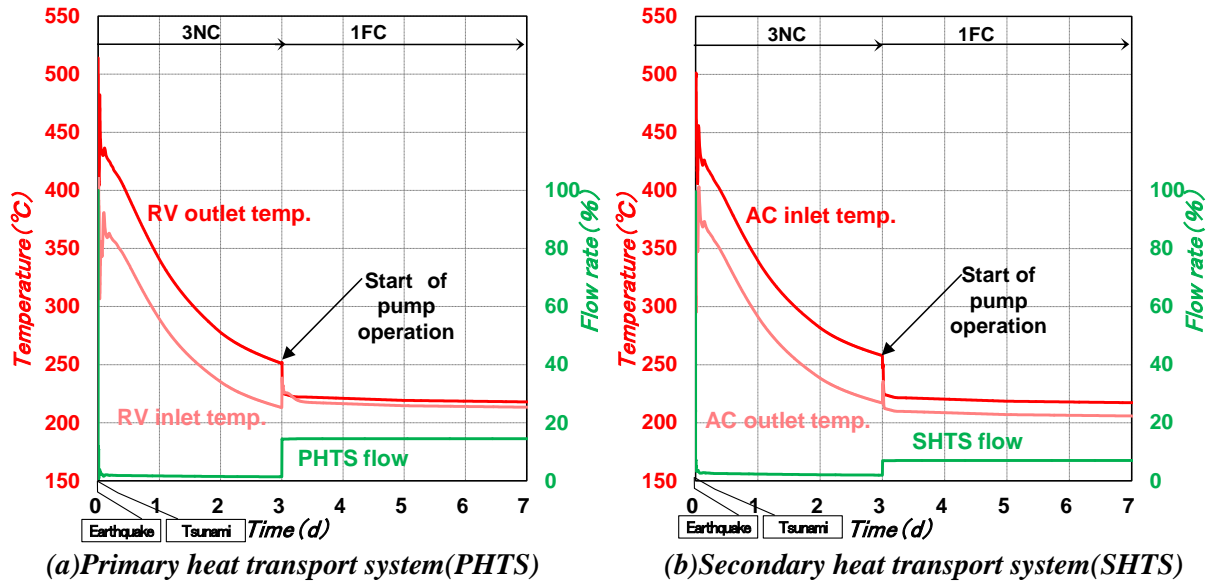


FIG. 4. Analytical results of Base case(0s. ~7days)

### 3.3 Concluding results

The fuel, fuel cladding, core sodium, reactor vessel inlet and outlet maximum temperatures do not exceed the criteria for the design basis accident of the safety analysis, although a SBO event is far beyond the design basis accident. The reactor can be led to a cold shut-down state by the natural circulations of the 3 sets of primary and secondary HTSs. This cold shut-down state can be maintained by a restored single set of HTSs, operated at a low-flow-rate mode by the primary and secondary pony motors (See Table 1.).

As a result it is concluded that the decay heat of the core can be safely removed by the natural circulations of the coolant sodium in the 3 sets of HTSs, even at a SBO event induced by an earthquake and a subsequent tsunami.

Table 1. Base case of summarized results

	Maximum temperatures (°C)					Cold shut-down state*1	
	Fuel pellet	Fuel cladding	Core sodium	RV outlet sodium	RV inlet sodium	Lead (days)	Maintaining
After earthquake (0s~13min)	1990	620	610	510	410	3	
After tsunami (13min~)	680	670	670	480	410		
DBE*2	Criteria for accidental transient The core does not suffer a significant damage, And the core can be sufficiently cooled.			< 650	< 650		
	Criteria for abnormal transient	<2650	<830	Less than boiling point*3	<600		

\*1: Primary sodium temperature 180°C<250°C

\*2: Design basis accidents

\*3: Approximately 920°C at 0.15 MPa

#### 4. Numerical simulation under varied analytical conditions

Numerical simulations have been performed by Super-COPD under varied analytical conditions to quantify the influence of the possible disincentives against the natural circulation, in order to confirm the success of the natural circulation and the resultant core cooling capability.

External hazards such as the tsunami attack delay time and the atmospheric temperature have been assumed as changing factors. The reactor power (decay heat) has also been considered as an internal obstructive factor. Failures of needed components for natural circulation have been also considered. Failures of the stop valves located at the inlet and outlet of the steam generators and air coolers, and failures of the vanes and dampers of the air coolers have been simulated. Failures of the passive components have been excluded in this study. Their integrity has been assumed to be secured a priori. The magnitude of the earthquake has been assumed to be within the design-basis.

*Table 2. Variation in analytical conditions for natural circulation*

<i>Case No.</i>	<i>Varied analytical conditions</i>	<i>Base case condition</i>
<i>Case 1</i>	<i>Tsunami attack delay time (0s. ~25min.)</i>	<i>13min.</i>
<i>Case 2</i>	<i>Rated power operation at the EOEC of the high burn-up core with design margin(Case 2.1) 40% power operation at the initial core(Case 2.2)</i>	<i>Rated power operation at the initial core</i>
<i>Case 3</i>	<i>AC inlet atmospheric temperature (+40 °C or -10)</i>	<i>20 °C</i>
<i>Case 4</i>	<i>Failure in SG inlet stop valve</i>	<i>Non failure</i>
<i>Case 5</i>	<i>Failure in AC vane and damper</i>	<i>Non failure</i>
<i>Case 6</i>	<i>Combination of severe analytical conditions (Case 1, Case 2 and Case 3)</i>	<i>-</i>

##### 4.1 Tsunami attack delay time (Case 1)

The possible maximum temperatures of the fuel cladding and the sodium are identified to be approximately 730 degrees-Celsius (C.) when the tsunami delay time is 9 minutes after the earthquake (See FIG. 5(a).), based on a series of parametric numerical simulations assuming the tsunami delay time as a parameter. These temperatures do not exceed the criteria for the design basis accident of the safety analysis (the fuel cladding temperature should be equal to or less than 830 degrees-C., and the sodium temperature should be less than the boiling point (approximately 920 degrees-C. at 0.15 MPa)), similar to the basic sequence of events.

The temperature (sodium density) difference between the inlet and the outlet of the reactor vessel is minimized at 9 minutes after the earthquake (reactor shut-down). This reduction in the temperature difference reduces the buoyancy effect and delays the recovery of the flow rate induced by the natural circulation. In case of an earlier tsunami delay time, larger temperature difference contributes more to faster recovery of the core flow rate, despite the larger core decay heat, resulting in lower maximum fuel cladding and sodium temperatures. This temperature difference does not change drastically after 9 minutes, while the core decay heat decreases gradually. Therefore the maximum temperatures of the fuel cladding and the core sodium are also decreased gradually (See FIG. 5(b)).

It is confirmed that the reactor can be led to a cold shut-down state approximately after 3 days for all the assumed tsunami delay times, the same as in the basic sequence of events.

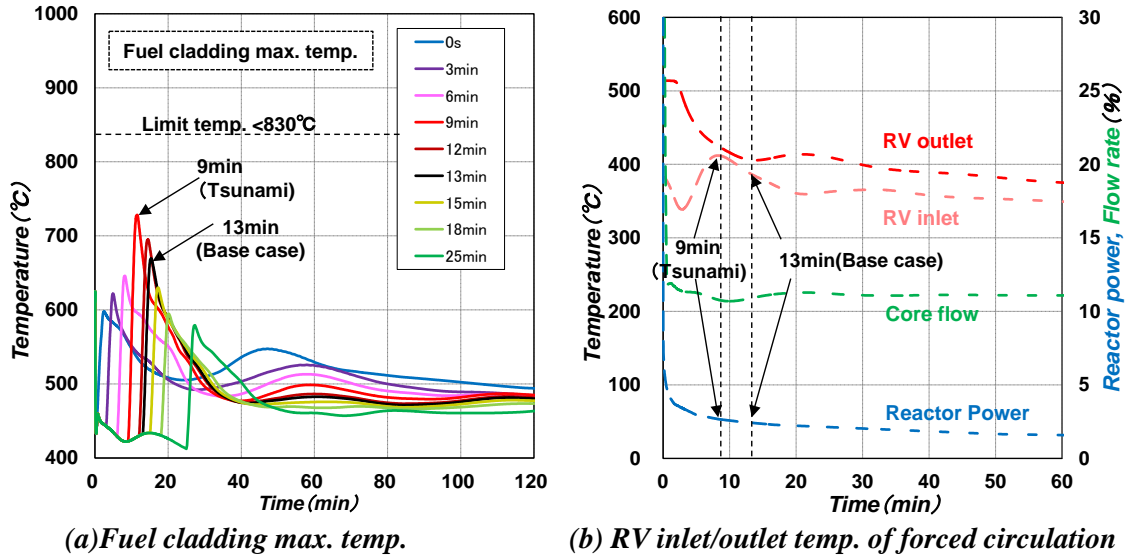


FIG. 5. Analytical result of Case 1

4.2 Reactor power and atmospheric temperature (Case 2 and Case 3)

The maximum core decay heat has been identified assuming the reactor shut-down after the rated power operation at the end of the equilibrium cycle (EOEC) of the high burn-up core, considering the design margin (Case 2.1). The minimum core decay heat has been evaluated assuming the reactor shut-down after the 40% rated power operation at the initial core (Case 2.2).

The maximum (Case 3.1) and minimum (Case 3.2) atmospheric temperatures (+40 and -10 degrees C.) have been identified based on the past experiences at the Monju site.

These changes in the core decay heat and the atmospheric temperature influence the rates of change in the sodium temperatures (See FIG. 5). However the reactor can be safely led to a cold shut-down state after a certain period of time. The maximum temperatures of the fuel cladding, the core sodium and the reactor vessel inlet and outlet do not exceed the criteria for the design basis accident of the safety analysis, as in the basic sequence of events.

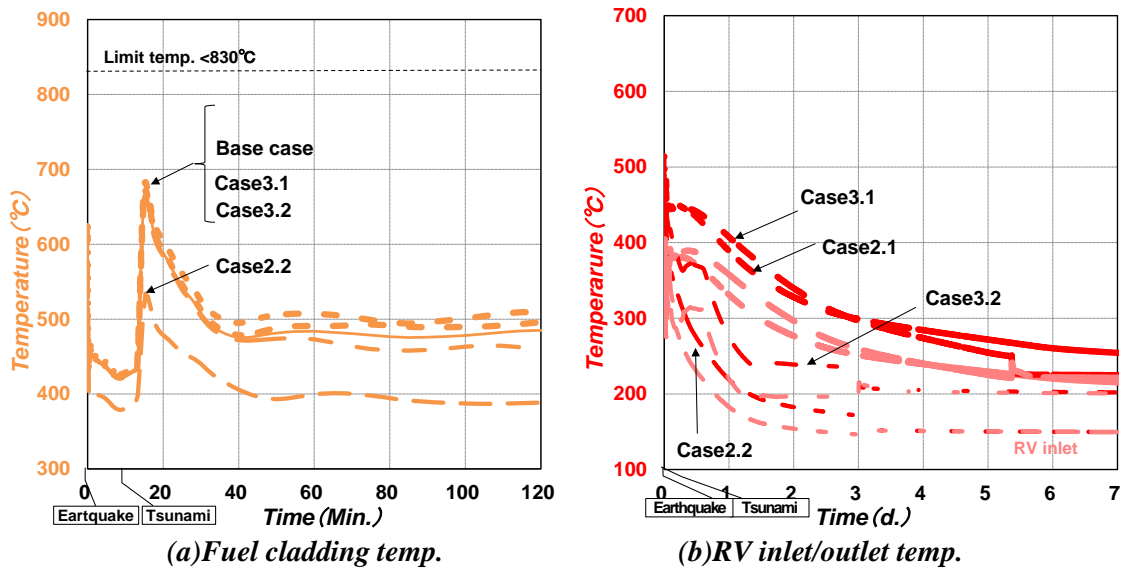
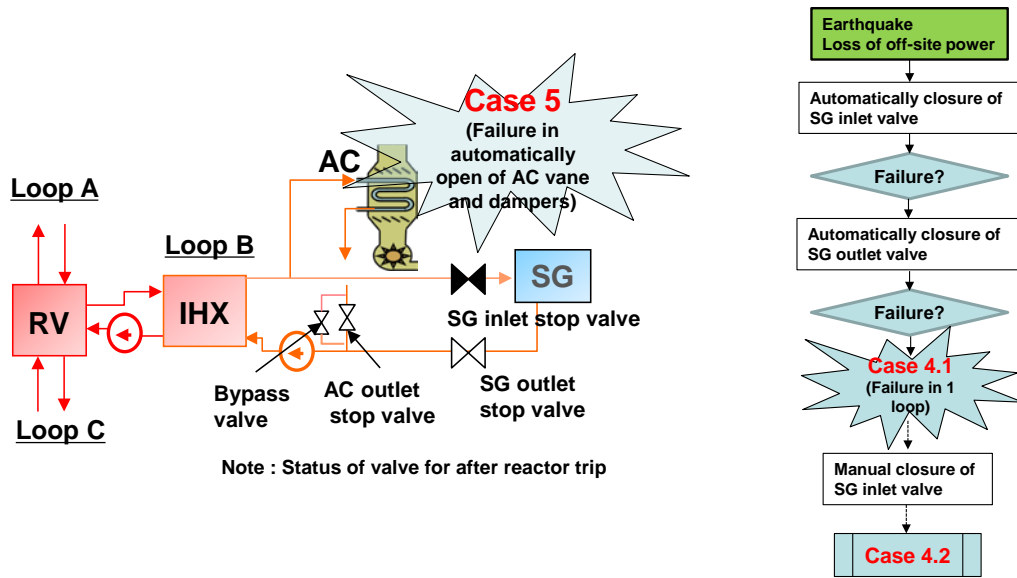


FIG. 6. Analytical result of Case 2 and Case 3

### 4.3 Failure of needed components for natural circulation

The stop valves at the inlet of the steam generators (SGs) should be closed and the stop valves at the outlet of the air coolers (ACs) should be opened in order to establish the sodium flow circuits for the natural circulations by switching the flow circuits from the SG side to the AC side. Moreover the apertures of the vanes and dampers of the ACs should be adjusted in order to control the heat removal capacity (See FIG. 7.). The core coolability under the failure conditions of these valves, vanes and dampers has been investigated as follows. These valves, vanes and dampers can be manually operated at the field site, in case they are not activated automatically by failure.



(a) Schematic view of needed components for natural circulation (b) Sequence of Case 4

FIG. 7. Needed components for natural circulation

#### 4.3.1 Failure of valves at sodium flow circuit (Case 4)

The stop valves at the inlet of the SGs are to be automatically closed activated by the reactor trip signal. This action separates the SGs from the system and establishes the sodium flow circuits for the decay heat removal by the ACs. The sequence of events has been investigated assuming that this automatic closure action of the inlet valve fails (See FIG.7(b)).

As a result it has been clarified that the stop valves at the outlet of the SGs are to be automatically closed, instead of the inlet valves, activated by the interlocking system and the flow circuits can be established.

Moreover failures of the closure action for both the stop valves at the inlet and outlet of a single SG have been assumed (Case 4.1). The results show that the core can be cooled down to a cold shut-down state by the natural circulations in the residual sound and normally operated 2 sets of HTSs. The hot sodium from the intermediate heat exchanger (IHX) at the failed HTS flows mainly to the highly-positioned AC. Therefore the core decay heat removal can be expected to a certain extent even at the failed HTSs. The manual closures of the SG inlet valves after 12 hours have been assumed in order to identify the effectiveness of the manual action (Case 4.2). The results show that the natural circulations are stabilized and accelerated by the separation of the SGs (See FIG. 8(a)).

The flow circuits for the ACs can be established even though a failure of the automatic opening action of the AC outlet stop valve is assumed. The bypass valves for the outlet stop valves are always opened. Therefore the sodium can flow through these bypass valves.

### 4.3.2 Failure of air cooler vanes and dampers (Case 5)

The vanes and dampers of the air coolers are controlled by a permanently-installed direct-current power supply. They can be also opened or closed manually. However in case that all these actions are assumed to be failed, the heat removal capability by the air coolers will be lost.

Therefore the following 4 cases have been assumed to clarify the core cooling capability by the air coolers: the air cooler vanes and dampers of a single AC (Case 5.1), double ACs (Case 5.2) and triple ACs (Case 5.3) would not be opened automatically and the failed vanes and dampers of a single AC would be opened manually later (Case 5.4).

The results show that the reactor can be led to a cold shut-down state by manually opening the failed vanes and dampers of a single AC within around 30 hours, even under a triple AC failure condition (See FIG. 8(b)).

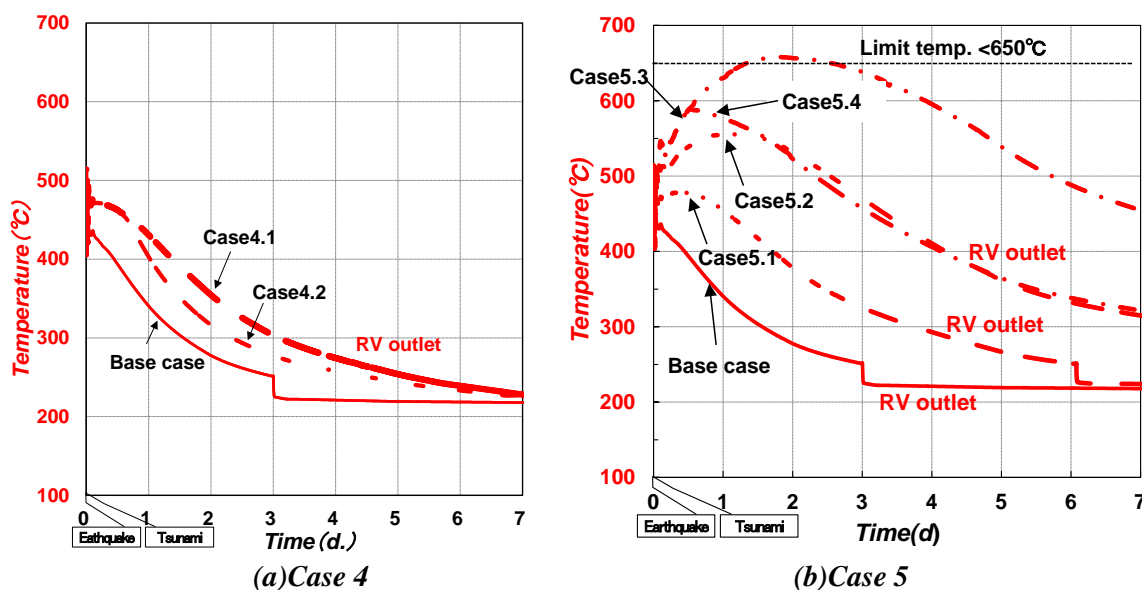
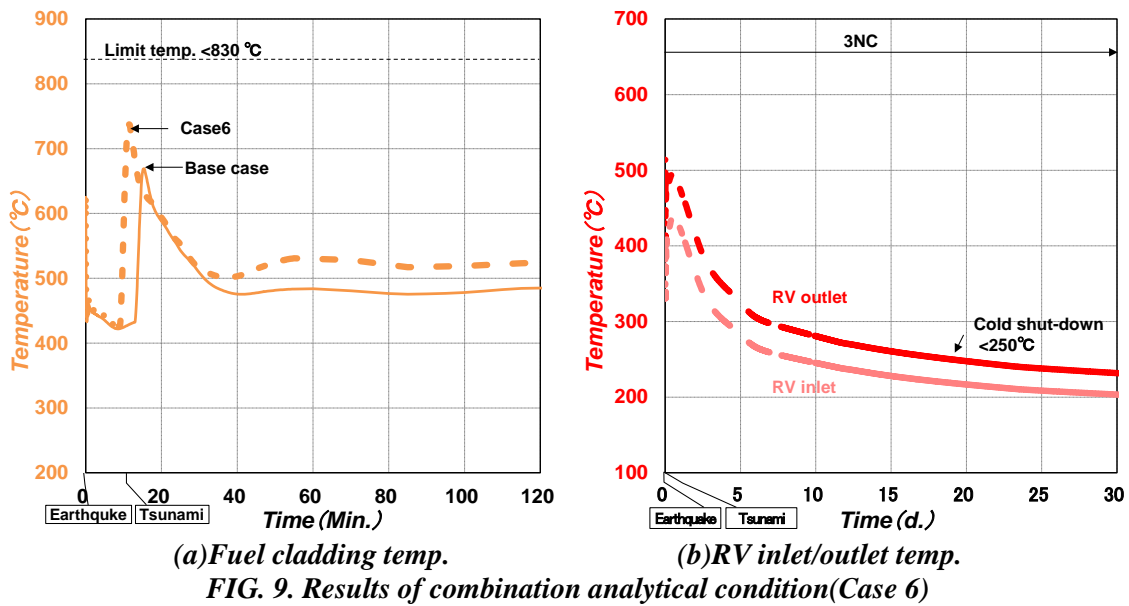


FIG. 8. Results of Case 4 and Case 5

### 4.4 Combination of severe analytical conditions (Case 6)

Some of the above-mentioned conditions have been combined from the viewpoints of the possible maximum temperatures.

The tsunami delay time of 9 minutes (Case 1) with the maximum core decay heat (Case 2.1) have been combined with the maximum atmospheric temperature (Case 3.1) to identify the possible maximum temperatures. The results show that the maximum temperatures do not exceed the criteria for the design basis accident of the safety analysis and the reactor can be led to a cold shut-down state by the natural circulations after 19 days, certainly later than the ordinary condition (See FIG. 9).



#### 4.5 Summary and interpretation of numerical simulations

The followings have been clarified based on the above-mentioned numerical simulations by Super-COPD.

The reactor can be safely led to a cold shut-down state after a certain period of time and the maximum temperatures of the fuel, the fuel cladding, the core sodium and the reactor vessel inlet and outlet do not exceed the criteria for the design basis accident of the safety analysis, despite under far-beyond-the-design-basis-accident conditions. These results are maintained even under the possible varied conditions of the tsunami attack delay time, the reactor power and the atmospheric temperature. The reactor can be also led to a cold shut-down state by manually opening the failed vanes and dampers of a single AC within around 30 hours, even under a failure condition of the automatic opening actions for all the vanes and dampers at the triple ACs. There will be sufficient time to manually open the vanes and dampers at the field site. The rate of change in the sodium temperature is moderate (see Table 3.).

Table 3. Summary of results under varied analytical conditions

	Maximum temperatures (°C)					Cold shut-down state (days)	Note
	Fuel pellet	Fuel cladding	Core sodium	RV outlet sodium	RV inlet sodium		
Base case	680	670	670	480	410	3	After tsunami(13min. to cold shut-down)
Case 1	740	730	730	490	410	3	9min. Tsunami
Case 2.1	700	680	680	490	400	8	Rated power, EOE core
Case 2.2	540	530	530	410	370	0.7	40%power, Initial core
Case 3.1	690	670	670	480	400	5	Atmospheric temp. 40°C
Case 3.2	680	670	670	480	400	1.2	Atmospheric temp. -10°C
Case 4.1	680	670	670	510	410	5	Failure in 1 loop of SG inlet stop valve
Case 5.4	760	750	750	590	560	10	Manual opening of the failed vanes and dampers of a single AC in 12 hours, under a triple AC failures
Case 6	750	740	740	500	440	19	Combination of Case 1, Case 2.1 and Case 3.1
DBE	The core does not suffer a significant damage, And the core can be sufficiently cooled.			<650	<650	-	-
	<2650	<830	Less than boiling point	<600	<588	-	-

## 5 Conclusion

This study clarified that the decay heat of the core can be safely removed in Monju by the natural circulations of the coolant sodium even at a SBO event induced by an earthquake and a subsequent tsunami, as far as the sodium coolant flow circuits are intact and secured. Moreover parametric numerical simulations revealed that the natural circulations will be maintained for a sufficiently long period of time and the safety of the reactor will be ensured even under wide range of varied conditions.

## ACKNOWLEDGEMENTS

The authors wish to express their greatest gratitude to Mr. T. Deshimaru and Mr. A. Miyakawa from Monju, who gave the authors beneficial suggestions on the analytical conditions and interpretation of the results, together with the members of the Technical Committee on Severe Accident Countermeasures referring to the Tohoku-district Off-the-Pacific-Ocean Earthquake, established in JAEA. The authors also would like to acknowledge the contributions of Mr. M. Minami, Mr. M. Kato and Mr. N. Yoshioka from NESI Inc, who collaborated with the authors to conduct the numerical calculations by Super-COPD and to arrange the figures and tables.

## REFERENCES

- [1] Nakai, S., et al., "Development of Module Integrated Plant Dynamics Analysis Code -Development of Super-COPD Code-," PNC Technical review No. 68-3 (1988) (in Japanese).
- [2] Tanji, M., et al., "Development and Verification of a Thermo-Hydraulic Simulation Code for System Transient in "Monju" (COPD code)," MHI Technical review Vol. 23, No. 6 (1986) (in Japanese).
- [3] Yamada, F., Ohira, H., 2010. Numerical simulation of Monju plant dynamics by SUPER-COPD using previous startup tests data, ASME 2010 3rd Joint US-European Fluids Engineering Summer Meeting.
- [4] FBR Plant Engineering Center et al., "External Evaluation on the Logical Adequacy of the Safety Measures and Coolability of the Reactor Core and others in Monju considering Earthquake and Tsunami," JAEA-Evaluation 2011-004,pp55-76(2011)(in Japanese)

## New transient analysis of the Superphénix start-up tests

K. Mikityuk<sup>a</sup>, M. Schikorr<sup>b</sup>

<sup>a</sup>Paul Scherrer Institute, Villigen PSI, Switzerland

<sup>b</sup>Karlsruhe Institute of Technology, Eggenstein-Leopoldshafen, Germany

**Abstract.** Open literature data were used to create computer models of the Superphénix sodium-cooled fast reactor (SFR) core and in-vessel structures with two codes: TRACE/FRED (PSI) and SIM-SFR (KIT). In both models 2D heat structures, 1D thermal-hydraulic channels and 0/1D reactor kinetics were used to account for dynamic reactivity feedbacks due to fuel temperature evolution as well as differential thermal expansions of fuel, cladding, sodium, diagrid, strongback, vessel and control rod drivelines. Six Superphénix start-up transient tests were analyzed using dynamic boundary conditions based on the test data for core inlet temperatures, flow rates and control rod position. Good agreement between calculations and measurements for reactor power and outlet temperature were obtained for all six cases using a single reactivity coefficient input data set. This analysis contributes to better understanding of SFR core/primary system dynamic behavior and to validation of the tools currently used for transient analysis of the Generation-IV SFR.

### 1. INTRODUCTION

Within currently ongoing European projects, transient (safety) analyses of various fast reactor concepts (SFR, LFR, GFR, MSR) are an important integral part of the comprehensive concept analyses performed. Concept-adapted versions of system codes such as RELAP, CATHARE, TRACE/FRED, SIM-SFR, SPECTRA, MAT5DYN, etc. are used to perform safety studies. In case no experimental plant data should be available for benchmarking these codes to the specific reactor concept, several of the above code systems are used within a project to allow intercode-comparison and -benchmarking. Fortunately, for the SFR concept, plant data from operating reactors (i.e., SPX1, PHENIX) is available allowing dedicated system code benchmarking. Two of the above listed code systems (TRACE/FRED and SIM-SFR) were used to analyse available plant transient data generated during the commissioning phase of SPX1.

The intrinsic purpose of performing this work was not only to benchmark codes, but also to study the generic dynamic behaviour of sodium-cooled fast reactors (SFRs). This requires an understanding of the various reactivity feedback mechanisms relevant in SFR such as the Doppler effect, coolant density changes, axial and radial expansions of the core, as well as other reactivity expansion effects basically driven by temperature changes outside the core region, in particular the control rod driveline expansion, the diagrid and strongback (radial and axial) expansion, and the reactivity effects associated with the change of the primary vessel wall temperature.

During the commissioning phase of SPX1 (see Fig. 1) several transients at different power levels were activated intentionally to study the dynamic response of SPX1 to certain transient initiators and to evaluate reactivity feedback coefficients. Six of these transients are documented in Ref.[1] (the entire volume of the journal being dedicated to SPX1), and these transients are used in this paper for deeper analyses. Basic input data to the system codes (geometries, fuel characterization, primary system design etc.) are also found in the various papers in Ref.[1], and are thus not explicitly repeated here. Only major assumptions relevant to the computer models are specifically addressed in this paper.

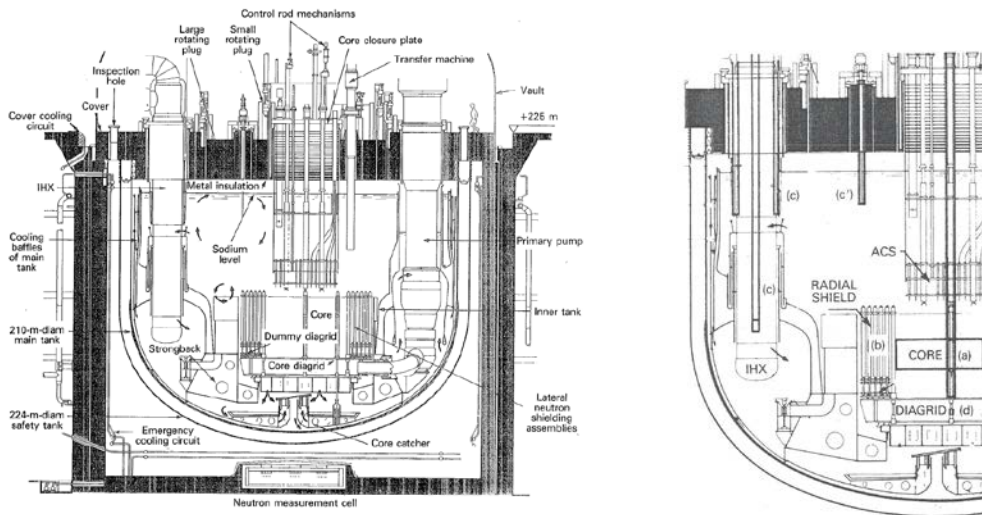


FIG. 1. Primary system of Superphenix (SPX1)

## 2. SFR (SPX1) REACTIVITY FEEDBACK COMPONENTS

The actual challenge in retracing real plant transients (such as the SPX1 start-up tests) covering the entire power range from hot full power (HFP) to cold zero power (CZP) is the determination of a single, unique set of reactivity coefficients applicable for all transients at all power levels for the particular plant configuration under investigation. If individual reactivity coefficients are allowed to be modified/adjusted during different simulation runs while retracing transients, then basically all fairly modern codes should be able to come up with a calculated transient solution replicating the plant data. However, requiring that all plant transients at different power levels are replicated with a single, unique reactivity coefficient set and without any further model/code changes (i. e. setting a “convenient” gap conductance) makes this exercise significantly more challenging, requiring essentially an extremely high fidelity simulation model. It also requires that all pertinent feedback effects are understood and properly simulated.

Table 1 provides this list of unique SPX1 reactivity feedbacks coefficients as used by PSI (TRACE/FRED) and KIT (SIM-SFR) to benchmark the respective system codes.

Table 1: Unique sets of SPX1 reactivity feedback coefficients as used by PSI (TRAC/FRED) and KIT (SIM-SFR) for retracing the SPX1 experimental plant transients as discussed below. (Core conditions during commissioning phase were assumed to be consistent with BOL core state).

Reactivity Component	PSI: TRACE/FRED	KIT: SIM-SFR
Doppler Constant [pcm]	-900	-890
Sodium Expansion [pcm/°C]	+0.500	+0.445
Axial Fuel Expansion [pcm/°C]	-0.60	-0.20
Diagrid Expansion [pcm/°C]	-1.0	-2.4
Strongback Expansion [pcm/°C]	-2.0	
Control rod driveline expansion [pcm/°C]	-1.0	Calculated dynamically
Vessel wall expansion [pcm/°C]	+4.0	-2.0 × Control rod driveline expansion

Two sets of coefficients were developed independently by PSI and KIT and these coefficients were not changed for the six transients analysed. It should be noted that characterization of the individual reactivity effects due to thermal expansions of reactor components with just few coefficients is a strong approximation of the actual complex core thermal-mechanical/neutronic configuration. Each reactivity coefficient describing the effect from thermal expansion of a reactor structure (diagrid,

strongback, vessel) was used in conjunction with a specific thermal model of this structure used to calculate its temperature evolution. The application of the two different sets of reactivity coefficients presented in Table 1 can be therefore considered as a sensitivity study of the transient response of the large SFR core to the simplified modeling/simulation of the in-core and out-core thermal mechanics / neutronics.

Major reactivity effects, essentially determining the course of most SPX1 transients, are found to be reactivities associated with the expansion of the control rod drivelines, vessel wall, diagrid and strongback. All effects are relatively slow in their response time before these effects to become effective as temperatures external to the core region have to change first.

*The Doppler Effect:* The fastest reacting reactivity is the Doppler effect, inserting positive reactivity during decreasing fuel temperature on account of the decreasing power level, or negative reactivity in case the fuel temperatures, or power level should rise.

*The Axial Fuel Expansion:* This reactivity effect becomes effective very quickly as it is associated with the bulk temperature changes of the fuel. The fuel temperature changes quickly upon any changes in reactor power. A free expansion of the fuel column was assumed in the simulation (BOL core conditions). The axial expansion of the fuel column decreases the fuel-to-coolant ratio and slightly increases the insertion of control rods, both effects introducing a negative reactivity.

*The Sodium Temperature Effect:* An increase in the core coolant temperature in average inserts a net positive sodium expansion reactivity due to its reactivity coefficient being positive. The sodium temperature reactivity effect acts quicker than other feedback effects (except Doppler and fuel expansion) since the time response of core coolant temperature are much faster than response of the reactor structures.

*The Diagrid Reactivity Feedback Effect:* The diagrid reactivity contribution during any transient is essentially due to changes in the core inlet temperature to which the large diagrid plate will adjust slowly on account of its relatively large mass, namely about 173 tons for SPX1. Should the core inlet temperature increase during any transient, such as is the case when the secondary pump is tripped concurrently with the primary pump, then the radial diagrid expansion will insert a negative reactivity, lagged in time.

*The Control Rod Driveline Expansion Reactivity Effect:* A major negative reactivity effect, that essentially determines the course of many SPX1 transients, is clearly the negative reactivities associated with the expansion of the control rod drivelines, immersed in the upper plenum sodium pool and located between the upper vessel head and the top of the reactor core. The temperature of the surrounding sodium pool of the upper plenum in which the drivelines are housed needs to change first. If the entire upper plenum temperature is to increase homogeneously (uniformly) the temperature change of the rod drives would be too slow to be effective. It is thus imperative to direct the core outlet flow into a shrouded region housing the rod drivelines before the core outlet flow is allowed to mix with the remaining upper plenum. This effect is taken into account in the modelling in SIM-SFR, by assuming a ~85% flow preference of the core outlet temperature into the shrouded driveline upper plenum (assumed 15% volume fraction of upper plenum) before mixing with the upper plenum sodium mass inventory.

*The Vessel Wall Expansion Reactivity Effect:* The other temperature influencing the control rod position is the vessel wall temperature. Thermal expansion of the vessel wall has the effect of moving the core downward and therefore withdrawing the control rod banks from the core region, thus counteracting, or adding positive reactivity into the core. The effect of vessel wall temperature changes are however very much delayed (by about 200 to 400 sec) due to the nature of the tortuous paths of the vessel wall cooling system (see Fig. 1). Part of the core inlet flow is diverted for cooling of the vessel walls; the temperatures of the vessel wall will thus gradually adopt the temperature of the core inlet flow, or primary outlet flow of the heat exchanger.

*The Strongback Reactivity Feedback Effect:* Similar to vessel expansion effect, the strongback thermal expansion is driven by the inlet coolant temperature increase with a significant time delay determined by the strongback mass. The thermal expansion of the strongback results in a slight shift of the core upwards and insertion of the control rods, therefore a negative reactivity is inserted when coolant temperatures increases at the core inlet.

In SIM-SFR the reactivity feedback coefficient associated with the control rod driveline expansion is dependent on the insertion depth of the control rods. During SPX1 commissioning, BOC core conditions, the rods were inserted at least 45% under nominal power conditions. For the -74 pcm reactivity transient activated at ~ 50% power (1556 MWth), the rods were inserted 53 cm. The total number of control rods is 21 and their total worth is 8106 pcm.

The expansion of the control rod drivelines themselves is calculated as:  $\Delta L / \Delta T = \alpha_{AIM1} L$ , where L is the length of the control rod driveline (~6720 mm) and  $\alpha_{AIM1} \approx 1.8 \times 10^{-5} [1/^\circ\text{C}]$  at 400°C. Therefore,  $\Delta L / \Delta T \approx 0.121 [\text{mm}/^\circ\text{C}]$ .

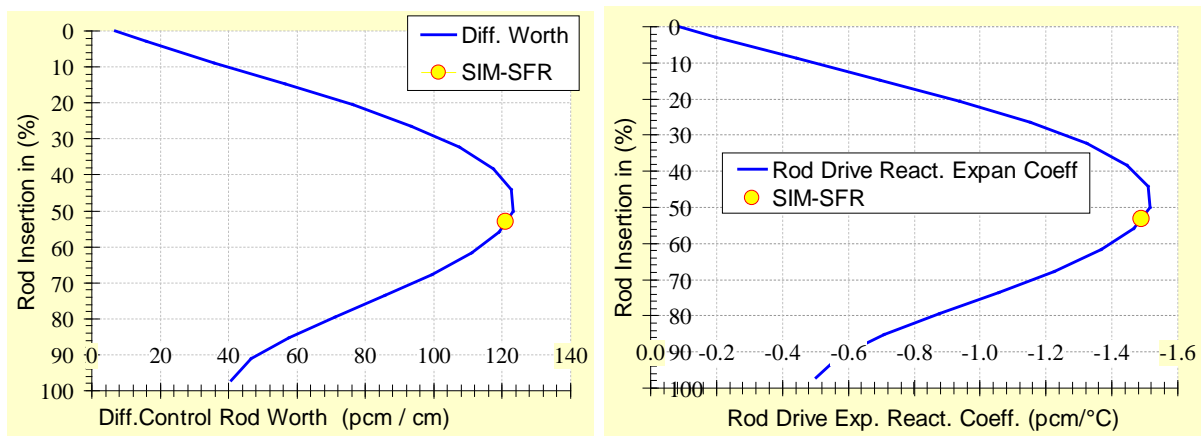


FIG. 2. Differential Control Rod Worth [pcm/c] and Rod Drive Expansion Reactivity Coefficient [pcm/°C] for SPX1 and corresponding rod position during BOC based on 21 rods and 8106 pcm total rod reactivity during commissioning phase

Using the differential control rod worth distribution for SPX1 in terms of (pcm/mm) and multiplying it by  $\Delta L / \Delta T$  (mm/°C) as calculated above, we can calculate the control rod driveline expansion reactivity feedback coefficient. This data is displayed for SPX1 in Fig. 2

To maximize the rod driveline extension feedback, the position of the rod banks should be ideally positioned at the peak of the differential control rod worth curve (see Fig. 2), i.e., at about core center, as is the case for BOC core conditions. When the rods are withdrawn under EOC conditions, this effect is then corresponding minimized.

### 3. SPX1 TRANSIENTS ANALYSED

From the commissioning phase of SPX1, three (3) reactivity insertion transients at different power levels (1552, 692 and 0 MWth) and three (3) mass flow change (two (2) primary mass flow changes and one (1) secondary mass flow change) transients were documented in Ref.[1].

The list of analyzed transients for SPX1 is as follows:

- -74 pcm stepwise reactivity insertion at 1542 MWth,
- -50 pcm reactivity insertion at 692 MWth,
- + 30 pcm reactivity insertion at hot zero power (HZP),
- -10% primary mass flowrate reduction at 1415 MWth,
- -10% primary mass flowrate reduction at 666 MWth,
- +10% secondary mass flowrate increase at 692 MWth,

The main results of all the analyzed transients are summarized in the following sub-sections.

### ***3.1. -74 pcm Reactivity Insertion Transient at 1542 MWth***

In Fig. 3 the SPX1 (and the system code models) was stabilized at about 50% power (1542 MWth), and the control rods were then inserting -74 pcm in a stepwise manner (-25, -25, and -24 pcm per step at 382 s, 442 s, and 502 s transient time, respectively). Input data provided to the codes was the measured time evolution of core inlet temperature and vessel wall temperature, also displayed in Fig. 3. The codes then calculated the corresponding power and core temperature evolution in response to the stepwise reactivity insertion. To be noted is the sensitivity of SPX (and the models) to the decrease in core inlet temperature of 1 °C from 400 °C to 399°C during the first 382 s transient time (prior to the start of the negative reactivity insertion) leading to a power increase from 1542 to 1552 MWth. To be noted also is the dynamic response of the stepwise power decrease (slight undershot followed by power recovery) at each rod insertion step reflecting the high fidelity of the dynamic fuel-cladding gap modelling in TRACE/FRED and SIM-SFR. Both codes are observed in Fig. 3 to retrace the power evolution of this 3000 s transient quite well (to within 0.7% error), as the major reactivity feedbacks of this reactivity insertion transient are the positive Doppler, counteracting the power decrease due to decreased fuel temperatures, and expansion feedbacks from the diagrid (driven by the decreasing core inlet temperature) and the rod + vessel expansion feedbacks (mainly driven by the combination of the upper plenum temperature changes and core inlet temperature). The reactivity components calculated by CEA [1] are also presented in Fig. 3. The good agreement of both code systems with the experimental transient data are an indication of 1. the selection of an applicable set of reactivity feedback coefficients (see Table 1) and 2. the appropriate thermal-hydraulic modelling of both the core internals (fuel pin/SA configuration: i.e. fuel, gap, clad, and coolant temperatures) and the primary system of SPX1 as the major expansion reactivity feedback components (rod driveline, strongback, diagrid, vessel wall) are driven by temperatures outside the core region.

### ***3.2. -50 pcm Reactivity Insertion Transient at 692 MWth***

In Fig. 4 the SPX1 (and the system code models) was stabilized at 692 MWth, and the control rods were then inserting -50 pcm. Input data provided to the codes was the measured time evolution of core inlet temperature and vessel wall temperature, also displayed in Fig. 4. The codes then calculated the corresponding power and core temperature evolution in response to the reactivity insertion. Both codes are observed in Fig. 4 to retrace the power evolution of this 3000 s transient quite well (to within 5 MWth error), as the major reactivity feedbacks of this reactivity insertion transient are again the positive Doppler, counteracting the power decrease due to decreased fuel temperatures, and expansion feedbacks from the diagrid and strongback (driven by the decreasing core inlet temperature) and the rod + vessel expansion feedbacks (mainly driven by the combination of the upper plenum temperature changes and core inlet temperature).

### ***3.3. +30 pcm Reactivity Insertion Transient at 0 MWth (HZP)***

The following transient is one of most challenging transient to retrace as it requires a high fidelity, dynamic fuel pin model as the feedback reactivities are initially solely due to the Doppler (fuel temperature increase), later followed by the expansion feedbacks. An incorrect modelling of the fuel-cladding gap characteristics will not allow retracement of this transient. In Fig. 5 the SPX1 (and the system code models) was stabilized at 0 MWth, reactor critical, with the primary loop temperatures

isothermal at  $\sim 179$  °C, The control rods were then withdrawn inserting +30 pcm of reactivity. Input data provided to the codes was the measured time evolution of core inlet temperature and vessel wall temperature, also displayed in Fig. 5. The codes then calculated the corresponding power and core temperature evolution in response to the reactivity insertion. Both codes are observed in Fig. 5 to retrace the power evolution of this 3000 s transient quite well (to within 1 to 2 MWth error), as the major reactivity feedbacks of this reactivity insertion transient is initially the negative Doppler, counteracting the reactivity insertion, followed by the expansion feedbacks from the diagrid and strongback (driven by the decreasing core inlet temperature) and the rod + vessel expansion feedbacks (mainly driven by the combination of the upper plenum temperature changes and core inlet temperature).

### **3.4. 10 % Primary Flow Reduction Transient at 1415 MWth**

In Fig. 6 the SPX1 (and the system code models) was stabilized at 1415 MWth, and the primary flow rate was then reduced by 10% flowrate. Input data provided to the codes was the measured time evolution of core inlet temperature, which reduced by 11 °C during this transient, and vessel wall temperature, as displayed in Fig. 6. The codes then calculated the corresponding power and core temperature evolution in response to the 10% flow reduction. The core temperature drop increases due to the flow reduction, and the resulting temperature changes in the core and the primary system lead to a transient reactor power change as displayed in Fig. 6. The primary changes in reactivity are due to the diagrid + strongback temperature changes as well as the control rod driveline expansion as can be seen in Fig. 6, both driven by temperature changes outside the core region. Both codes, TRACE/FRED and SIM-SFR are observed to retrace the transient power evolution of this 3000 s transient quite well (to within 0.7% error), indicating again 1. an appropriate selection of the set of reactivity feedback coefficients (see Table 1) and 2. the appropriate thermal-hydraulic modelling of both the core internals (fuel pin/SA configuration: i.e. fuel, gap, clad, and coolant temperatures) and the primary system of SPX1.

### **3.5. 10 % Primary Flow Reduction Transient at 662 MWth**

In Fig. 7 the SPX1 (and the system code models) was stabilized at  $\sim 662$  MWth, and the primary flowrate was then reduced by 10%. Input data provided to the codes was the measured time evolution of core inlet temperature, which reduced by 11 °C during this transient, and vessel wall temperature, as displayed in Fig. 7. The codes then calculated the corresponding power and core temperature evolution in response to the 10% flow reduction. The core temperature drop increases due to the flow reduction, and the resulting temperature changes in the core and the primary system lead to a transient reactor power change as displayed in Fig. 7. The primary changes in reactivity are due to the diagrid + strongback temperature changes as well as the control rod driveline expansion as can be seen in Fig. 7, both driven by temperature changes outside the core region. Both codes, TRACE/FRED and SIM-SFR are observed to retrace the transient power evolution of this 3000 s transient quite well (to within 0.7% error), indicating again 1. an appropriate selection of the set of reactivity feedback coefficients (see Table 1) and 2. the appropriate thermal-hydraulic modelling of both the core internals (fuel pin/SA configuration: i.e. fuel, gap, clad, and coolant temperatures) and the primary system of SPX1.

### **3.6. 10 % Secondary Flow Increase Transient at 632 MWth**

In Fig. 8 the SPX1 (and the system code models) was stabilized at 632 MWth, and the secondary flow rate was then increased by 10% flowrate. This lead to a distinct decrease in the core inlet temperature from 385°C to 374°C, resulting in a positive reactivity component of +20 to +30 pcm due to decreasing diagrid and strongback temperatures with a resultant increase in power from 632 to 690 MW, later stabilizing at 665 MW, as can be observed in Fig. 8. Input data provided to the codes was again the measured time evolution of core inlet temperature, which reduced by 11 °C during this transient as displayed in Fig. 8. The codes then calculated the corresponding power and core temperature evolution in response to the 10% secondary flow increase. The core temperature drop increases due to the power increase, and the resulting temperature changes in the core and the primary

system then lead to the transient reactor power change as displayed in Fig. 8. Both codes, TRACE/FRED and SIM-SFR are observed to also retrace this transient power evolution of this 3000 s transient quite well (to within a few MW error).

#### **4. CONCLUSIONS**

In the framework of the ongoing European GEN-IV projects, the system codes TRACE/FRED and SIM-SFR were independently benchmarked on six Superphenix (SPX1) transient data sets obtained and documented during the commissioning phase of this reactor.

The purpose of the exercise was twofold, foremost to study the generic dynamic behaviour of SFRs, and second to benchmark these two code systems to SFRs in order to use the predictive capability of these codes in the safety analysis of newer, more current SFR designs.

To account for the various reactivity feedback components driving the dynamic behaviour of SPX1, various expansion driven reactivity effects have to be understood and properly simulated/modelled in the respective code systems before the SPX1 plant transient could be replicated. Aside of the conventional Doppler, axial fuel expansion (fuel temperature) and coolant density feedbacks, all basically driven by temperature changes inside the core, expansion feedbacks driven by temperature changes outside the core region (diagrid, strongback, control rod driveline, vessel wall) were found to play dominant roles in the dynamics of SPX1.

The above recognition required a detailed thermal-hydraulic modelling of the entire primary system of SPX1 in addition to the high fidelity modelling required to account for the appropriate dynamics of the fuel-gap-clad (fuel pin) system.

Only when one unique set of reactivity coefficients and associated models of the fuel rods and structures are used for all six SPX1 transients investigated (different power levels), only then one can claim that the dynamics of the reactor system is correctly understood and also properly modelled/simulated in the respective code system. Should changes in individual reactivity feedback coefficient components, or model changes be necessary when switching from one SPX1 transient to the other, then the reactor system is not yet either completely understood, or improperly simulated/modelled.

To retrace the six SPX1 transients, as documented above, both system codes TRACE/FRED and SIM-SFR used a high fidelity, dynamic fuel-clad-gap model, accounting for all pertinent physical phenomena (such as thermal expansions of both fuel and clad, inner gas pressure evolution, gas gap conductance, etc.) in conjunction with thermal-hydraulics modelling of important parts of the primary system. This turned out to be a very sensitive issue in particular when trying to retrace the +30 pcm reactivity insertion transient at hot zero power (HZP).

A unique set of reactivity coefficients for SPX1, applicable at the commissioning phase of SPX1, could be found (requiring of course a tedious and lengthy iteration process), indicating that all relevant dynamic processes governing SPX1 are properly understood and reasonably correct simulated/modelled in the TRACE/FRED and SIM-SFR system codes.

#### **Acknowledgements**

The authors acknowledge the European Commission for funding the various GEN-IV projects in its 7th Framework Programme. Acknowledgment is also due to all the colleagues of the participant organizations for their contributions in many different topics.

#### **References**

- [1] NUCLEAR SCIENCE AND ENGINEERING, 106 (1990)

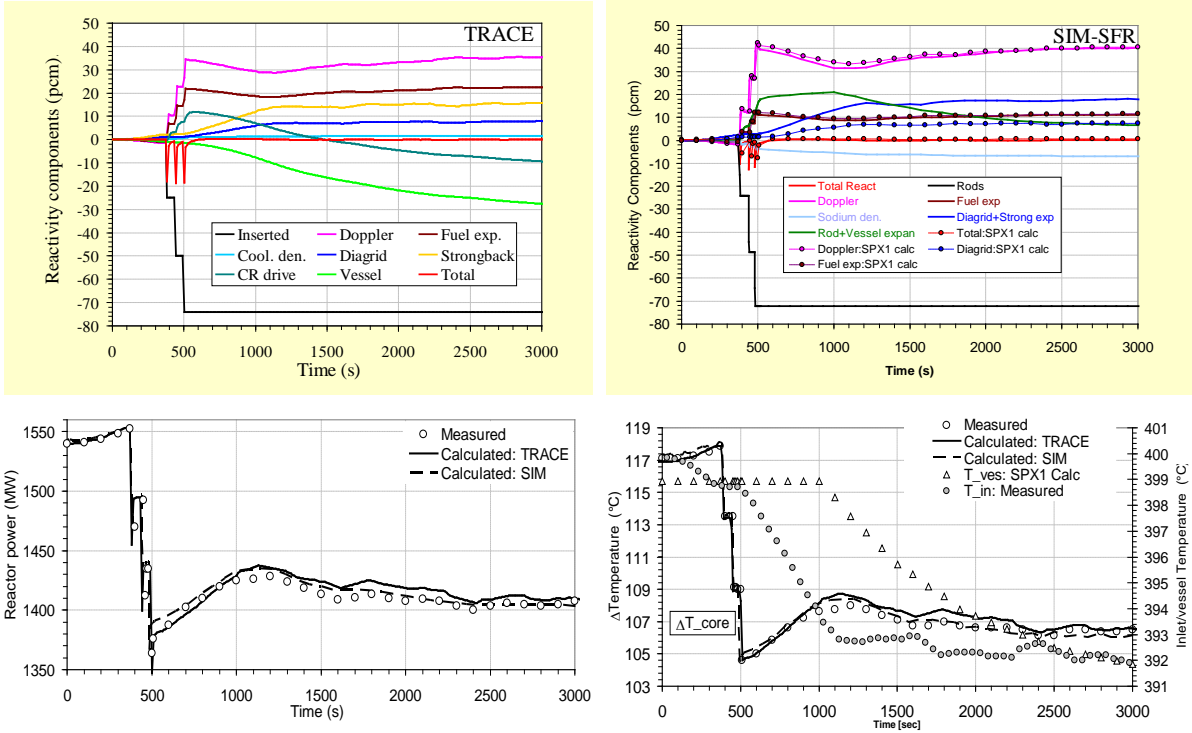


FIG. 3. Evolution of reactivity components, power, and temperatures in the  $-74$  pcm stepwise reactivity insertion transient (at 1542 MWth) as calculated by TRACE/FRED and SIM-SFR

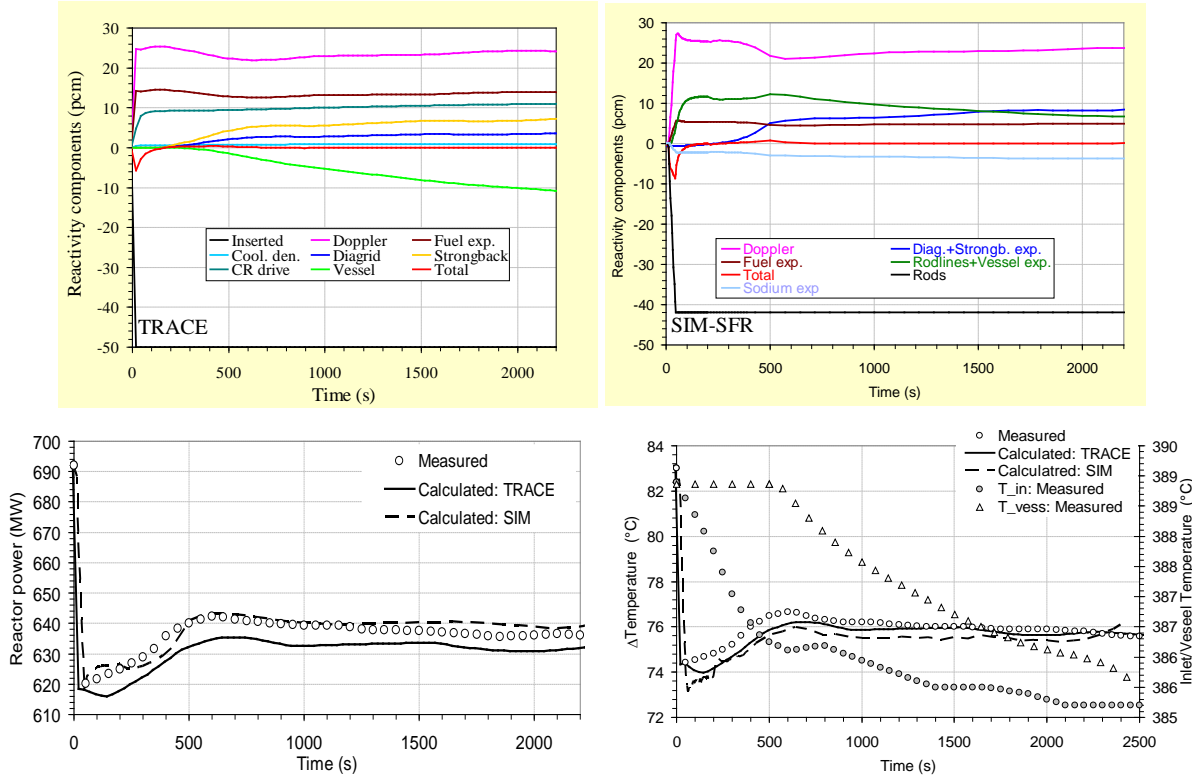


FIG. 4. Evolution of reactivity components, power, and temperatures in the  $-50$  pcm reactivity insertion transient (at 692 MWth) as calculated by TRACE/FRED and SIM-SFR

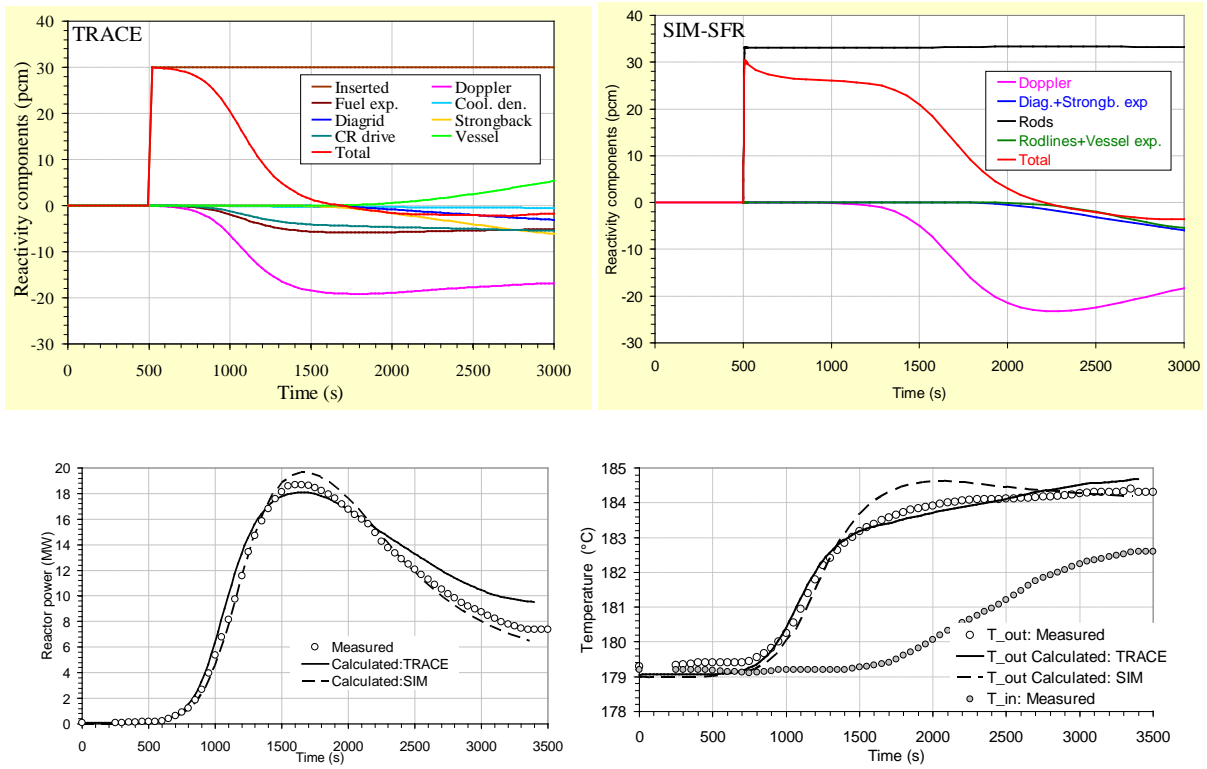


FIG. 5. Evolution of reactivity components, power, and temperatures in the +30 pcm reactivity insertion transient (at 0 MWth, critical reactor at 179.5°C isothermal primary system temperatures) as calculated by TRACE/FRED and SIM-SFR

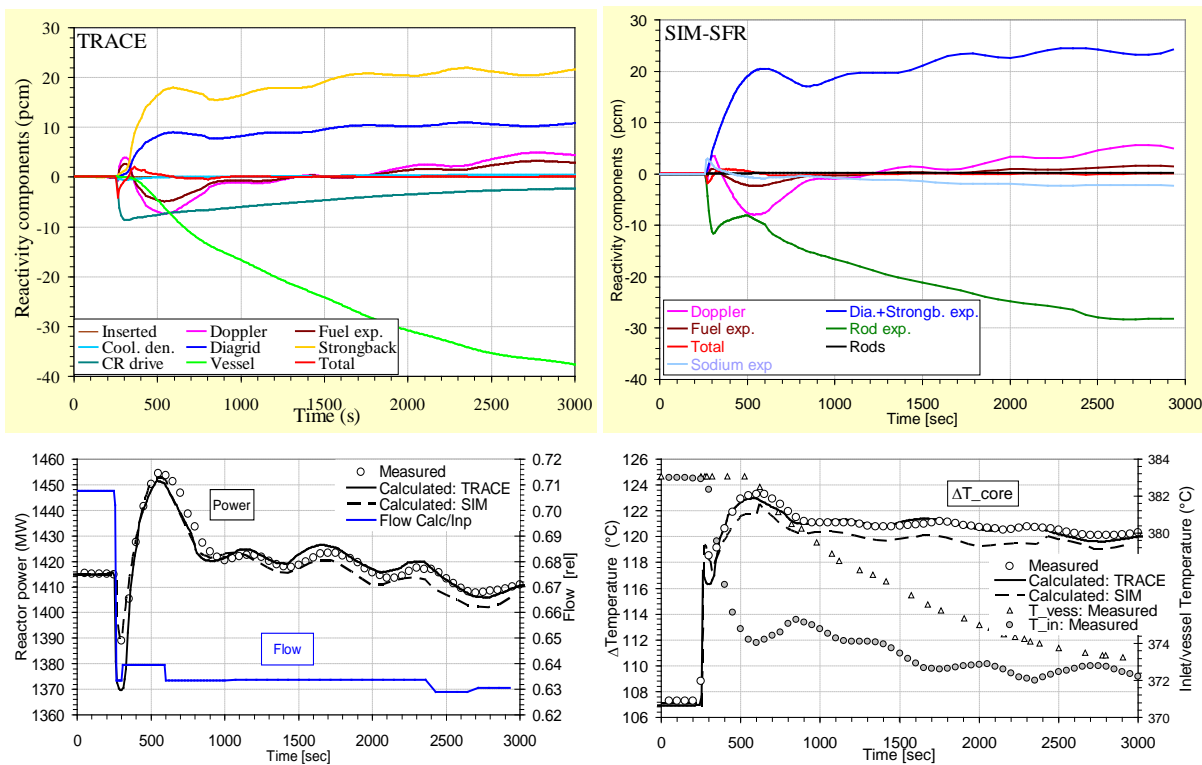


FIG. 6. Evolution of reactivity components, power, and temperatures in the 10% Primary Flow Reduction transient (at 1415 MWth) as calculated by TRACE/FRED and SIM-SFR

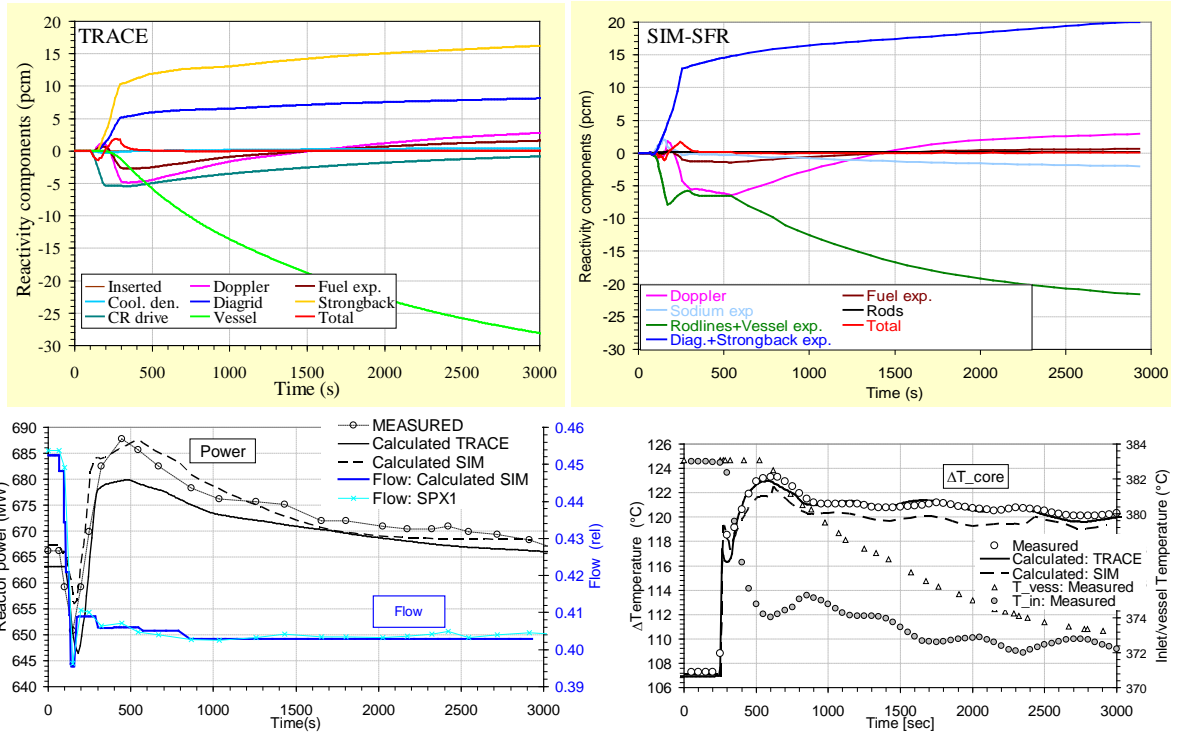


FIG. 7. Evolution of reactivity components, power, flow and temperatures to the 10 % Primary Flow Reduction transient (at 666 MWth) as calculated by TRACE/FRED and SIM-SFR

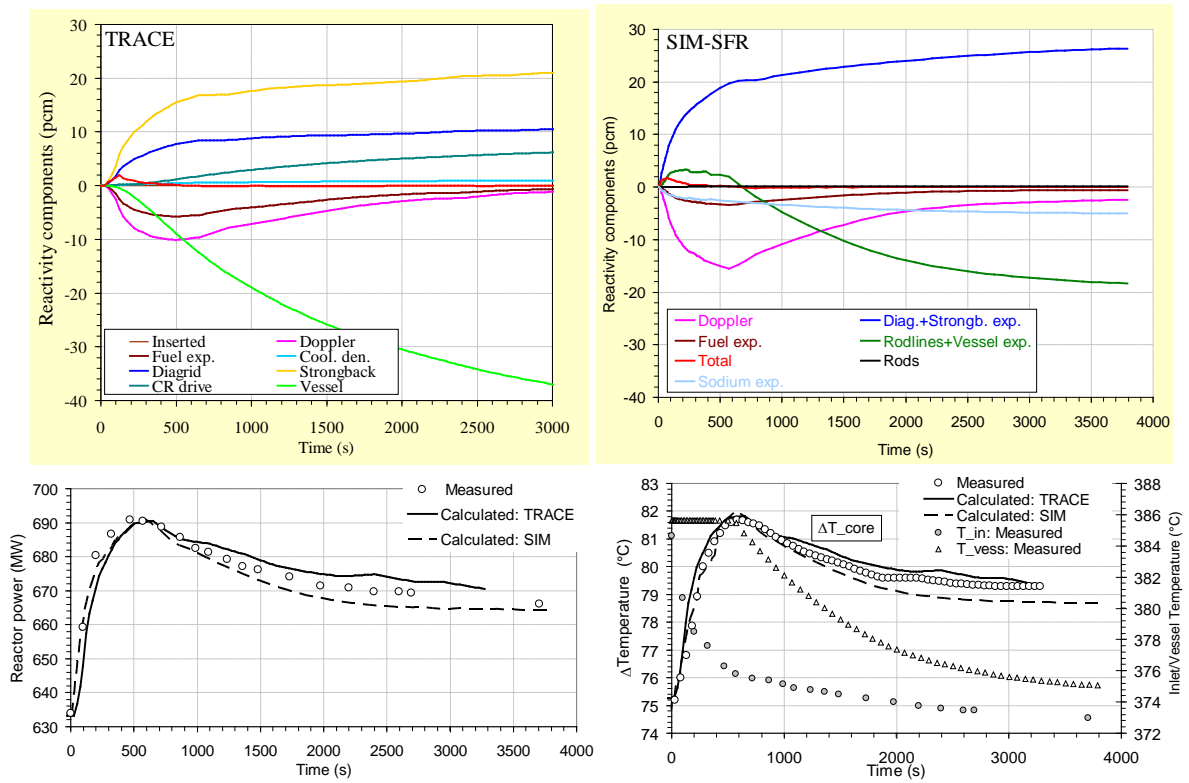


FIG. 8. Evolution of reactivity components, power, and temperatures in the 10% Secondary Flow Increase transient (at 632 MWth) as calculated by TRACE/FRED and SIM-SFR

# PHENIX : A REPROCESSING AND MULTIPLE RECYCLING EXPERIMENT, UNIQUE IN THE WORLD.

FR13 Paris France 4 to 7 March 2013

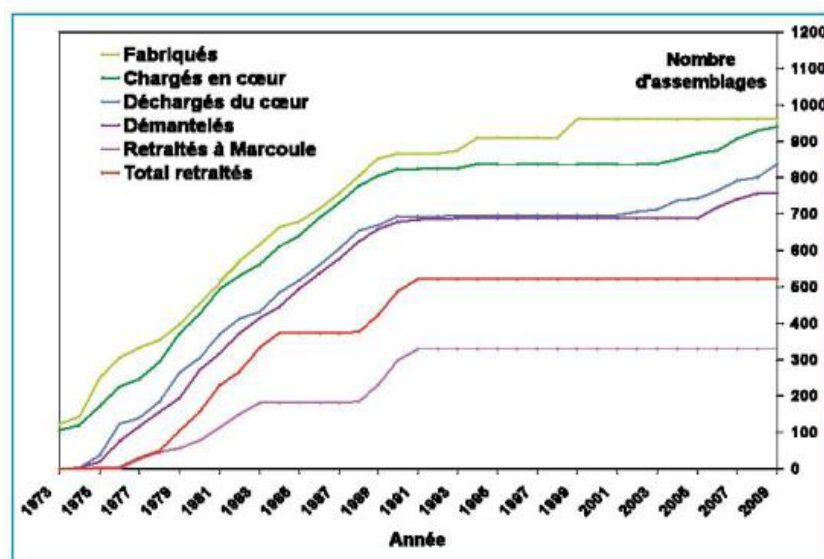
Joël GUIDEZ – CEA/DEN/DIR CEN Saclay 91190 Gif sur Yvette

**Abstract** The fast reactors can produce more plutonium than they use. After reprocessing, fresh fuel sub-assemblies can be made, from a part of the recovered plutonium, supplemented by natural or depleted uranium. This means all the uranium can be burned and thus increase a lot the world's available energy reserves. Phénix has reprocessed 520 assemblies, in three different facilities, i.e. slightly more than 26 metric tons of fuel. 4.4 metric tons of plutonium have been extracted in this way. The breeding rate has been confirmed and measured at 1.16. Then 3.3 metric tons of plutonium were used to manufacture fresh fuel sub-assemblies for Phénix which have been burned in the reactor. This paper presents the entire experiment that is unique in the world, and which demonstrates that the fuel cycle of fast reactors is an industrial reality.

## PHÉNIX FUEL REPROCESSING EXPERIMENT

### General data:

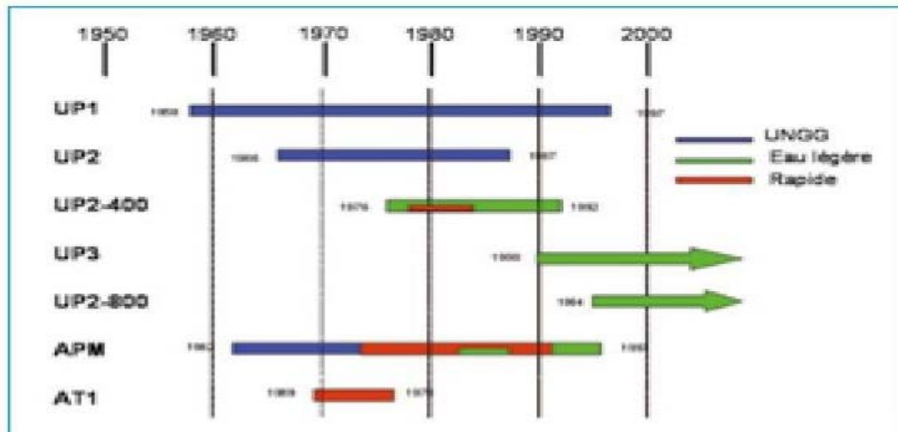
520 Phénix assemblies were reprocessed from 1976 to 1993, which represents 4.4 metric tons of metal PU extracted.



**This reprocessing took place successively in three facilities:**

- experimental pilot facility for reprocessing FBR fuels: AT1 facility in La Hague from 1969 to 1977. The capacity was 1 kg/day (150 kg/year),
- pilot facility at Marcoule (APM) from 1973 to 1997 the capacity of which increased from 2 t/year to 5 t/year,
- UP2-400 plant at La Hague where reprocessing is performed by dilution with GCR fuels.

All of the reprocessing facilities in operation at that time, are given in the table below, and the place of fast reactor spent fuels in the three matching aforementioned facilities.



**Experiment in the AT1 facility in La Hague:**

This facility was the prototype for French fast reactor spent fuel reprocessing technology. It was operated from 1969 to 1977 and primarily tested reprocessing techniques on fuels from Rapsodie, before testing a few fuels from Phénix.

As always in reprocessing operations for Phénix assemblies, they were dismantled in the examination bay (CE) of the Phénix power plant, and the pins removed, placed in a holster, and sent for reprocessing. Shearing operations were carried out pin by pin in the AT1. Then dissolving was carried out intermittently, with successive extraction cycles to initially separate the fission products, then uranium and plutonium.



AT1 facility in La Hague

The table below lists all the AT1 campaigns that helped validate the principles of fast reactor spent fuel reprocessing, on more than 15,000 pins (Rapsodie and Phénix combined), with burn-up ranging from 40,000 to 120,000 MWd/t and cooling time between 6 and more than 24 months.

Campaign	Number of needles	Quant U+Pu (kg)	Core max. burnup (MWd/t)	CT (months)
1969	281	16.5	40 000	6
1970	576	43.4	53 000	6
1971	641	49.1	52 000	12
1972-A	934	37.1	52 000	2.5
1972-B	634	46.5	55 000	> 6
1972-C	1808	70.5	85 000	2 to 6
1973-A	697	49.2	55 000	12
1973-B	760	25.7	68 000	12
1974-A	3103	115.5	90 000	4 to 12
1974-B	1687	80.4	90 000	12
1975-A	190	34.3	8350	
1975-B	908	33.6	95 000	1.5 to 5
1976-A	534	11.3	24 000	
1976-B	303	10.8	120 000	6
1976-C	454	17.2	85 000	12
1976-D	152	5.5	85 000	12 to 24
1977-A	166	28.4	44 200	8
1977-B		11.9		> 24
1977-C	156	7.9		> 24
1977-D	1493	58.8	90 000	> 24

Table summarizing reprocessing campaigns at the AT1.

It should be noted that only 142 kg of U+PU of this reprocessing was from Phénix. The reprocessed quantities mainly came from Rapsodie+Fortissimo.

## Reprocessing experiment at APM

The reprocessing at the Marcoule pilot facility took place on the TOP line (2 t/year) from 1973 to 1983. Then renovation work was carried out from 1984 to 1987 at the APM to increase capacity to 5 t/year, on the TOR line.

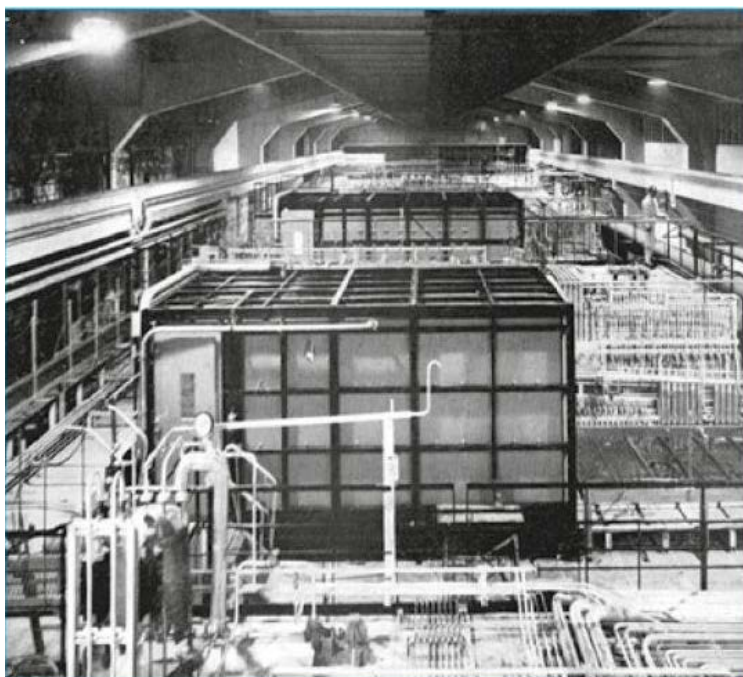


Marcoule pilot facility.

Phénix's first core, on the TOP line (UO2 enriched by 26% in U-235) was reprocessed from 1976 to 1978 (2.3 t), then from 1978 to 1983, 6.8 t of Pu was reprocessed from Pu cores at Phénix. The table below summarizes the last campaigns.

Campaign	Quantity U+Pu (kg)	Core max burnup (MWd/t)	Ct months
P0-Core 1	154	37 000	10 to 30
P1-Core 2	198	37 000 to 48 000	14
P2-Core 1	740	55 000 to 65 000	30 to 50
P3-Core 2	1840	55 000 to 72 000	23 to 40
P4-Core 2	2193	55 000 to 83 000	14 to 40
P5 - Cores 1 and 2	1644	35 000 to 101 000	15 to 42
<b>Total</b>	<b>6769</b>		

Table summarising TOP campaigns



TOP line at the Marcoule pilot facility.

The operations started up again on the TOR line in 1988 and enabled 7.3 t from the Phénix PU cores to be processed from 1988 to 1991. The campaigns were conducted, with burn-up up to 105,000 MWd/t.

At the APM, operations also took place with individual pin shearing, intermittent dissolving, and with extraction cycles using pulsed column and mixer-settler.

It should be noted that at the end of the APM's life, pilot R&D units will test techniques for improving processes with spacer wire removal methods, continuous dissolving, trapping dissolving off-gas, shell melting, etc.



TOR dissolver.

It should also be noted that research was conducted on the vitrification of the fission products obtained. Marcoule's PIVER unit thus vitrified the solutions of fission products originating from the reprocessing two metric tons of Phénix fuel.



Shell melting unit.

## Reprocessing experiment at UP2-400 in La Hague:

The UP2-400 unit in La Hague was not specifically dedicated to fast reactor spent fuel. It processed approximately ten metric tons of Phénix fuel from the internal core, i.e. the least PU-enriched with burnup ranging from 24 to 91,000 MWd/t.

Year	U+Pu (t)	Burnup (GWd/t)
1979	2.1	43 to 56
1980	1.5	
1981	2.2	
1982	2	24 to 91
1984	2.1	
<b>Total</b>	<b>9.9</b>	

Table summarising reprocessing campaigns at UP2-400.

Operations were conducted with Phénix holster shearing, intermittent dissolving and adjusting with GCR solutions for extraction.

## Feedback review on reprocessing techniques

- **Dismantling of assemblies**

The very thick hexagonal tube of fast reactors prohibits shearing the entire assembly, as with water reactors. Assemblies, relieved of their sodium, had to be dismantled to extract the pins. This operation was performed at the plant's examination bay (EC), by mechanical milling on the TH's corner, then separation and extraction of the bundles of pins arranged in holsters.

- **Shearing of pins**

For this operation, the question arises of whether or not to remove the spacer wire first. The answer depends on how the shears and dissolver operate.

It should be noted that the Phénix experiment took place without prior removal of the wire. The shearing into sections, was carried out without any problems, either one pin at a time (AT1 and TOP), or rows of pins (TOR) or by direct shearing of holsters (UP2-400).

- **Fuel dissolving**

Two aspects are to be considered: the most thorough dissolving possible of uranium and plutonium in nitric acid at boiling point, and the behaviour of cladding material in the same environment.

The uranium oxide and plutonium oxide form solid solutions at a certain ratio beyond which they become insoluble.

The Phénix cores (core 1 at 18% and core 2 at 25%) did not cause any problems within the limits of the burn-up tested.

As for the cladding materials, the materials tested: 316 L, 316 Ti and 15-15 TI showed good behaviour.

- **Clarification**

The separation of insoluble products before the extraction operations, does not pose any specific problem to fast reactor spent fuel.

- **Extraction cycles**

These operations are not specific to fast reactor spent fuels either and the improvements made in the context of water reactors are transferable.

However, it should be noted that assemblies cooled for at least five years must be used in order to remain within the usual standards of thermal power solutions.

- **Waste**

Once again few specific problems. The validation of fission product vitrification (PIVER) should be noted and the specific problem of fast reactor spent fuel stainless steel shells in which melting seems the best process to develop.

### **Conclusion**

520 assemblies, i.e. the equivalent of about 4 and a half Phénix cores have been reprocessed. Taking into account the 2.3 metric tons from the first UO<sub>2</sub>-enriched cores, this represents a little over 26 metric tons.

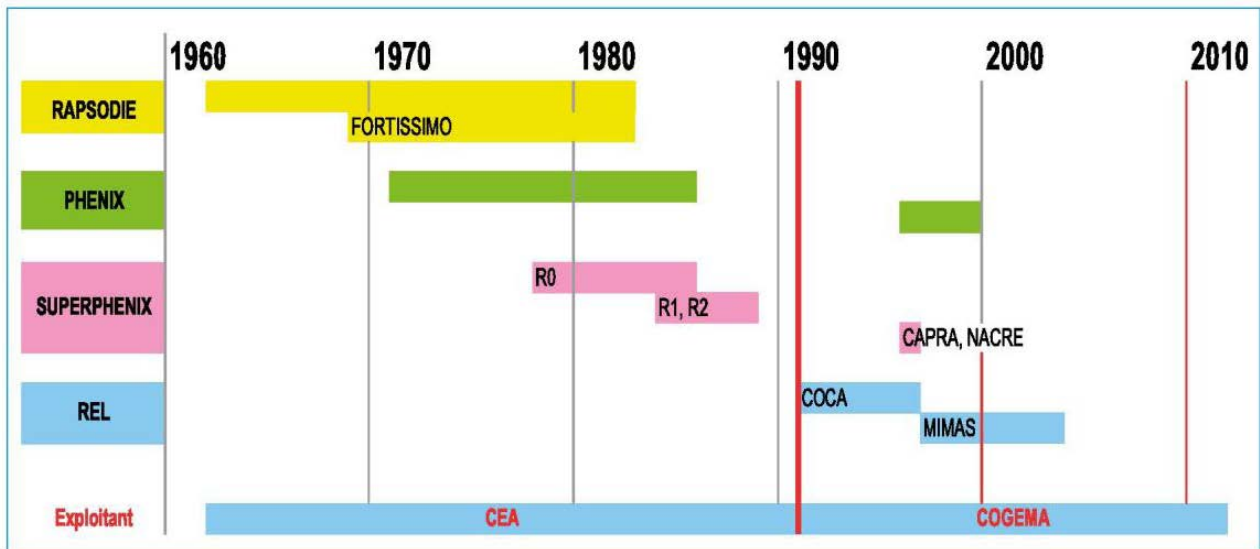
It should also be noted that the measurements and assessments made during the reprocessing operations, were used to measure an overall breeding rate of 1.16 and thus experimentally confirm the expected theoretical values (1.13).

## **Feedback on fuel production**

All the Phénix fuels were produced in the ATPu facility at Cadarache which also produced the Rapsodie, PFR and Superphénix pellets.

Reactors	No. of pins	No. of pallets (millions)	Pallets (tml)	Pu mass Pu (t)
Rapsodie	28 536	1	1.2	0.35
<b>Phénix</b>	<b>180 941</b>	<b>12.6</b>	<b>32.4</b>	<b>8.2</b>
Superphénix	208 396	16.9	71.2	12.7
PFR (GB)	9 555	0.7	1.6	0.54
<b>Total</b>	<b>427 428</b>	<b>31.2</b>	<b>106.4</b>	<b>21.8</b>

Production of oxide fuels for fast reactors from 1963 to 1999.



The 181,000 Phénix pins were made before 1991 by the FBR process and then the COCA process.

An important goal was to reuse the plutonium produced by reprocessing it to make new Phénix assemblies and show the industrial possibilities of fast reactor multi-recycling.

Of the 4.4 metric tons of Pu produced, 3.3 metric tons were reused to make fuel for Phénix as per the attached diagram.

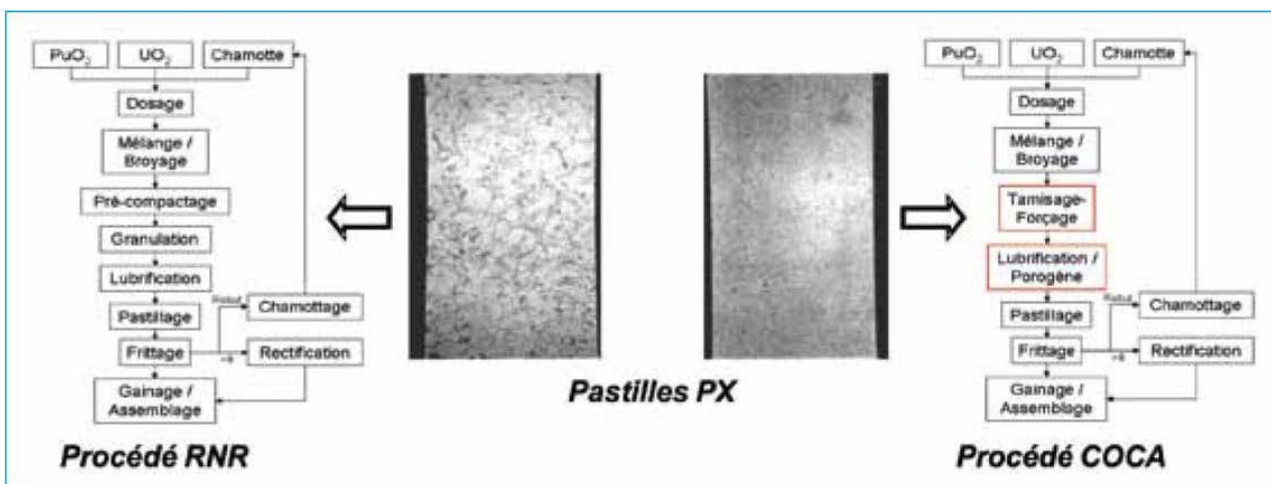
In 1980, the first assembly produced using Phénix recycled Pu was loaded in the reactor and performed the first cycle closure.

This experiment culminated in the CPD 408 assembly (Fontenoy Experiment) which used recycled plutonium for the third time.

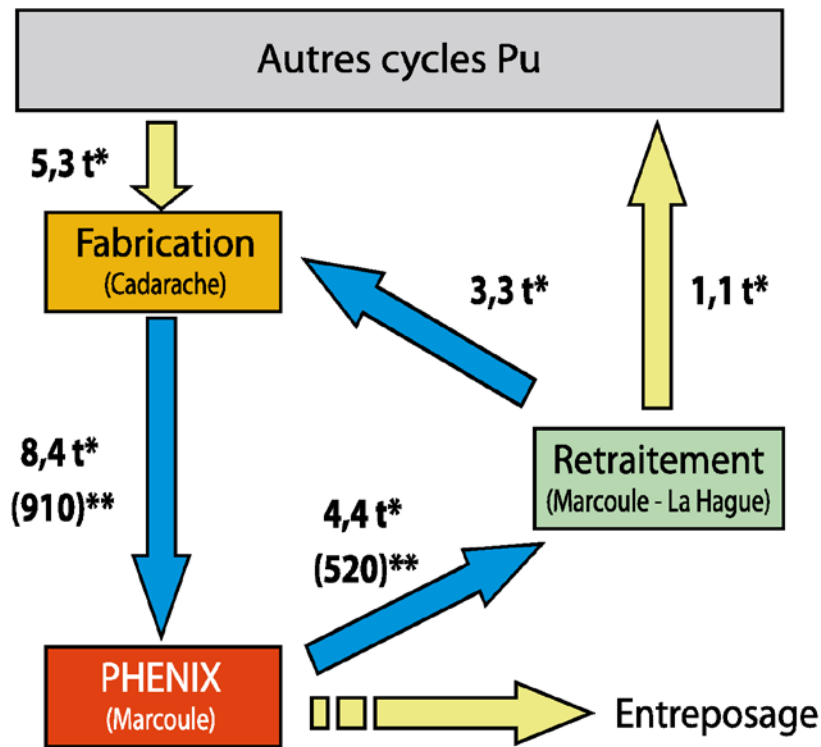
The plutonium obtained at APM was sent to La Hague, in the form of nitrate, for oxide conversion. As this conversion was performed with dilution in GCR fuel products, it was not possible to monitor the isotopic evolution of the fuel as it went through the reactor.

This isotopic evolution was, historically, more closely linked to the origin of the Pu used: GCR, Phénix, and then

REL as well as its ageing (increase in Americium content).



## Phénix - Flux plutonium totaux (fin 1995)



\*Masse de Pu métal - \*\*Nombre d'assemblages

### Applications for future reactors

Breeding rates and the ability to reprocess industrially have been demonstrated through the reprocessing of 520 Phénix assemblies.

3.3 metric tons of the 4.4 metric tons of Pu thus extracted were reused to make new Phénix assemblies that were re-burned in the reactor.

For reactors of the future, it should be noted, that increases in Pu content, increases in burn-up, or changes to cladding material would require validation in terms of dissolving processes.

Aside from these reservations, and notwithstanding improvements that are still possible, the feasibility of reprocessing has been proven.

Similarly, an industrial demonstration of the feasibility of fuel production was achieved, by using this reprocessed plutonium, and its recycling in the reactor.

### REFERENCE

[1] BOOK "Phénix Retour d'expérience" Chapter 25. J Guidez October 2012

# Preliminary considerations on the startup phase for the ASTRID core

G Mignot

CEA, DEN, DER, 13108 Saint Paul lez Durance, France

**Abstract.** This paper presents preliminary considerations on the startup phase for the ASTRID core, as well as an overview of the different steps before reaching the optimised equilibrium core. The start-up phase is assumed to cover the period between loading the dummy core into the reactor (for commissioning tests) and achieving the optimised equilibrium core. Four main stages are considered: a first stage of start-up tests before fuel core loading, a second stage related to zero power and power ramp-up tests, a third stage corresponding to the transition from the first core to the equilibrium contractual core, and the last stage to reach the optimised performance for the equilibrium core. In the two last stages, a sub-assembly surveillance plan based on post-irradiation examinations is taken into account.

As this work is in its preliminary stages, the first scenarios shown for the start-up phase must not be considered as the ASTRID reference scenarios. The scenarios strongly depend on the assumptions considered in the analysis, whereas those discussed in this paper aim at outlining the content and the duration of the starting phases for the ASTRID core, which will be useful in subsequently assessing the core sub-assembly fabrication needs. Assumptions for the start-up phase will be updated in accordance with progress on the ASTRID core design development and core qualification programme.

## 1. Introduction

In this paper, preliminary considerations on the startup phase for the ASTRID core are presented, with focus placed on the transition period ranging from the first core to the optimized equilibrium core.

Four main stages are considered:

- A first stage of commissioning tests before fuel core loading,
- A second stage related to zero power and power ramp-up commissioning tests,
- A third stage corresponding to the transition from the first core to the equilibrium contractual core,
- A last stage to reach the optimised performance for the equilibrium core.

The assumptions considered for the reactor start-up are based on feedback from the Superphénix1 commissioning tests [1] and the results of preliminary calculations dealing with equilibrium core management.

It is considered that the optimised equilibrium core is the 1500 MWth CFV v1 core design [2].

## G Mignot

During the transition phase from the starting core to the equilibrium optimised core, a surveillance plan of fuel sub-assemblies is taken into account in the calculations. This programme aims at verifying the behaviour of some fuel sub-assemblies by post-irradiation examinations at intermediate burn-ups before achieving the target burn-up.

### 2. ASTRID core design

As already mentioned, the optimised equilibrium core considered in the analysis is the 1500 MWth CFV (very low sodium void coefficient) V1 core [2] which is the current reference core design for ASTRID.

Figure 1 and Table 1 show the core layout and main features of the CFV V1 core design.

<i>1500 MWth CFV V1 Core</i>	
Fuel sub assemblies (internal / external core)	291(177+144)
Control rods	18 (12+6)
Fuel	(U,Pu)O <sub>2</sub>
Clad material	Austenitic steel (AIM1)
Number of batches / Fuel cycle length (EFPD)	4 x 360
Fuel residence time (efpd)	1440
$\Delta\rho$ core burn-up reactivity loss (pcm/efpd)	-4,3
Na void worth (\$)	-0,5
Breeding gain	-0,02
Plin max at beginning of life (W/cm)	483

**Table 1: 1500 MWth CFV V1 AIM1 core data**

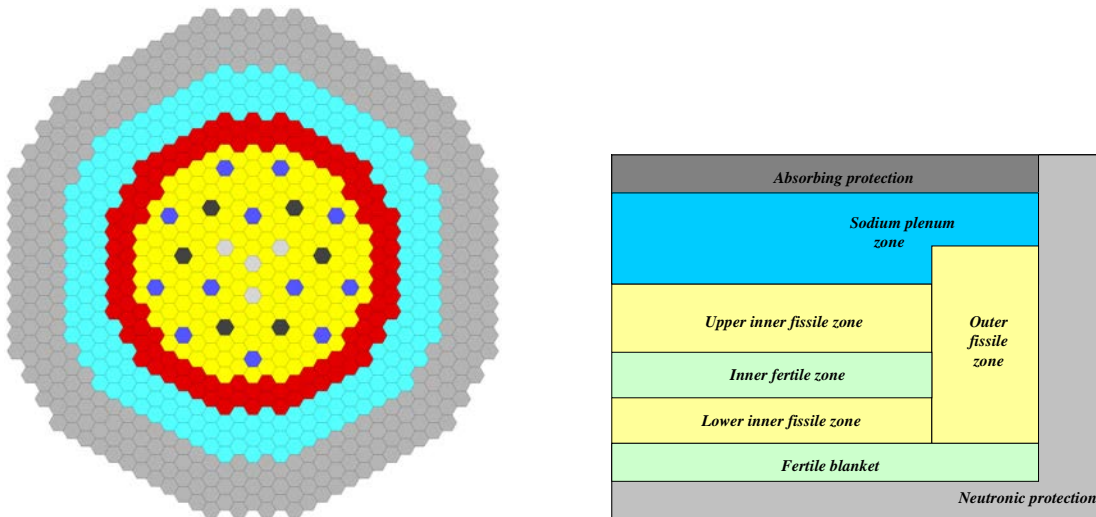


**Figure 1: 1500 MWth CFV V1 AIM1 core design**

### 3. The main stages of the startup phase

Four stages have been defined for the start-up phase for the ASTRID core (Fig. 2):

- commissioning tests before fuel core loading; during this stage, the dummy core is set up in the reactor, and the gas and sodium tests are carried out on the fuel handling systems as well as thermohydraulic and mechanical tests on the reactor components.

- zero power and power ramp-up commissioning tests; this stage begins with fuel loading in the reactor for the first divergence and zero power tests. Power ramp-up tests are then performed until 100% nominal power is reached.

- transition from the start-up core to the equilibrium contractual core; the contractual equilibrium core is characterised by a limited fuel burn-up which has been authorised by the licensing authorities, based on fuel qualification elements given before reactor start-up and the planned sub-assembly surveillance programme.

- increase of fuel performance to reach the optimised equilibrium core; the performance of the optimised equilibrium core corresponds to the maximum core performance according to the technology limits of the fuel cladding material. The maximal performance levels are reached progressively on the basis of a fuel surveillance plan.

The scenarios of these 4 stages are discussed in the following paragraphs.

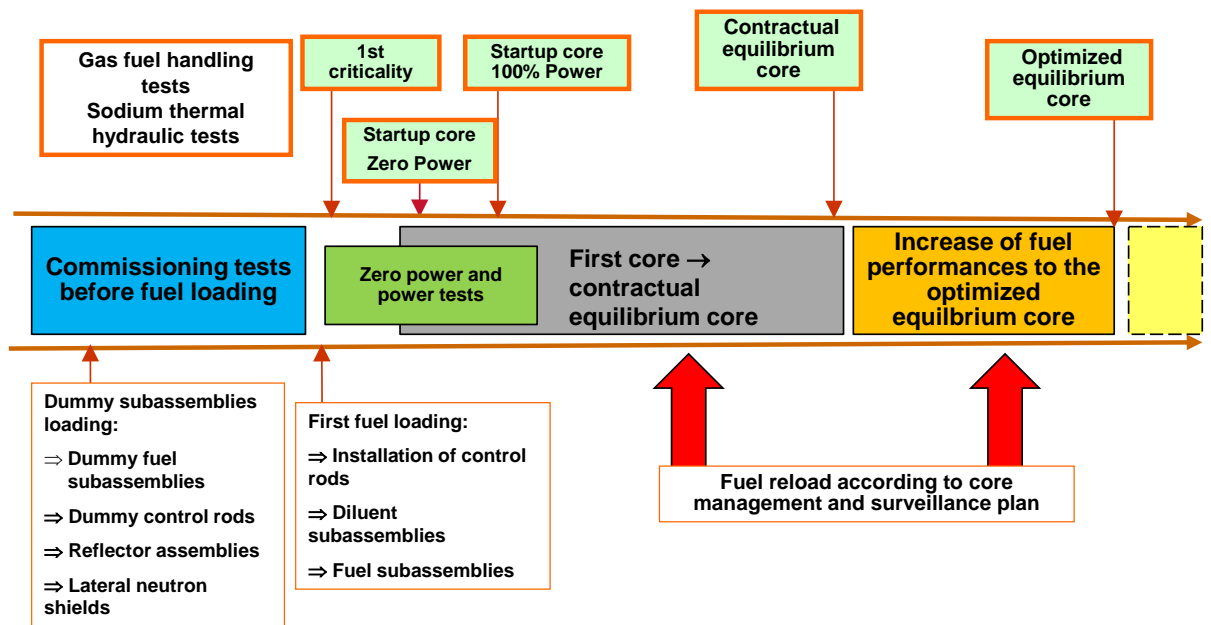


Figure 2: Core configurations during startup periods

#### 3.1. Commissioning tests before fuel core loading

It currently seems reasonable to consider assumptions similar to those of Superphenix for the ASTRID commissioning tests before fuel loading [1].

For Superphenix, these tests were divided in two parts:

## G Mignot

- the first part aimed at individually testing in a gas environment the different basic systems in relation to the nuclear reactor and the balance of plant. In the reactor, air tests were performed on components to check vibration, confinement and interface issues. In particular, after the implementation of the dummy core in the reactor vessel, tests were carried out on control rod drive mechanisms and handling systems (transfer machines, casks and rotating plugs).

At the end of this first part, the nuclear reactor was ready to be filled with sodium. This period lasted about 2 years.

- the second part was dedicated to integral tests in the nuclear reactor after filling the primary and secondary systems with sodium. Isothermal tests were performed, in particular fuel sub-assembly handling tests with dummy sub-assemblies and hydraulic tests inside the reactor vessel. Experimental assemblies equipped with instrumentation were introduced into the core to carry out measurements inside the core and in the diagrid.

This period lasted about 18 months. At the end, the dummy control rod assemblies were unloaded and replaced with the real control rod assemblies; neutron counters for the first criticality were also installed inside the core.

### **3.2. *Zero power and power ramp-up commissioning tests***

Like for the first phase of the commissioning tests, tests similar to those performed for Superphenix are being considered for ASTRID.

In the beginning, the fuel is loaded in the reactor and the fuel sub-assemblies replace the dummy core. These tests consist of:

- first divergence and zero power tests,
- power ramp-up tests up to 100% of nominal power.

The first criticality in Superphenix occurred 2 months after the beginning of the fuel loading. Fuel was introduced progressively by batches of sub-assemblies in order to produce a first critical core. This first divergence core layout is composed of fewer fuel sub-assemblies than the start-up core. After the first divergence, the start-up core was completed by adding fuel sub-assemblies to get the start-up core layout, and zero power tests were performed over 3 months.

Power ramp-up tests were then carried out over 30 months, at intermediate power levels (20%, 50% and 100% full power). Specific core tests were performed to verify the absorber worth, neutron flux distribution and reactivity coefficients. Complementary tests were also carried out to explore incident operating conditions (operating with a defective component) and natural convection conditions. During this test period, the average reactor availability factor was about 30%.

### **3.3. *Transition from the start up core to the equilibrium contractual core***

The third stage involves the transition from the start-up core to the equilibrium contractual core and includes the phase of power ramp-up tests, as shown in Figure 2.

All the fuel sub-assemblies in the start-up core consist of fresh fuel. To limit excess reactivity, diluting sub-assemblies are placed inside the core in substitution of some of the fuel sub-assemblies. From this start-up core, the equilibrium core is achieved by successive fuel batch reloading to finally obtain a core pattern composed of fuel sub-assembly batches with different burn-ups. The maximum fuel burn-up is the contractual burn-up allowed by licensing authorities with regards to fuel qualification elements available before reactor start-up.

The following assumptions are considered for this stage:

## G Mignot

- When the power ramp-up tests are finished, the average availability factor is assumed to be 70% which is similar to the Phenix and BN600 reactors during the first 10 years of reactor operation,
- The Pu enrichment in the fuel sub-assemblies is the same as for the optimised equilibrium core. This assumption is satisfactory in terms of simplifying fuel fabrication processes and core management.
- The fuel residence time of the contractual core is assumed to be equal to 720 EFPD, which is half of the optimized core residence time. The core pattern is divided into 4 batches with fuel reloading every 180 EFPD.
- The core management assumption to reach the contractual equilibrium core aims at reducing the irradiated fuel storage requirements.
- A fuel surveillance plan will be carried out during this stage. The surveillance programme aims at assessing the behaviour of some of the fuel sub-assemblies by post-irradiation examinations at intermediate burn-up before achieving the target burn-up. The fuel surveillance plan has not yet been defined and it is considered that it should not change the core management schedule established to achieve the contractual equilibrium core.

A preliminary scenario for this stage is given in Figure 3. It can be seen that the contractual equilibrium core is obtained about 5 years after fuel loading in the reactor.

At the end of every cycle,  $\frac{1}{4}$  core is unloaded and is replaced by fresh fuel. The strategy of reusing the irradiated fuel is not discussed in this paper.

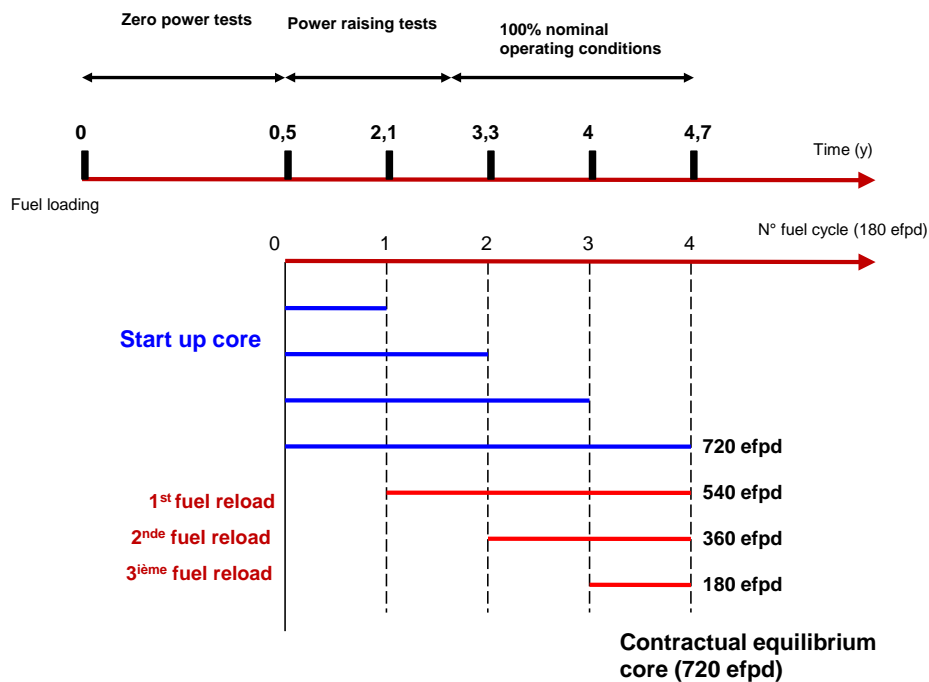


**Figure 3: Transition period from start-up core to contractual equilibrium core**

### 3.4. *Increasing of fuel performances to the optimised equilibrium core*

As shown in the table 1, the fuel residence time of the optimised equilibrium core with AIM1 fuel clad material is equal to 1440 EFPD.

The following assumptions are considered for this stage:

- the reactor availability factor is 70% over the whole period,
- the Pu enrichment of fuel sub-assemblies is similar to the optimised equilibrium core,
- the increase in the fuel performance is obtained step by step, according to a specific fuel surveillance plan.

At the beginning, the allowed maximum fuel residence time is considered to be equal to 720 EFPD. When a core fuel batch is irradiated up to 720 EFPD, it is then unloaded from the core except for some fuel sub-assemblies which remain inside the core and are irradiated up to the next target residence time. The step between two target values is assumed to be 360 EFPD. So, when these precursor sub-assemblies are irradiated up to 1080 EFPD, post-irradiation examinations are performed to check the condition of the fuel elements. The time to obtain the results of post-irradiation examinations (PIE) on the precursor sub-assemblies – including the fuel cooling time and transport – is assumed to be 2 years. If the results of post-irradiation examinations are satisfactory, the core fuel sub-assemblies should be allowed to be irradiated up to the new target value, which equals 1080 EFPD in this example.

- the core reloading pattern is divided in 4 batches with fuel batch reload every 360 EFPD
- as in the previous stage, the core management to reach the optimised equilibrium core aims at reducing the irradiated fuel storage needs.

A preliminary scenario for this period is given in Figure 4. The figure shows the core batch management from the contractual core until achieving the optimized equilibrium core performances (red lines on the figure 4). Also, the irradiation time of the precursor subassemblies and the duration of post irradiation examinations are shown. It can be observed that the fuel subassemblies in the core are allowed to be irradiated up to 1080 EFPD at the end of the 9<sup>th</sup> cycle, and up to the optimum performances (1440 EFPD) at the end of the 15<sup>th</sup> cycle. So, the performances increase is allowed after 8 years to change the fuel residence time from 720 to 1080 EFPD and after 13 years to change the fuel residence time from 1080 to 1440 EFPD.

Moreover, it can be noticed the time from the initial fuel loading to obtain the optimized equilibrium core is about 15 years, considering a reactor availability of 70% during this period. For availabilities of 60% or 80%, the duration can vary between 16 and 13 years.



## G Mignot

- The stage of commissioning tests is based on Superphenix feedback.

A first preliminary scenario for the start-up phase can be defined as shown in Figure 5.

It can be seen that:

- the dummy core is loaded 42 months before fuel core loading in the reactor,
- the end of the commissioning tests is 36 months after fuel core loading,
- the contractual equilibrium core is reached about 5 years after fuel core loading,
- the optimised equilibrium core is obtained about 15 years after fuel core loading.

This first scenario must not be considered as the optimised reference scenario for the ASTRID start-up phase. This paper only sets out to provide a preliminary indication and an estimate of the duration of the start-up phase so as to highlight the most influential assumptions. A sensitivity study will be performed in the near future to quantify the impact of the most important parameters on the start-up phase. Once the scenarios have been consolidated, they will then be used to assess the core sub-assembly fabrication needs.

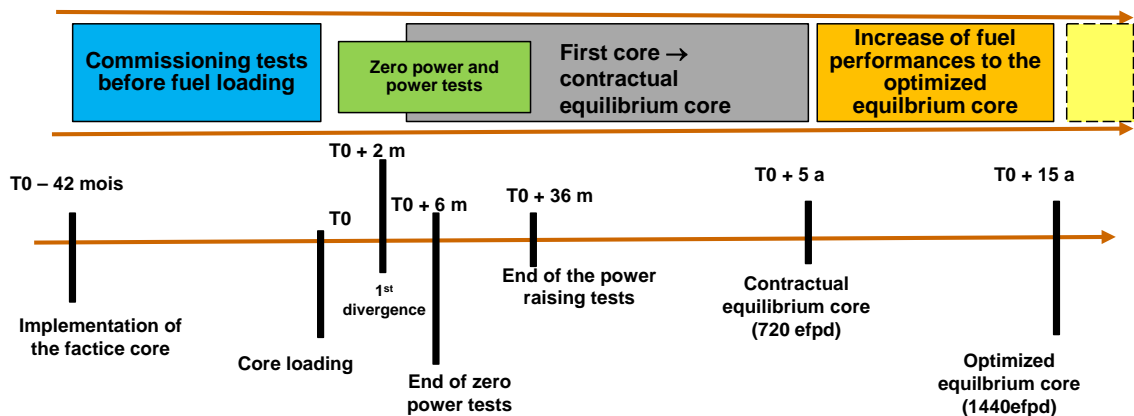


Figure 5: Preliminary overview of the start-up phase for ASTRID core

## REFERENCES

- [1] Fundamental aspects on the design and performances of the Superphenix reactor core Nuclear Science and Engineering – Vol. 106 N° 1 Sept. 1990
- [2] B. Fontaine et al. “The French R&D on SFR core design and ASTRID Project” Proc. of GLOBAL 2011 - Makuhari, Japan, Dec. 11-16, 2011

# Study of the tritium distribution in the effluents resulting from the sodium hydrolysis

A. Chassery<sup>a,b,c</sup>, H. Lorcet<sup>a</sup>, J. Godlewski<sup>a</sup>, K. Liger<sup>a</sup>, C. Latge<sup>a</sup>, X. Joulia<sup>b,c</sup>

<sup>a</sup>CEA, DEN, Cadarache, DTN, F-13108 Saint-Paul-Lez-Durance, France

<sup>b</sup>Université de Toulouse ; INPT, UPS ; Laboratoire de Génie Chimique ; 4, Allée Emile Monso, F-31030 Toulouse, France

<sup>c</sup>CNRS ; Laboratoire de Génie Chimique ; F-31030 Toulouse, France

**Abstract.** Within the framework of the dismantling of Sodium Fast Breeder Reactors (SFBR), several processes are under investigation regarding sodium disposal. One of them rests on the implementation of the sodium-water reaction, in a controlled and progressive way, to remove residual sodium mainly from cold traps. This particular sodium contains impurities such as sodium hydrides, sodium oxides and tritiated sodium hydrides. During the hydrolysis of these various species, the tritium is distributed between the liquid and the gaseous effluents, according to its forms HT and HTO. HTO being 10,000 times more radiotoxic than HT, a precise knowledge of the mechanisms governing the distribution of tritium is necessary in order to design the process needed to treat the off-gas before its release into the environment. This paper presents some experimental results of the tritium distribution between the various effluents generated and provides a phenomenological description of a polluted sodium hydrolysis.

## 1. INTRODUCTION

Liquid sodium, used as a coolant fluid in Sodium Fast Breeder Reactors (SFBR), can contain several impurities such as oxygen or hydrogen, present from the start or introduced during certain servicing or handling operations on components or fuel assemblies. Another contaminant that can be found in the sodium is the tritium, a radioactive hydrogen isotope, produced by fission reactions. In order to operate in safe conditions, the sodium is purified in devices called cold traps, in which the crystallization of the sodium oxide ( $\text{Na}_2\text{O}$ ), sodium hydride ( $\text{NaH}$ ) and co-crystallization of tritiated sodium hydride ( $\text{NaT}$ ) is induced by cooling. The crystals thus formed are trapped on a woven steel wool support (FIG.1). When these devices need to be dismantled, the residual sodium and impurities must be removed.



FIG. 1. Section of a woven steel wool support loaded with polluted sodium ( $\text{Na}+\text{Na}_2\text{O}+\text{NaH}+\text{NaT}$ ).

Various methods have been proposed or developed in the past to remove residual sodium from cold traps [1]. One of them rests on the implementation of the sodium-water reaction (SWR) to remove films or clusters of residual sodium. This reaction is highly exothermic and is characterized by the generation of large volumes of hydrogen gas and the production of soda. In order to use this reaction in a controlled and progressive way, a process called ELA (Enceinte de Lavage en Actif) is under development mainly for the cleaning of cold traps from the prototype fast breeder reactor PHENIX.

In ELA, the hydrolysis reaction should be performed in a vessel that can be opened for introduction of a batch of waste. Wastes are placed in a basket made of perforated metallic sheets to give access to sprayed water. The spray system consists of ramps of upward-oriented nozzles located at the bottom of the vessel underneath the basket. Such an arrangement facilitates sodium hydroxide evacuation and avoids formation of retained pools and strong reactions between water and sodium. A high flow rate of inert gas is also injected, resulting in local cooling and effective sweeping of the reaction area.

The resulting sodium hydroxide solution is drained into a separate collection tank for further processing. Generated hydrogen is vented via an off-gas line. The control of the reaction is done by on-line measuring of hydrogen concentration in gas release and controlling the water flow rate. Inert gas is partly vented together with an off-gas and partly recirculated. ELA's vessel is shown in FIG. 2.

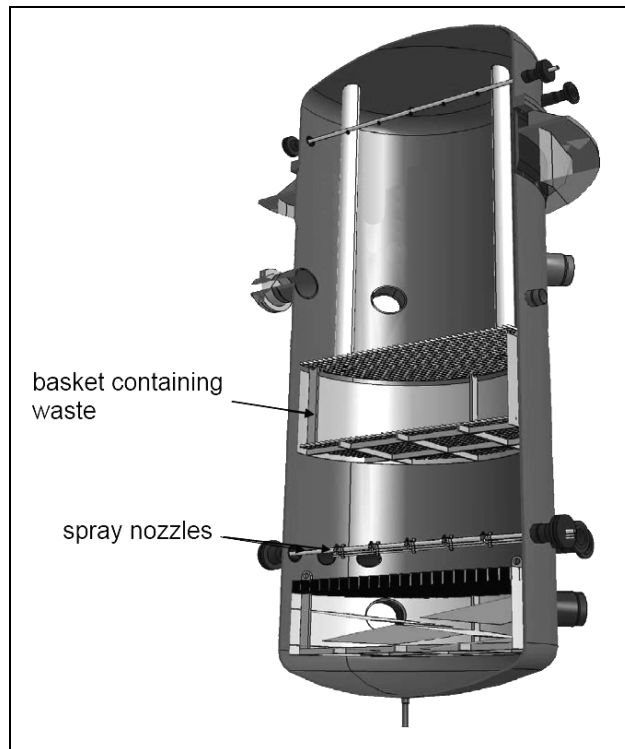


FIG. 2. ELA preliminary design.

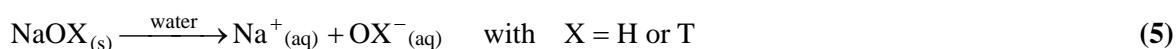
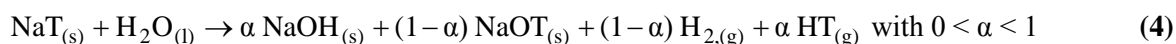
In order to design the process, a precise knowledge of the composition of the effluents is needed. Indeed, the tritium distribution between the gaseous and liquid effluents, and within the gaseous effluent, according to its chemical form HT(g) or HTO(v), is critical for designing the elements needed to treat the off-gas before its release into the environment.

Based on previous studies carried out on the chemical reactions between water and elements containing sodium, this paper provides a phenomenological description of a polluted sodium hydrolysis performed according to ELA's experimental conditions. This study is carried out in order to provide a numerical modelling of the phenomena involved in such an operation to predict the composition of the effluents produced, especially regarding tritium contamination. After a description

of the chemical reactions involved in such an operation, some experimental results of the tritium distribution in the gaseous effluent according to its chemical form will be presented. Some propositions will be made to explain this experimentally observed distribution and the one expected to be in ELA. Finally, a phenomenological study has been carried out to develop a model that is partially described in the last part of this paper.

## 2. CHEMICAL REACTIONS INVOLVED IN A POLLUTED SODIUM HYDROLYSIS

When water comes into contact with Na(s), Na<sub>2</sub>O(s) and NaH(s), it induces the generation of reaction products such as NaOH and H<sub>2</sub>. The number of chemical reactions involving these various elements can lead to a complex reactional scheme. Several studies have been previously carried out on the chemical system Na-H-O [2], [3]. These studies have shown that the occurrences of all the possible chemical reactions depend mainly on the pressure and temperature conditions. Within ELA experimental conditions, the process runs at atmospheric pressure. The temperature inside the vessel is below 313 K in normal operating conditions and it is assumed for the development of the model that the maximum temperature reached at the reaction surface area is the one of a boiling solution of soda (423 K – 473 K). Under these conditions, the following main reactions have been considered:



All these reactions are exothermic, the heat generated by a mole of sodium is, respectively for each reaction,  $\Delta_r H^0_1 = -141 \text{ kJ}\cdot\text{mol}^{-1}_{\text{Na}}$ ,  $\Delta_r H^0_2 = -82 \text{ kJ}\cdot\text{mol}^{-1}_{\text{Na}}$ ,  $\Delta_r H^0_3 = -76 \text{ kJ}\cdot\text{mol}^{-1}_{\text{Na}}$ ,  $\Delta_r H^0_4 = -82 \text{ kJ}\cdot\text{mol}^{-1}_{\text{Na}}$  and  $\Delta_r H^0_5 = -45 \text{ kJ}\cdot\text{mol}^{-1}_{\text{Na}}$  [4]<sup>1</sup>.

According to the reaction (4) described above, the only gaseous by-product containing tritium should be HT(g). The rest of the tritium should be present in the liquid effluent as OT<sup>-</sup> ions or as tritiated water HTO(l), according to the dissolution reaction (5) occurring when water is added in excess.

## 3. TRITIUM DISTRIBUTION BETWEEN THE EFFLUENTS

Tritiated water HTO being 10,000 times more radiotoxic than HT, it is important to know precisely what the composition of the off-gas will be in ELA in order to design the process needed to treat the off-gas. Therefore, a few experimental results of the tritium distribution in the gaseous effluent, obtained from radioactive sodium hydrolysis operations performed at the CEA Cadarache, have been gathered in this paper.

During these hydrolysis operations, the gaseous effluent was sent towards a set of four feeding bottles. HTO(v) was trapped in the first two bottles, by means of the bubbling principal. The remaining tritium, in its HT(g) form, was then converted to HTO(v) in a oven by an oxidation reaction, and finally trapped into the last two bottles. The quantity of tritium was finally measured in each bottle by

---

<sup>1</sup> For the calculation of  $\Delta_r H^0_4$ , it has been assumed that the standard enthalpies of formation of NaT, NaOT and HT were the same as the standard enthalpies of formation of NaH, NaOH and H<sub>2</sub> respectively.  $\Delta_r H^0_5$  is the heat of solution of NaOH at infinite dilution.

liquid scintillation counting in a laboratory. The tritium distribution in the gaseous effluent according to its chemical form is shown for each experiment in FIG. 3.

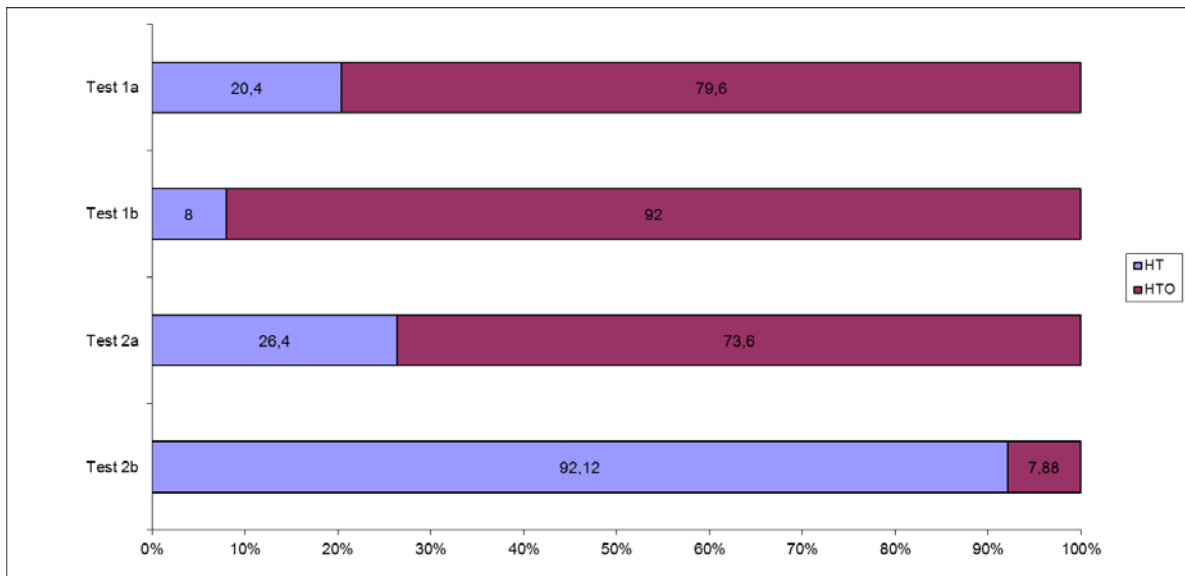


FIG. 3. Experimental results showing the tritium distribution in the gaseous effluent according to its chemical form HT or HTO.

Two different types of experimentations were carried out :

- The experimental results referred to as *Test 1a* and *Test 1b* are from hydrolysis operations performed in the CEA facility KALINA, where large amounts of sodium (respectively 27 kg and 210 kg) have been hydrolyzed using water jet pipes. These operations were performed under atmospheric conditions with an extraction flow rate of the gaseous effluent of  $10,000 \text{ Nm}^3 \cdot \text{h}^{-1}$ . The results point out that a large amount of tritium is in the gaseous effluent as HTO(v).
- The results referred to as *Test 2a* and *Test 2b* are from hydrolysis operations performed on smaller quantities of sodium (inferior to 10 g), in a vessel swept by an inert gas flowing at about  $1 \text{ l} \cdot \text{min}^{-1}$ . Water was added drop by drop to the sodium. Even if *Test 2a* seems to be in good accordance with the results from KALINA, *Test 2b* shows a small amount of HTO(v) in the gaseous effluent (7,88% of the total tritium). There is no significant difference in the experimental conditions between these two tests. Further experiments are needed to explain these results.

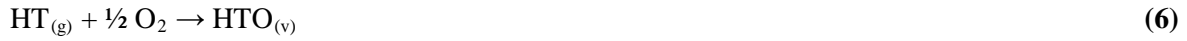
These hydrolysis operations have not been performed with the aim to study the tritium distribution. Therefore, most of the experimental conditions are not available and may vary from one experiment to another, but these results can nevertheless point out that, depending on the experimental conditions of the hydrolysis, HTO(v) can be present in the gaseous effluent (in an amount up to 90% of the tritiated gaseous products).

This unexpected presence of HTO(v) may be explained by two different possible mechanisms :

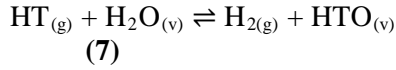
- a conversion of HT(g) in the gas phase,
- a phase change of HTO(l) produced by the hydrolysis reactions.

### 3.1. Conversion of HT(g) into HTO(v)

In the atmosphere, HT can be converted into HTO either by the oxidation reaction :



or by the isotopic exchange reaction :



These reactions have been studied previously and information on their feasibilities and kinetics can be found in the references [5], [6].

According to these previous studies, the oxidation reaction (6) is negligible at ordinary temperatures unless catalyzed. Efficient catalysts for this reaction could be :

- a metallic catalyst (Pb, Pt, PtRh, CuO...),
- $\beta$ -radiation induced from tritium decay,
- UV radiation,
- humidity (the presence of water vapor in  $\text{O}_2$  increases the conversion rate by a factor of 3 [5]).

Even if the experiments in KALINA have been carried out in presence of oxygen, no metallic catalyst was involved neither UV radiation. As for the  $\beta$ -radiation, the maximum activity in KALINA for these experiments was estimated to  $2.53 \times 10^{-11} \text{ mCi} \cdot \ell^{-1}$ , which is not sufficient to efficiently catalyze the oxidation reaction according to the studies carried out by Casellato et al. and mentioned in reference [5].

As for the isotopic exchange reaction (7), in absence of an efficient catalyst, the reaction does not proceed. It has been demonstrated that a more rapid equilibrium is possible when the reaction is catalyzed by:

- a metal or metal oxide,
- $\gamma$  or X-ray irradiation,
- $\beta$ -radiation [6].

For the same reasons, as described above for the oxidation reaction, the isotopic exchange cannot be efficiently catalyzed in KALINA. As for the results referred to as *Test 2a* and *Test 2b*, the maximum activity expected to be reached in the vessel was  $1.125 \times 10^{-4} \text{ mCi} \cdot \ell^{-1}$ , assuming a flow rate of inert gas of  $1 \ell \cdot \text{min}^{-1}$ . According to the reference [6], this activity is not high enough to catalyze the reaction.

In both cases, these mechanisms cannot provide an explanation of the presence of  $\text{HTO}_{(v)}$  observed in the experimental results. Other phenomena must be involved in tritium distribution. In this study, the assumption is made that tritiated water may be produced in the liquid phase and then converted into vapor by various mechanisms.

### 3.2. Conversion of $\text{HTO}_{(l)}$ into $\text{HTO}_{(v)}$

Part of the tritium initially present in the tritiated sodium hydride  $\text{NaT}_{(s)}$  could be converted into  $\text{NaOT}_{(s)}$  according to the reaction (4). This  $\text{NaOT}_{(s)}$  thus formed, as for the  $\text{NaOH}_{(s)}$ , should be dissolved by the continuous water supply. In the liquid film formed at the surface area,  $\text{OT}^-$  ions produced by reaction (5) could contribute to the self-ionization of water and produce tritiated water by the following reaction (8).



### A. Chassery et al.

This liquid tritiated water could then be converted into vapor which could explain the experimental results. In this study, three different phenomena have been selected to explain the possible transformation of  $\text{HTO}_{(l)}$  to  $\text{HTO}_{(v)}$ .

- The thermodynamic equilibrium at the interface between the solution of electrolytes and the surrounding gas. Assuming that this equilibrium could be reached, some amount of HTO present in the liquid film could be transferred to the gas phase.
- The effective sweeping caused by the inert gas supply could lead to a partial evaporation of water and tritiated water present in the drop.
- The heat of the reactions (1) to (5) could rise the temperature of the electrolyte solution up to its boiling point causing its partial vaporization.

Applying the conclusions of this preliminary study to predict the composition of the effluents in ELA, it can be pointed out that, because the atmosphere in ELA does not contain oxygen, the oxidation reaction cannot proceed. As for the isotopic exchange, among all of the catalysts cited above, the  $\beta$ -radiation is the only mechanism that should be present in ELA. But regarding to the maximum activity that can be reached in the process, estimated under  $10 \text{ mCi} \cdot \ell^{-1}$ , only 0.1% of HT could be converted in a day time [6]. The residence time in ELA being estimated inferior to 5 min, a negligible amount of  $\text{HT}_{(g)}$  should be converted to  $\text{HTO}_{(v)}$ . The only possible explanation for a hypothetical presence of  $\text{HTO}_{(v)}$  in the off-gas could be the vaporisation of liquid tritiated water. Some additional experiments are required in order to study the different phenomena cited above to explain this phase change. Nevertheless, these mechanisms have been selected in this study to propose a phenomenological description of a polluted sodium hydrolysis performed in ELA.

## 4. PHENOMENOLOGICAL DESCRIPTION OF A POLLUTED SODIUM HYDROLYSIS

A first scenario has been developed based on several studies previously cited and carried out on the chemical system Na-H-O and on the SWR. Some of the hypotheses made to set up this model are also deduced from experiments performed at the CEA on the sodium hydrolysis, with or without tritium involved. This phenomenological description is shown in FIG. 4.

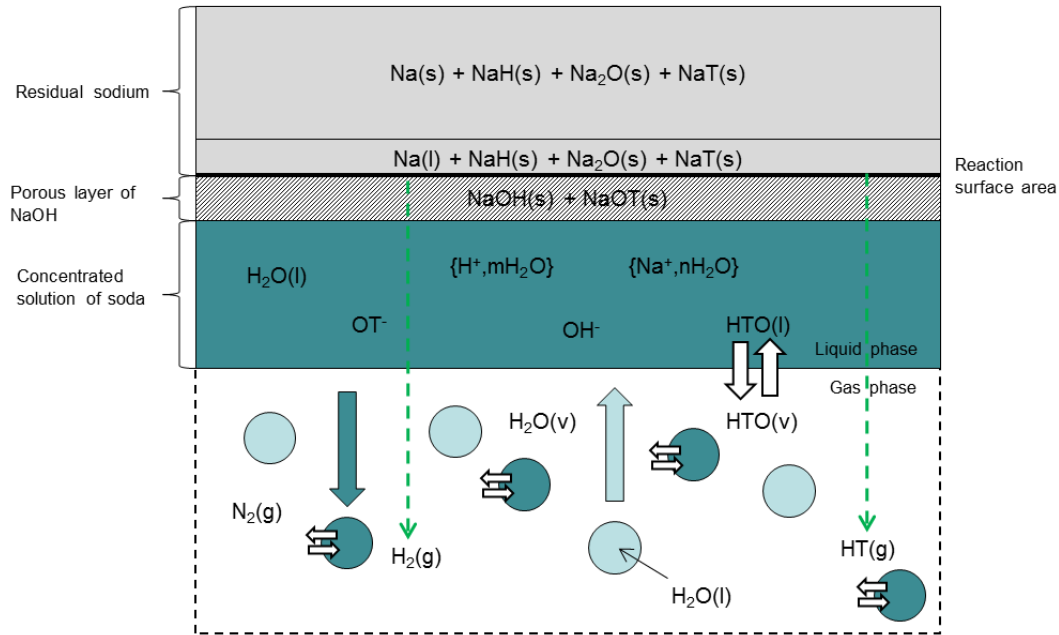


FIG. 4. Scenario of a polluted sodium hydrolysis.

It describes a polluted sodium hydrolysis performed in the experimental conditions expected to be reached in ELA. Water, sprayed underneath a cluster of polluted sodium, will react according to the chemical reactions (1) to (4) described in part 2. The NaOH and NaOT produced will form a porous layer between the sodium and the liquid film. The thickness of this layer should be defined by an equilibrium between the production of NaOX (X standing for H or T) and its dissolution into the liquid film. Assuming the reactions (1) to (4) to be instantaneous, the diffusion of water through the porous layer of NaOX should be a limited step for the overall sodium hydrolysis. The liquid film composed of a saturated solution of sodium hydroxide, falls down in droplets under the influence of gravity. These droplets of electrolyte solution, containing some amount of HTO(l), may be partially evaporated by the counter-current flow rate of inert gas. Gaseous products, H<sub>2</sub>(g) and HT(g), are vented with the inert gas.

The heat produced by the highly exothermic reactions between sodium, its impurities and water and by the dissolution of NaOX(s) heats the sodium up to its melting point (371 K at atmospheric pressure) and makes it melt close to the reaction surface. An amount of this heat of reactions is expected to be absorbed by the liquid film, causing its partial vaporization. The rest of the energy produced would be absorbed by the inert gas.

This scenario is based on the main hypotheses cited below:

- The surface reactions are instantaneous.
- Heat of reaction is absorbed by :
  - the fusion at 371 K of the sodium.
  - the vaporization of the liquid film which is at its boiling point ; its temperature depends on the concentration of the solution of soda (expected to be close to the saturation).
  - the high flow rate of inert gas. In ELA, the reaction area should be swept by a large amount of inert gas, added to a massive recirculation of thousands of cubic meters per hour.
- Gaseous by-products are transported with the inert gas.

- NaOX is in solid state near the surface reaction, making a porous layer limiting the transport of water to the reaction surface.
- The porous layer of NaOX is dissolving into the liquid film. The concentration is expected to be the one of a saturated solution of soda at the solid-liquid interface.
- The sodium hydroxide solution is in thermodynamic equilibrium with the surrounding gas.

A first step in the modelling of the hydrolysis based on this scenario is the modelling of the vapor-liquid equilibrium (VLE) between the solution of electrolytes and the gas phase. A study has been carried out on this VLE and is presented below.

## **5. TOWARDS A NUMERICAL MODEL : THE MODELLING OF THE VLE BETWEEN THE LIQUID FILM AND THE SURROUNDING GAS**

One of the hypotheses presented above to explain the transfer of HTO from liquid phase to gas phase is the achievement of the vapor-liquid equilibrium between the liquid film and the surrounding gas.

A special thermodynamic model is needed to describe the VLE of a system in which the liquid phase is an electrolyte solution. In this study, three models, available in Simulis Thermodynamics<sup>2</sup>, have been tested to predict the composition of the vapor phase in equilibrium with liquid solutions of sodium hydroxide. The experimental results presented are from a study carried out by Krey [7] and the models used in the calculation of the activity coefficients are:

- UNIQUAC Electrolyte SW [8], [9], [10]
- Sour Water [11], [12], [13]
- ULPDHS [14]

A modelling of the vapor-liquid equilibrium at the temperature of 373.15 K is shown in FIG. 5.

---

<sup>2</sup> <http://www.prosim.net/en/software-simulis-thermodynamics-3.php>

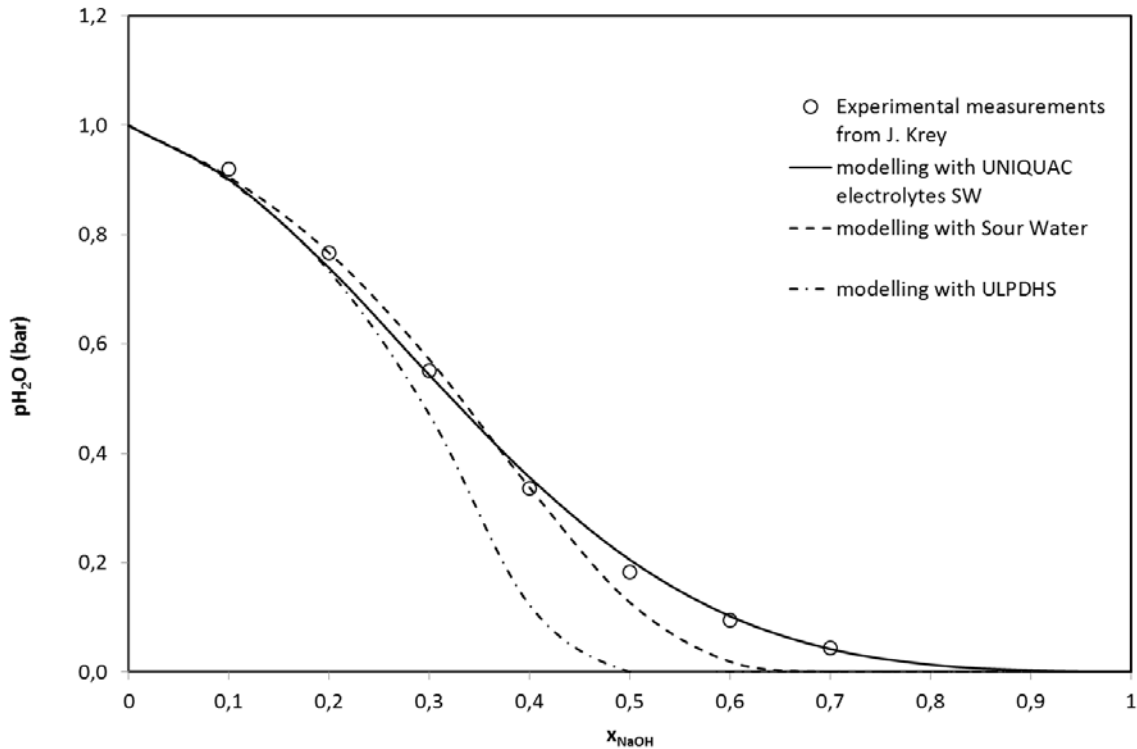


FIG. 5. Modelling of the vapor-liquid equilibrium for the system  $\text{NaOH-H}_2\text{O}$  at 373.15 K

The modelling results show that the best correspondence with experimental measurements, with a maximum percent error of 11%, is achieved with *UNIQUAC Electrolytes SW*. Regarding to these results, this thermodynamic model has been chosen to be used in the modelling of the overall hydrolysis, assuming the thermodynamic behavior of the chemical species HTO and NaOT to be the same as the one of  $\text{H}_2\text{O}$  and  $\text{NaOH}$ .

## 6. CONCLUSIONS AND PERSPECTIVES

Based on experimental results, some hypotheses have been made to explain the unexpected presence of tritiated water in the gaseous effluent observed during a polluted sodium hydrolysis. The chemical reactions able to convert  $\text{HT(g)}$  into  $\text{HTO(v)}$  cannot provide an explanation to these observed results. The assumption has been made that  $\text{HTO(v)}$  may be produced by one or more of this three phenomena listed below:

- The vapor-liquid equilibrium at the interface between the solution of electrolytes and the surrounding gas.
- The evaporation of  $\text{HTO(l)}$  caused by the high flow rate of inert gas.
- The vaporization of  $\text{HTO(l)}$  caused by the heating of the liquid film.

Based on these assumptions, a first scenario has been developed to describe the phenomena involved in a polluted sodium hydrolysis performed in ELA. This phenomenological description is used to develop a numerical model that will enable to predict the gaseous effluent composition, especially in terms of tritium, in order to design the process needed to its treatment.

Some additional experiments are actually performed at the CEA Cadarache in order to validate the hypotheses presented in this paper.

REFERENCES

- [1] LATGE, C., “A new process for the removal of impurities in the cold traps of Liquid Metal Fast Reactors”, IAEA Technical Committee Meeting, Aix-en-Provence (1997) 244-267
- [2] MAUPRE, J.P., “Etude des systèmes ternaires Na-C-O et Na-H-O dans la partie riche en sodium”, PhD Thesis, Université de Provence – Centre Saint-Charles (1978)
- [3] FORD, J.A., « Literature review of sodium-water reactions » (1965)
- [4] GREEN, D.W., PERRY, R. H., “Perry’s Chemical Engineers’ Handbook”, 8<sup>th</sup> Edition, McGraw-Hill (2008)
- [5] BURGER, L.L., “The Conversion of Tritiated Hydrogen to Water in the Atmosphere”, Pacific Northwest Laboratories, Richland, Washington (1976)
- [6] YANG, J.Y., GEVANTMAN, L.H., “Tritium  $\beta$ -Radiation-Induced Isotopic Exchange with Water Vapor”, Journal of Physical Chemistry, Volume 68, Number 11 (1964)
- [7] KREY, J., Z. Phys. Chem. Neue Folge 81:252 (1972)
- [8] THOMSEN K., RASMUSSEN P., Chem. Eng. Sci., Vol.54, pp.1787-1802 (1999)
- [9] THOMSEN K., RASMUSSEN P., GANI R., Chem. Eng. Sci., Vol.51 N°14, pp.3675-3683 (1996)
- [10] PEREDA S., THOMSEN K., RASMUSSEN P., Chem. Eng. Sci., Vol.55, pp.2663-2671 (1999)
- [11] EDWARDS T. J., MAURER G., NEWMAN J., PRAUSNITZ J.M., AIChE Journal, Vol. 24, n°6, pp. 966-976 (1975)
- [12] BEILING V., RUMPF B., STEPP F., MAURER G., Fluid Phase Equilibria, 53, pp. 251-259 (1989)
- [13] RUMPF B., MAURER G., Fluid Phase Equilibria, 81, pp. 241-260 (1992)
- [14] ACHARD, C., “Modélisation des propriétés d’équilibre de milieux biologiques et alimentaires à l’aide de modèles prédictifs”, PhD Thesis, Université Blaise Pascal (1992)

# Validation of BN reactor plant long-term operation

**B.A. Vasilyev, O.Yu. Vilensky, V.B. Kaidalov**

JSC “Afrikantov OKBM”, Nizhny Novgorod, Russia

**Abstract.** Sodium-cooled fast reactor operation is characterized by impact of high temperatures, thermocyclic loads during transients and intensive neutron flux on structural materials. Main material failure mechanisms are creep, fatigue, embrittlement and irregular swelling. During service life extension for BN-600 and new generation RP, possible technological and operational component defects are taken into account. Within 2006 - 2011, material studies for austenitic steel 18Cr-9Ni used as base structural material for BN reactor components were carried out, swelling, fatigue, long-term strength, and crack velocity as a function of different temperatures and neutron flux intensities were obtained. Provisions of corresponding regulatory document were approved on validation of integrity for critical non-replaceable components of BN-600 reactor and being constructed BN-800 RP within 45 years of operation. One of the objectives for BN-1200 RP is provision of 60-year operation life. Hence, extension of steel 16Cr-11Ni-3Mo application for BN-1200 reactor partially used in BN-800 reactor is provided.

## 1. Introduction

Possible long-term operation of BN reactor plant (RP) depends mainly on life characteristics of non-replaceable equipment. First of all, this equipment is vessel and reactor in-vessel metal structures. During operation, most of this equipment is inaccessible for non-destructive testing to detect the defects and to repair them. Therefore, design analysis is very important to validate the operability of mentioned structures. In view of the above-mentioned and due to specific operation conditions of some BN reactor in-vessel metal structures (high temperatures and intensive neutron flux), it was required to develop the new methodology (as compared with the industrial “Codes for NPP Equipment and Piping Strength Analysis norms for strength” [1]) for structure strength validation in view of radiation swelling effects, radiation-thermal creep, degradation of mechanical properties of structural materials within the time period up to  $3 \cdot 10^5$  hours and under irradiation as well as growth of postulated crack-like defects to provide the increased operation life (up to 45 years).

This methodology is presented in the standard regulatory document (RD) “Procedure of strength analysis for main components of sodium cooled fast neutron reactor plants” [2]. The provisions of this RD were approved during validation of operability of BN-600 “critical” non-replaceable components when extending the operation life from 30 to 45 years; and the long-term properties of structural materials within the time period up to  $3 \cdot 10^5$  hours and under irradiation were also used to validate strength of non-replaceable components of BN-800 RP under construction within the specified term of 45-year operation.

To validate the increased operation life of BN RP, it is also necessary to validate the life time of the secondary circuit high-temperature equipment (heat exchangers, pipelines, steam generators (SG)), which can be replaced or repaired only once during operation.

One of the main objectives for BN-1200 RP (generation 4) is provision of 60-year operation life. In this connection, it is proposed to extend steel 16Cr-11Ni-3Mo application in RP vessel and heat exchange components partially used in BN-800 and new steel 12Cr-Ni-Mo-V-Nb application in SG components carrying out the required material and methodological studies.

## 2. Operation loading conditions and main failure mechanisms in non-replaceable BN RP components

The list of “critical” non-replaceable BN RP components, which determine the plant lifetime, was made based on the following criteria:

- safety effect;
- impossibility to replace and repair;
- inaccessibility for visual inspection and technical condition monitoring;
- maximum values of main damaging factors - radiation exposure, primarily, as well as temperature and thermo-cyclic load impacts.

According to these criteria for provision of BN-600 operation life increase, the following reactor equipment was identified as “critical” (Fig. 1): vessel, pressure chamber, reflector, headers, support belt, pressure pipeline unit, heat exchanger support, side shielding pipes.

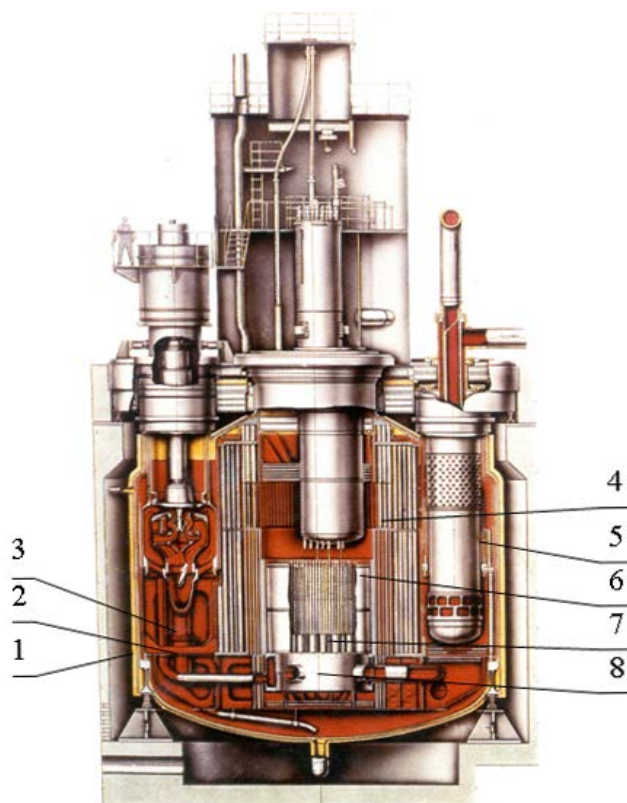


FIG. 1. BN-600 reactor “critical” non-replaceable components:

1 – vessel; 2 – support belt; 3 – pressure pipe unit; 4 – side shielding pipes; 5 – IHX support; 6 – reflector; 7 – headers; 8 – pressure chamber.

From the viewpoint of radiation damage, the structures located near BN-600 core are in the most unfavourable conditions; in the first place, it is the reflector shaping the array of core assemblies. Besides the high temperature levels and gradients along the height and thickness of the upper load-bearing shell of the reflector, this structure is subjected to the most intensive neutron irradiation, which varies considerably along the height and circumference of the shell that can result in irreversible form change. The maximum levels of neutron irradiation and temperature on the headers, where the core assemblies are installed, are considerably lower as compared with the reflector.

Heat exchange supports and side shielding pipes in the area of sodium overflow work in the area of increased temperatures and temperature variance.

The reactor vessel is subjected to rather low-dose irradiation under temperature of 430 °C maximum; the main loading factor here is weight loads and temperature gradients. Maximum excess pressure in reactor vessel is rather small – 0.14 MPa. The pressure chamber and pressure pipeline unit operate under the higher pressure of 0.8 MPa and under the temperature up to 375 °C in the conditions of cyclic loading and temperature variance (for pressure chamber).

The support belt is also subjected to temperature variances under temperature of 450 °C maximum; and also takes weight loads from the equipment arranged on.

Table 1 presents the operation conditions (in view of operation life increase up to 45 years) and corresponding main damage accumulation mechanisms for “critical” non-replaceable BN-600 reactor components (material is steel 18Cr-9Ni).

Table 1. The operation conditions and main damage mechanisms for BN-600 reactor components

Component	Maximum temperature, °C	Maximum neutron fluence (E>0.1 MeV), cm <sup>-2</sup>	Main damage accumulation mechanisms
Vessel	430	2.5·10 <sup>18</sup>	LCF*
Pressure chamber	370	6·10 <sup>19</sup>	LCF
Reflector	530	~10 <sup>23</sup>	Swelling, creep, LCF, embrittlement
Headers	385	~10 <sup>22</sup>	Embrittlement, LCF
Support belt	450	<10 <sup>18</sup>	LCF
Pressure pipe unit	375	<10 <sup>18</sup>	LCF
IHX support	540	10 <sup>18</sup>	HCF**, creep
Side shielding pipes	540	4·10 <sup>19</sup>	HCF, creep

\* LCF – low-cycle fatigue;

\*\* HCF – high-cycle fatigue.

Temperature and radiation loading conditions of the vessel and most non-replaceable in-vessel components of BN-800 reactor with the specified 45-year operation life are close to operation conditions of corresponding BN-600 reactor components and similar damage accumulation mechanisms appear in them. However, maximum temperature for BN-800 reflector is considerably lower (up to 460°C) due to its design variation and cooling conditions improvement; and maximum accumulated neutron fluence reduces by 30% owing to the additional absorber material (boron carbide) located in shielding assemblies installed near the elevator compartment.

BN-1200 RP design with 60-year operation life provides noticeable increase of sodium temperature at the core inlet (by 45-56 °C as compared with BN-600 and BN-800 reactors) and thus, reactor vessel components (up to 480 °C). Intensive irradiation of BN-1200 reflector shell (it decreases by ~ 10<sup>6</sup> times as compared with BN-600) is avoided due to substantial increase of in-core shielding and thus, its swelling and deformation consequently. In this case, maximum neutron fluence on non-replaceable structures of BN-1200 RP will achieve 6·10<sup>21</sup> cm<sup>-2</sup> (with E>0.1 MeV) on the headers over the operation life.

Table 2 presents maximum operation temperatures and fast neutron fluences (with  $E > 0.1$  MeV) over the operation life and associated variations in application of structural materials for the most loaded BN RP equipment components.

Table 2. Variations in the materials for BN equipment as a function of maximum operation parameters

Component	Material/temperature (°C)/ neutron fluence (cm <sup>-2</sup> )		
	BN-600	BN-800	BN-1200
Reactor vessel	18Cr-9Ni/430/2.5·10 <sup>18</sup>	18Cr-9Ni/430/6·10 <sup>17</sup>	16Cr-11Ni-3Mo/480/10 <sup>13</sup>
Reflector	18Cr-9Ni/530/10 <sup>23</sup>	16Cr-11Ni-3Mo/460/7·10 <sup>22</sup>	18Cr-9Ni/415/~10 <sup>17</sup>
IHX (tube sheets, shells)	18Cr-9Ni/550	16Cr-11Ni-3Mo/550	16Cr-11Ni-3Mo/550
Hot pipelines of the secondary circuit	18Cr-9Ni/518	16Cr-11Ni-3Mo/505	16Cr-11Ni-3Mo/527
SG:	(sectional)	(sectional)	(module-vessel)
- evaporator;	2Cr-Mo/452	2Cr-Mo/386	12Cr-Ni-Mo-V-Nb/527
- superheater	18Cr-9Ni/518	2Cr-Mo/505	–

### 3. Material studies and methodological provision for BN RP long operation life

In 2004, FSUE CRISM “Prometey” (St. Petersburg) together with JSC “Afrikantov OKBM” (Nizhny Novgorod) and other Rosatom organizations started a set of modern material studies to validate the operability of BN non-replaceable structures for extension of BN-600 RP operation life up to 45 years. The activities were emphasized to receive the long-term strength and ductility characteristics of BN-600 RP main structural material – austenitic steel 18Cr-9Ni within the time period up to 3·10<sup>5</sup> hours, and to take account of irradiation impact on swelling, ductility, creep, crack resistance and crack growth velocity for this steel. The full-scale parts of BR-10 and BOR-60 reactors and BN-600 package simulator were tested, and well-known data on standard mechanical properties, radiation swelling, creep, fatigue and crack resistance of foreign austenitic steels of 304 type were taken into account. As the result, the calculated temperature-dose dependences for steel 18Cr-9Ni and weld metal within the range of neutron fluence with energy  $E > 0.1$  MeV from 0 to 10<sup>23</sup> cm<sup>-2</sup>, irradiation and testing temperatures from 20 to 650 °C were obtained.

To analyze strength and to validate BN reactor main component operability during operation stages and to extend the specified RP operation life, FSUE CRISM “Prometey” and JSC “Afrikantov OKBM” developed and approved the procedures for analysis of various limiting states:

- initiation of crack under cyclic loading as per fatigue mechanism (for components with temperature of  $T \leq 450$  °C);
- initiation of crack under long-term static and cyclic loading at creep and fatigue (for components with temperature of  $T > 450$  °C);
- unstable crack development (initiated during operation or developed because of possible technical defects);
- loss of bearing capacity or leaktightness of pressure vessel or pipeline;
- inadmissible variations in geometric dimensions of structure component.

The results of material studies given above and methodological analytical procedures formed the basis of standard RD [2] used during operation stages and extension of RP specified operation life. This RD was approved by Rostekhnadzor, put in force by Concern “Rosenergoatom” in May 2007 and used for operability validation of “critical” non-replaceable components of BN-600 reactor for 45-year operation life [3].

In 2008-2010, FSUE CRISM “Prometey” and OKBM performed material studies of austenitic steel 16Cr-11Ni-3Mo, which is used for the reflector, IHX internals and secondary coolant circuit hot pipelines, to validate the operability of BN-800 RP non-replaceable components for 45-year operation life. This steel is more radiation- and heat-resistant and has lower regulatory requirements for austenization of welded joints (for operation temperature) as compared with steel 18Cr-9Ni. Based on metal studies of BN-600 reheater parts (steel 16Cr-11Ni-3Mo) and in view of well-known data on foreign austenitic steels of 316 type, the calculated temperature-dose dependencies were obtained for standard mechanical properties, radiation swelling, creep, fatigue and crack resistance of steel 16Cr-11Ni-3Mo for base metal and welded joint metal. Fig. 2-4 compare the calculated data on swelling deformations, radiation and temperature creep in view of irradiation effect for these steels under same loading conditions showing the advantage of steel 16Cr-11Ni-3Mo [4]. These properties were approved by Rostekhnadzor and included in updated RD [5] as a supplement. The temperature-dose dependencies for steels properties (16Cr-11Ni-3Mo and 18Cr-9Ni) were plotted as a function of damaging dose (up to 65 dpa that corresponds to neutron fluence with  $E > 0.1$  MeV of  $\sim 1.5 \cdot 10^{23}$  cm<sup>-2</sup>) and its gaining velocity instead of the dependence on neutron fluence and flux; this estimate is less conservative and more accurate.

The requirements for structural materials of commercial BN-1200 RP equipment being under design are stipulated mainly by maximum temperature and operation life of this RP (60 years) (~480000 h with plant capacity factor =0.9). To extend the operation life of high-temperature equipment and pipelines of BN-1200 RP up to 60 years, the corresponding operability validation of applied structural materials and welded joints is required. These activities have been performed by FSUE CRISM “Prometey” and OKBM since 2009 [6]. They include:

- study of mechanical properties of steel 1018Cr-9Ni and 0816Cr-11Ni-3Mo, which worked as a part of BN-600 RP components (IHX, CRDM, reheater);
- study of long thermal ageing effect on structural changes, standard mechanical properties and crack formation for steel 18Cr-9Ni and 0816Cr-11Ni-3Mo and welded joints;
- irradiation tests for creep and long-term strength of steel 18Cr-9Ni and 16Cr-11Ni-3Mo;
- development of the methodology to account the residual weld stresses in strength and longevity analyses, model of one-sided accumulation of deformations under cyclic loading, prediction of material surface damage depth at contact with sodium for a period of 60 years, etc.

It is planned to complete the work by issue of the Procedure for strength analysis of BN RP components at the design stage with corresponding Appendices for material properties in view of operation duration up to 500000 hours.

High-chromium steel 12Cr-Ni-Mo-V-Nb proposed to be used for vessel structures and for heat exchange tubes of BN-1200 SG refers to new materials. This steel has higher temperature and corrosion resistance as compared with perlitic steel 2Cr-Mo used in BN-600 and BN-800 SGs; it will allow increasing BN-1200 SG component service life from 20 to 30 years. Due to the fact that steel 12Cr-Ni-Mo-V-Nb is not included in the list of materials adopted for fabrication of NPP equipment [7], it is necessary to perform the integrated material studies to certify the base metal and weld joints.

As well, the activities are performed to develop the upgraded austenitic steels of 18Cr-9Ni and 16Cr11Ni3Mo type with increased content of nitrogen and decreased content of carbon for future application in commercial BN-1200 RP. It shall result in improved characteristics of corrosion resistance, long-term strength, creep and fatigue of these steels. Now, the upgraded steels have been melted, the test program has been agreed, base metal and welded joint samples have been fabricated,

and investigations of corrosion, short-term and long-term properties, as well as crack resistance and crack growth resistance started.

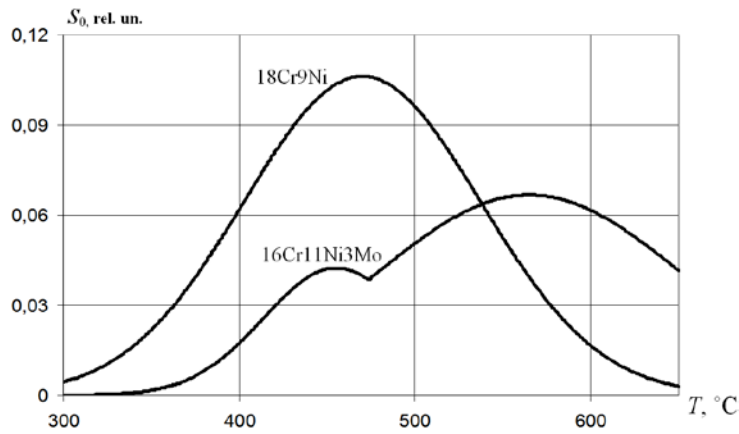


FIG. 2. Dependences of volumetric radiation swelling of steels at  $F=10^{23}$  n/cm<sup>2</sup>.

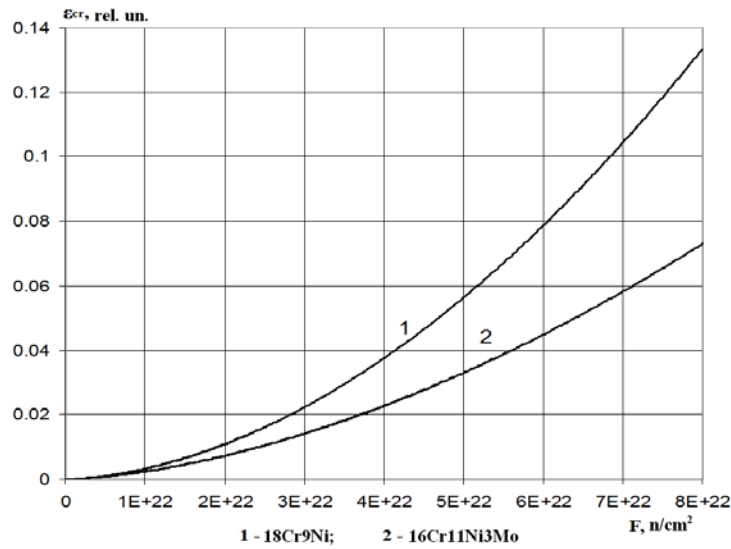


FIG. 3. Dependences of radiation creep at  $T=455$  °C.

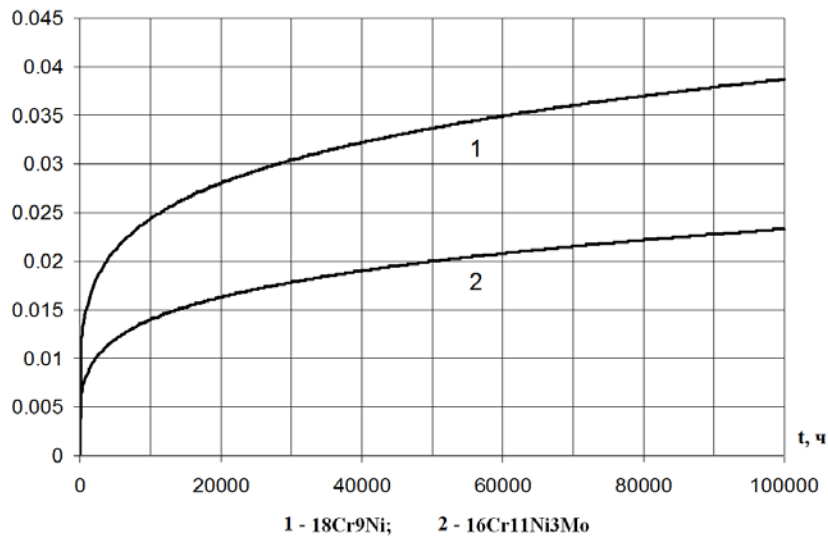


FIG. 4. Dependences of thermal creep at  $T=550$  °C and  $\Phi=2 \cdot 10^{13}$  n/cm<sup>2</sup>·s.

## 4. Validation of long-term operation life for non-replaceable components of BN RP

### 4.1. BN-600

The operability of non-replaceable components of BN-600 RP when extending operation life up to 45 years was validated using the developed RD [2].

Damageability under cyclic and long-term static loading in non-replaceable components of BN-600 reactor was estimated as per the results of stress-strained state analysis during various operation modes and showed that during 45 years, cracks initiation is possible in some components:

- upper load-bearing shell of the support (in the increased temperature areas under the elevator supports) due to creep under neutron irradiation;
- elevator supports (in the cut-out base for the guide tube) due to low-cycle fatigue under neutron irradiation;
- IHX support of isolated loop (near the lower part of inlet windows) under significant thermal pulsations during operation with two loops because of high-cycle fatigue.

As for the other non-replaceable components of BN-600 reactor, the damages accumulated during 45 years will be significantly lower than the allowable ones, and crack initiation is not anticipated. The analysis of postulated crack growth initiating during operation or propagating because of process defects showed that these cracks will not reach critical dimensions during BN-600 RP 45-year operation.

Under the conditions of neutron irradiation, the significant radiation damage is anticipated only in one non-replaceable component – upper load-bearing shell of the reflector. Deformation of this structure component is predicted due to non-uniform radiation and thermal impact by volume during 45-year operation. The analysis of reflector load-bearing shell deformation showed that this deformation will not result in loss of operability of equipment: core fuel assemblies, loading-unloading elevators and refuelling mechanism.

Thus, according to the investigation results [3], the operability of BN-600 reactor non-replaceable components is satisfied during 45-year operation. Based on the validation presented in 2010 after 30-year BN-600 RP operation life expiration, the license was received for operation life extension up to 2020. The Rostekhadzor will solve the issue of operation life extension up to 2025 (45 years) later.

### 4.2. BN-800

The operability of non-replaceable components of BN-800 RP within the specified operation life of 45 year was validated as per “Codes for NPP Equipment and Piping Strength Analysis” [1] using the provisions of actualized RD [5], referred to the long-term characteristics of structural materials within the period of time up to  $3.35 \cdot 10^5$  hours (45 years with plant capacity factor =0.85).

As per the results of cyclic and long-term static strength analysis, the damages accumulated during 45 years in non-replaceable components of BN-800 reactor do not exceed the allowable values; and crack initiation is not expected.

As it was mentioned above, the conditions of radiation and thermal loading of BN-800 reflector load-bearing shell are substantially lower than that of BN-600. Together with application of radiation-resistant steel 16Cr-11Ni-3Mo as BN-800 reflector structural material, it results in substantial decrease of radiation-thermal deformation of the reflector shell as compared with BN-600 reflector shall made of steel 18Cr-9Ni.

Figs. 5 and 6 present 20 x increased deformation of BN-600 and BN-800 reflector load-bearing shells respectively after 45-year operation. The predicted irreversible variation of main dimensions of reflector load-bearing shells due to radiation effect after 45-year operation is given in Table 3.

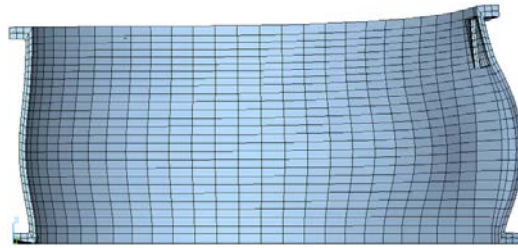


FIG. 5. Deformation of the upper load-bearing shell of BN-600 reflector after 45-year operation (central cross-section side view).

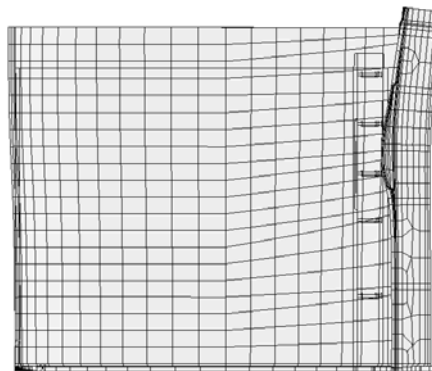


FIG. 6. Deformation of the load-bearing shell of BN-800 reflector after 45-year operation (central cross-section side view).

Table 3. The irreversible variation of main dimensions of reflector shells after 45-year operation

Reactor	BN-600	BN-800
Height increase on the side of maximum irradiation, mm	21	2.2
Height increase on the opposite side, mm	4	0.2
Radius increase in elevator compartment direction, mm	52*	5.3**
Radius increase in elevator compartment opposite direction, mm	10*	0.1**
Radius increase in elevator compartment perpendicular direction, mm	2.5*	≈0*
Variation of the distance between shell axis and compartment wall, mm	+8**	-6.7*

\* – in the centre of the core;

\*\* – at the reflector top.

Thus, it is shown that during 45-year operation, the irreversible dimension variations of BN-800 reflector load-bearing shell made of steel 16Cr-11Ni-3Mo are substantially less than those ones of BN-600 reflector load-bearing shell made of steel 18Cr-9Ni. The qualitative pattern of reflector load-bearing shell deformations (e.g., outside bending for BN-600 or inside bending for BN-800 in the area of maximum fluence) also differs considerably because of their design features, first, due to the wall welded near the elevator compartment along the entire height of BN-800 reflector load-bearing shell.

According to the results of the analysis, the irreversible variation of main dimensions due to irradiation effect will not result in operability loss of associated BN-800 reflector equipment: core assemblies, loading-unloading elevators and refuelling mechanism. At the same time, significantly less irreversible deformation of BN-800 reflector shell predicted for 45-year operation gives the possibility of positive consideration of BN-800 RP specified operation life extension.

#### **4.3. BN-1200**

To validate the operability of non-replaceable components of BN-1200 RP during 60-year operation life, the Procedure for strength analysis of BN RP components at the design stage is now under development. The procedure will define the methods and procedures of analysis of limiting conditions, which will allow, on one side, decreasing conservatism in damage accumulation estimates in the most loaded RP components under long-term operation at the design stage as compared with “Codes for NPP Equipment and Piping Strength Analysis norms for strength” [1], and, on the other side, taking into account of possible process defect development during long-term operation. The Procedure will also provide the Appendices on the properties of main structural materials for RP equipment and pipelines (austenitic steels 18Cr-9Ni and 16Cr-11Ni-3Mo) in view of long-term operation up to 500000 hours.

To provide additional long-term reliable and safe operation of BN-1200 RP equipment and pipelines it is assumed to develop and implement the lifetime operational monitoring system.

This system shall provide receiving of actual, less conservative estimates of lifetime characteristics of RP equipment and pipelines as compared with the design estimates due to:

- formation of list of equipment and components, which are critical by the conditions of strength, density, and technical, fire, radiation and/or nuclear safety;
- accounting of actual fabrication dimensions, design imperfections and initial defectiveness of material, which were revealed during RP equipment fabrication, installation and delivery trials ;
- accounting of actual (certificated) properties of base and welding structural materials used to fabricate the certain equipment;
- monitoring of actual loading conditions of RP equipment during controlled stages of operation as per automated process control system data;
- status control of base and welding materials as per the results of periodical equipment inspection during operation and as per instrument inspection during planned preventive maintenance;
- definition of structural material behaviour under actual operational conditions as per the results of witness sample periodical tests;
- revision of the moment of limiting condition achievement in the equipment and its residual lifetime estimation;
- revision of limiting condition progress kinetics stipulated by load-bearing capacity loss or allowable leak sizes, based on the condition of RP safety provision.

The novelty of this work for BN RP consists in application of procedure for definition and monitoring of the limiting conditions of the equipment based on the present-day developments in damaged medium mechanics and fracture mechanics, modern and advanced non-destructive inspection aids, computer codes and new information technologies.

## **5. Conclusion**

BN RP operation life duration is mainly determined by life characteristics of non-replaceable equipment – vessel and in-vessel structures of the reactor.

Due to specific conditions of BN reactor vessel and in-vessel structure operation (high temperature level, intensive neutron irradiation, inaccessibility for non-destructive tests of defects and repair) and to validate the long-term operation life (up to 45 years and more), new methodology was developed to validate structure strength in view of radiation effects and degradation of structural material mechanical properties within the time period up to  $3 \cdot 10^5$  hours and under irradiation, as well as development of postulated crack-like defects. This methodology is described in standard RD "Procedure of strength analysis for main components of sodium cooled fast neutron reactor plants".

Using this RD, the extension of operation life of BN-600 reactor non-replaceable components from 30 to 45 years, as well as strength and durability of the most loaded non-replaceable components of BN-800 RP under construction were validated for the specified 45-year operation life. Here, as per the conditions of radiation and temperature effect, austenitic steel 16Cr-11Ni-3Mo is used for the most loaded non-replaceable components of BN-800 RP, which is more radiation- and heat-resistant as compared with steel 18Cr-9Ni.

Wider application of austenitic steel 16Cr-11Ni-3Mo refers to new decisions in commercial BN-1200 RP design that allow increasing of operation life of the most loaded non-replaceable components of BN-1200 RP up to 60 years.

High-chromium steel 12Cr-Ni-Mo-V-Nb is a new material, which was proposed for SG design to increase the operation life up to 30 years. According to the regulatory requirements, the set of material tests shall be performed for this steel to validate and certify the base and welded joint material.

As for austenitic steels 18Cr-9Ni and 16Cr-11Ni-3Mo, the main task here is to study the long-term thermal ageing effect within the time period up to  $5 \cdot 10^5$  hours on structural variations and mechanical characteristics on the base and welded joint metal. In addition, the austenitic steels 18Cr-9Ni and 16Cr-11Ni-3Mo are now under upgrading for future application of them in commercial BN-1200 RP.

To provide additional long-term reliable and safe operation of BN-1200 RP equipment and pipelines, it is planned to develop and implement the lifetime operational monitoring system.

## **REFERENCES**

- [1] Codes for NPP Equipment and Piping Strength Analysis PNAE G-7-002-86. - M.: Energoatomizdat. – 1989. – 525p.
- [2] Procedure of strength analysis for main components of sodium cooled fast neutron reactor plants. RD EO 1.1.2.09.0714-2007. M: – 2007. – 181p.
- [3] VASILYEV, B.A. VILENSKY, O.YU., KAIDALOV, V.B., KAMANIN, YU.L., MARGOLIN, B.Z., GULENKO, A.G. Development of methodology and validation of operation life extension for BN-600 reactor vessel and non-replaceable components up to 45 years// Izvestiya VUZov, Yadernaya energetika, 2011. – No. 1, p.32-43.
- [4] KAPUSTIN, S.A., GOROKHOV, V.A., VASILYEV, B.A., VILENSKY, O.YU., KAIDALOV, V.B., OSETROV, D.L., MARGOLIN, B.Z., GULENKO, A.G. Comparative analysis of radiation-thermal deformation of BN-600 reactor reflectors (steel 18Cr-9Ni) and BN-800 reactor reflectors (steel 16Cr-11Ni-3Mo) as per the results of numerical simulation// Problemy mashinostroeniya i nadezhnosti mashin, Akademizdatstentr "Nauka" RAN. - 2011, No. 6, p.99-107.
- [5] Strength analysis for main components of sodium cooled fast neutron reactor plants. Procedure RD EO 1.1.2.09.0714-2011. M: – 2011. – 121p.
- [6] VASILYEV, B.A., VILENSKY, O.YU., KAIDALOV, V.B., SHEPELEV S.F. BN-1200 RP design features. Objectives for material studies provision. The 12<sup>th</sup> International conference "Material issues in design, manufacturing and operation of NPP equipment", CRISM "Prometey", St. Petersburg, June 5-8, 2012. Proceedings of the conference, vol.3, p.227-237.
- [7] Rules for Design and Safe Operation of NPP Equipment and Piping. PNAE G-7-008-89. M: Energoatomizdat, 1990. - 169 p.

# **Sodium loop decommissioning of PHENIX : Additional draining and preparation of carbonation IAEA-CN-199/430**

*F. DOMINJON<sup>a</sup>, C. BERETTI<sup>b</sup>, J.-M. HERBET<sup>a</sup>, J. MAS<sup>a</sup>*

<sup>a</sup>CEA MARCOULE - Commissariat à l'Energie Atomique, Département Exploitation des Installations de Marcoule (DEIM), Bagnols sur Cèze, FRANCE

<sup>b</sup>CEA MARCOULE Commissariat à l'Energie Atomique, Département des Projets d'Assainissement et de Démantèlement (DPAD), Bagnols sur Cèze, FRANCE

## **Abstract.**

French fast breeder nuclear power plant PHENIX stopped in July 2009.

The secondary circuits are formed of 3 loops of sodium. The treatment of the residual sodium in the loops will be realized in 3 steps: additional draining, carbonation and rinse. Additional draining and preparation of carbonation is ongoing.

The Commissariat à l'Energie Atomique (CEA) is the operator of PHENIX. Additional draining and preparation of carbonation is conducted by the CEA (PHENIX and decommissioning Department).

**After normal draining, sodium is still in the loop by two possibilities :**

## **1. Films of sodium,**

Best estimates are :

- 1 mm for horizontal surfaces,
- 30 microns for slope surfaces.

Estimate of the amount of sodium in film : 80 Kg per loop.

These films of Na will be directly treated by carbonation.

## **2. Retentions**

### **2.1. Large retentions**

These retentions are identified in sodium part of the steam generator.

These retentions will be treated by additional draining.

### **2.2. Small retentions**

- Expansion tank 23 mm max thickness of Na,
- Bottom of secondary loop 7 mm max thickness of Na,

- Thermal “get in” steam generator 65 g Na each,
- Auxiliary heater 10 mm max thickness of Na,
- Auxiliary pump 10 mm max thickness of Na,
- These retentions of Na will be directly treated by carbonation,
- Estimate of the amount of sodium in small retentions : 12 Kg per loop.

**2.3. Other retentions**

These retentions are identified in sodium loop, sodium valves not able to be drained, sodium discharge tank...

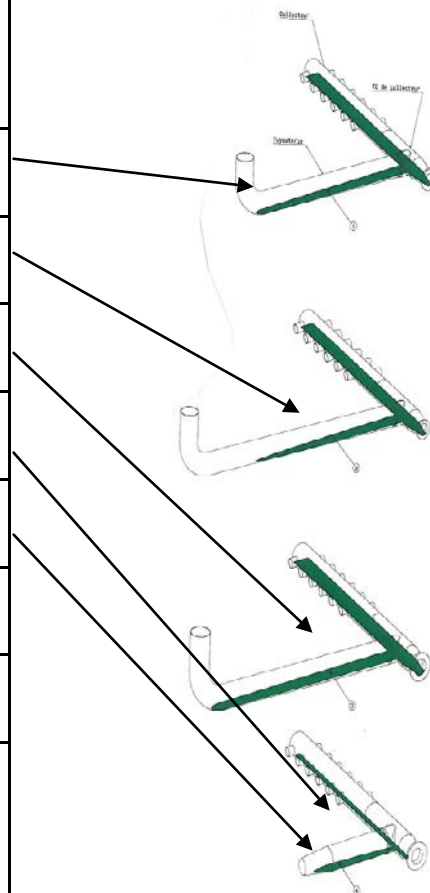
These other retentions are separated from the loop and treated individually.

**3. Aim of the additional draining :**

In order to realize the carbonation in 20 days, the aim after additional draining is a thickness of Na of 10 mm max (except for the expansion tank), acceptable up to 23 mm.

**Estimate of the amount of sodium before and after additional draining :**

	Before draining	After draining
Re superheater enter	211 l	5 l
Superheater enter	202 l	5.5 l
Eco-Eva enter	373 l	5.5 l
Line S* 1004	17 l	0.2 l
Isolation valve	260 l	0.2 l
Total per loop	1063 l	16.4 l
Small retentions	12 Kg	12 Kg
Films of sodium	80 Kg	80 Kg

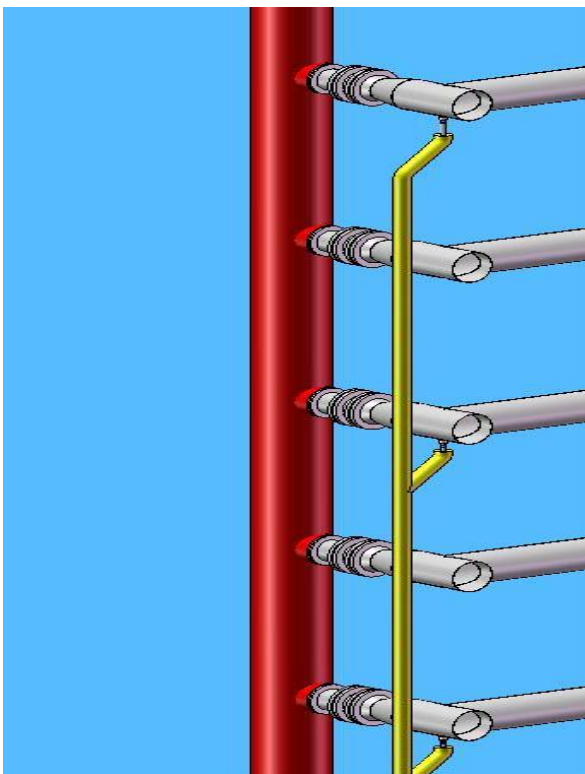


Implementation of the drain line.

Te entry collectors



Isolation Diaphragm Before work



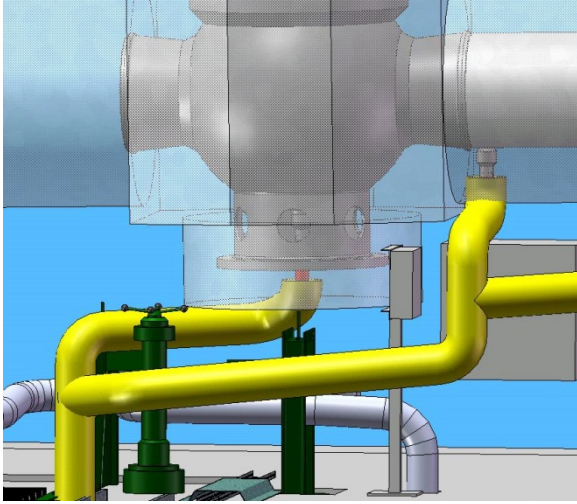
Drain line



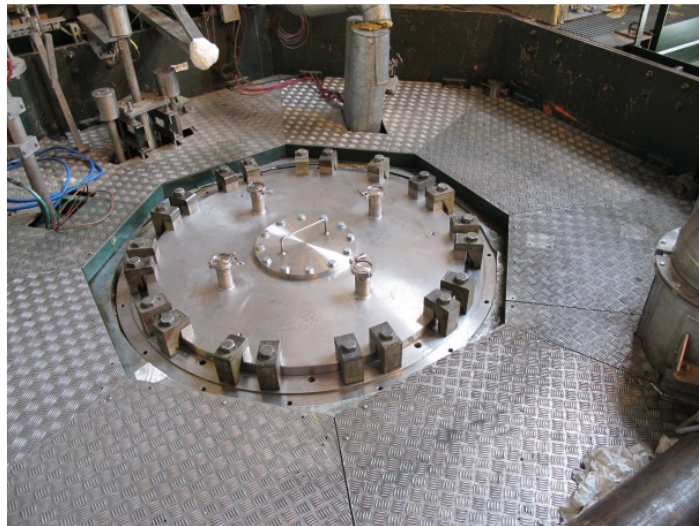
After work



Steam generator isolation valve



Removal of the secondary pump



Cutting tools



Circular cutting



Reciprocating saw



Corer



Grinder (not getting through)

TV Visits



Poussy inox Camera Ø23 mm with a cold light



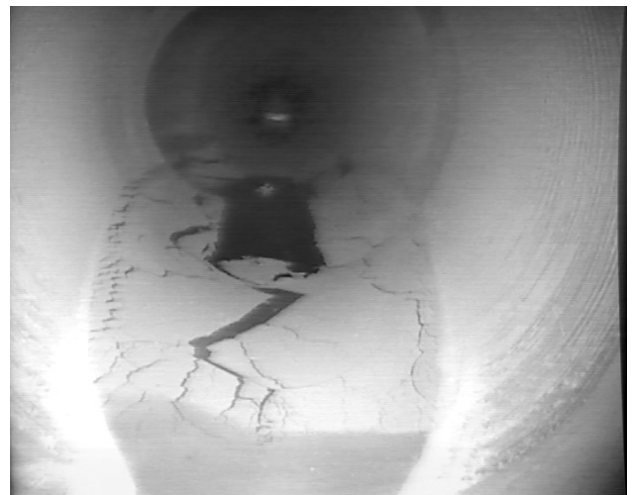
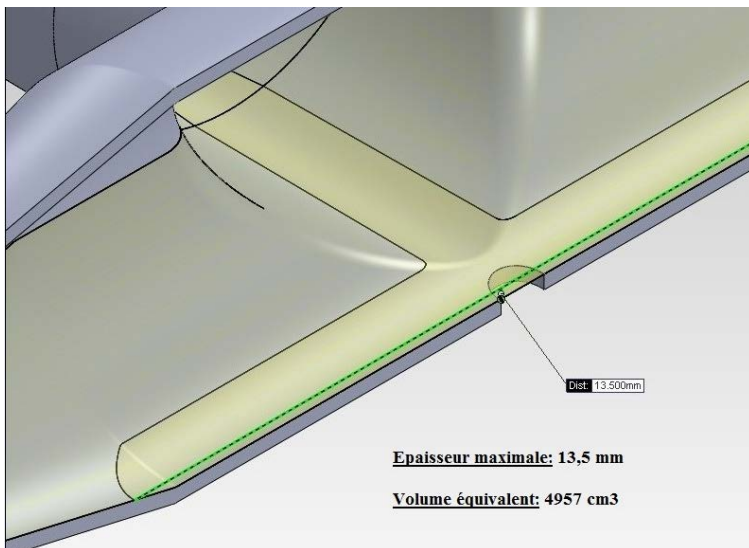
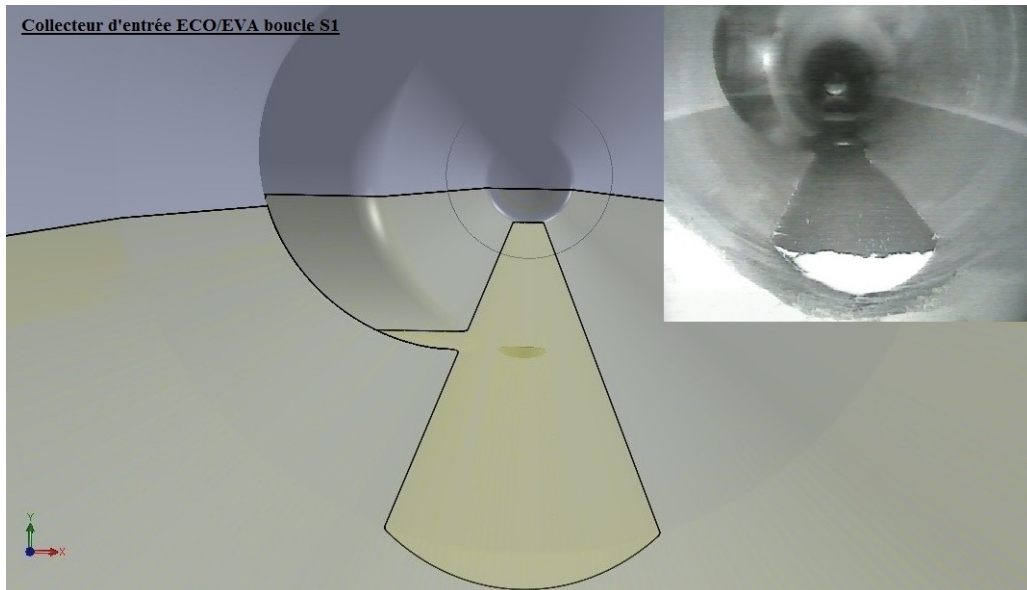
Opening of the sodium circuit with argon and get in of the camera and its support

TV views after additional draining

Estimates of the quantities of residual sodium with 3D modeling.

Maximum thickness 13,5 mm.

Residual volume 4,96 l.



Preparation of carbonation



Opening of the casing



Implementation of floors

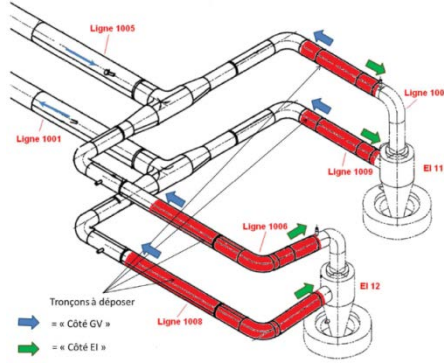


Implementation of curtains for the heating to 50 °C in the steam generator casing

Preparation of carbonation



Intermediate heat exchanger isolation of the secondary loop



Replacement of the valves by hoses



# Dismantling of large components from Phénix reactor

**A.-M.ROUX<sup>a</sup>, A.DURAND<sup>a</sup>, D.CERAT<sup>c</sup>, P.BLIN<sup>b</sup>, A.FAURE<sup>a</sup>**

<sup>a</sup>CEA MARCOULE - Commissariat à l'Energie Atomique, Département Exploitation des Installations de Marcoule (DEIM), Bagnols-Sur-Cèze, FRANCE

<sup>b</sup>CEA MARCOULE Commissariat à l'Energie Atomique, Département des Projets d'Assainissement et de Démantèlement (DPAD), Bagnols-Sur-Cèze, FRANCE

<sup>c</sup>CEA MARCOULE Commissariat à l'Energie Atomique, Département des Unités de Sécurité et Protection (DUSP), Bagnols-sur-Cèze, FRANCE

**Abstract.** The PHENIX reactor was definitively shut down in 2009. The cleaning and dismantling preparation operations are under way. These operations include dealing with large removable components such as primary coolant pumps, intermediate heat exchanger and heat exchanger blanking device (DOTE).

This presentation describes the waste transformation operations performed on a DOTE, from its extraction from the reactor core until transformation to waste for disposal.

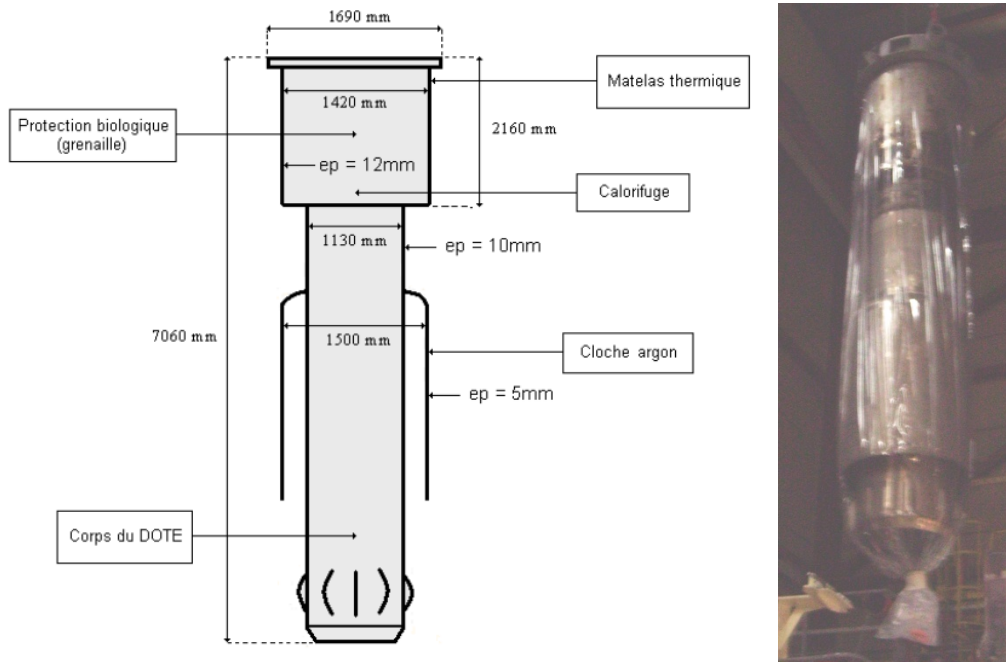
Before 2009, all the large components were dismantled and packaged in metal containers according to Low Level and Intermediate Level Short Lived (LLIL-SL) waste specifications. These operations induced several cuttings and thus consumed exposition of the operators.

In order to reduce the dose and the cost due to the treatment of the component, the objective is now to send the DOTE in one single part to the CSTFA (Very Low Level waste repository).

## 1. Description of a DOTE

A DOTE or dummy intermediate heat exchanger replaces an intermediate heat exchanger in order to first plug the slab penetration initially intended for an exchanger by providing a radiation shield and second make a leak tightness between the hot and cold headers with an argon cap.

A false intermediate heat exchanger is like a long cylinder (7m), 1.7m in diameter and weighing a total of 16 metric tons. Its stainless steel body is cylindrical in shape without tube bundle inside. The thermal mattress consisting of 3 layers of metal (one of stainless steel and 2 of copper) is at the head. Iron shot in this upper part provides a radiation shield and it is put in a sealed container. A cylindrical cap encircles the lower part of the component and a sealing plug at the joint between the upper and the lower part of the component is a layer of insulation between a stainless steel plate and 4 rigid panels.



<b><i>French</i></b>	<b><i>English</i></b>
Protection biologique (grenaille)	Radiation shield (shot)
Matelas thermique	Thermal mattress
Calorifuge	Insulation
Cloche argon	Argon cap
Corps du DOTE	DOE body

FIG. 1. DOTE DESCRIPTION.

## 2. Processing the DOTE

### 2.1. Cutting the thermal mattress

Once the DOTE has been removed from the reactor, it is transferred in a specific cask to the Handling building. The component is deposited in an Intervention Cell (IC) to take off the thermal mattress. Its component plates are cut up, washed in a decontamination box and radiologically tested. A radiological characterisation by gamma spectrometry is then performed to determine the appropriate packaging.

### 2.2. Washing and decontamination of the component

The component is then transferred to washing pits where it undergoes a series of washing baths in order to remove sodium residue. The washing process implies gradually destroying the residual sodium using water in the form of aerosols shaped by a carrier gas,  $\text{CO}_2$ , which favours the neutralization of sodium hydroxide produced by transforming it into carbonate. After direct spraying of steam, the component is dried using nitrogen and visually inspected. Lastly, it is rinsed and possibly submerged.

Decontamination baths will also help to significantly reduce the contamination and therefore the surface activity. The aim of the operation is, by the action of chemicals, to eliminate radioactive materials deposited on the surface of the component (activation products and fission products) by attacking only a small thickness of the component. The products used are sulphuric acid ( $\text{H}_2\text{SO}_4$  at  $12.5 \text{ g / l} \pm 0.5$ ) and phosphoric acid ( $\text{H}_3\text{PO}_4$  at  $30 \text{ g / l} \pm 0.5$ ) and several decontamination cycles are performed.

### 2.3. Characterisation

A mapping of the component is carried out upstream of the washing process (dose rate and contamination). Then a gamma spectrometry characterization is performed when removed from the wash pit. The component is measured by sections to determine the parts pertaining to VLLW and LL/ML channels. It was only after the measurement result is obtained that processing scenario is defined. The DOTE 4776, in its entirety, has VLLW ranking and will be processed as a single part.



FIG. 2. GAMMA SPECTROMETRY

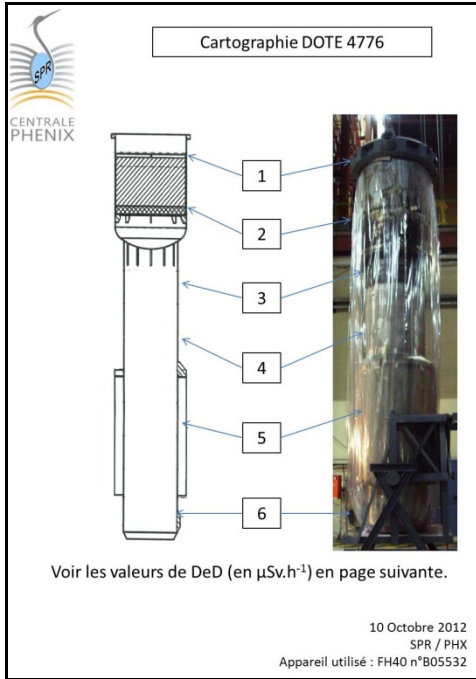


FIG. 3. RADIOLOGIC MAP

## 2.4. Processing

The component is delivered on the Handling Hall structural steelwork. To make tilting easier, the shot is first removed by suction at the upper part using a vacuum cleaner. The component is then tilted using the crane and tilter then inserted into the work airlock.

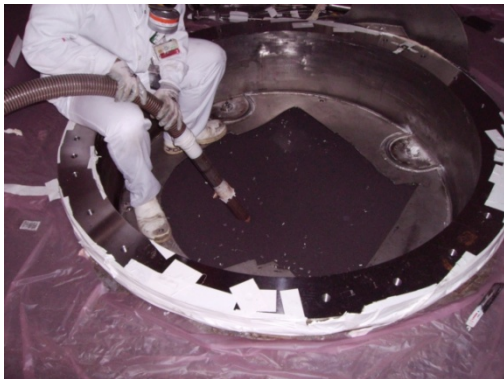


FIG. 4. REMOVING THE SHOT

As the DOTE mainly consists of empty spaces, waste will be inserted inside the body to optimize its hollow volumes. The shot is reinserted into the body through the carrier shell and spread out as evenly as possible. The VLLW heat mattress and VLLW metal waste coming from normal operation (and previously characterised) can be conditioned by creating an opening in the DOTE body which is then closed by a welded metal plate.

The argon cap is cut up and removed from the DOTE body for characterization. The VLLW cut pieces are reinserted into the upper part.



FIG. 5. ARGON CAP CUTTING

A special paint is applied to the single part to set any trace of lip contamination and to prevent any sweating.



FIG. 6. DOTE AFTER PAINTING

Injection ports and vents are made in the part to allow the injection of mortar during its processing at ANDRA's CSTFA storage centre. These openings are drilled and screwed into the metal cover. New lifting gear as well as slings are set up. A design note specifies the type of lifting gear and slings to be used as well as their location on the part.



FIG. 7. PREPARATION OF INJECTION PORTS

Given the length of the unit room (over 6m), sending the 20-foot ISO container is impossible and removal to the CSTFA requires premium transportation. The component is put in a frame.

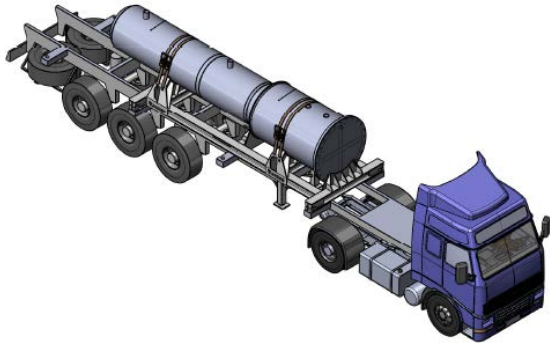


*FIG. 8. TRANSPORT OF THE COMPONENT*

Acceptance of the single part at the CSTFA involves considerable preparatory work consisting of specific meetings and discussion with ANDRA to establish the processing procedure, the characterization stages as well as the type of transport required. An acceptance file is drafted by the plant and must be drawn up in collaboration with ANDRA.

### **3. Conclusion:**

The objective is to recover the components free of sodium so as to carry out the required processing to condition the waste into suitable packaging and remove it to approved channels. Large components are processed by taking into account the feedback acquired on PHENIX since 2010:

- Limiting the number of cuts (ALARA approach) and operating them with the appropriate specific tools (wire saw),
- Optimizing the VLLW dispatch (characterizing as accurately as possible),
- Giving preference to sending single parts,
- Optimizing volumes.

### **ACKNOWLEDGEMENTS**

All these operations have been achieved through a close collaboration between each department and all services providers in charge of operations.